A CMOS SWITCHED CAPACITOR BASED AMPEROMETRIC READOUT CIRCUIT FOR MICRONEEDLE GLUCOSE SENSOR

by

SUNIL GOVARDHAN

Presented to the Faculty of the Graduate School of

The University of Texas at Arlington in Partial Fulfillment

of the Requirements

for the Degree of

MASTER OF SCIENCE IN ELECTRICAL ENGINEERING

THE UNIVERSITY OF TEXAS AT ARLINGTON

December 2013

Copyright © by SUNIL GOVARDHAN 2013

All Rights Reserved

Acknowledgements

I am thankful to my advisor Dr. Sungyong Jung for guiding me through to successfully complete this thesis defense. Along with engineering and research capabilities he has groomed me to look at ideas with deeper insight and conviction, since the fall of 2011. He has been persistent, motivating and encouraging. If not for him, it would not have been possible for me to submit an integrated circuit design in 0.35µm technology for fabrication and test it as a Master's student. He owns the credit for all that I have achieved today and for making me a good circuit designer.

I also thank, Dr. Yuze Sun and Dr. Ali Davoudi for their consent and time to serve on my thesis defense committee and evaluate my work. Special thanks to Dr. Davoudi for lending us equipment which helped me for my experimental work.

I am lucky to have worked with the best minds of AMIC lab and thank them all Dr. Varun Shenoy, Dr. Niranjan Karandikar, Dr. Shaoshu Sha, Mr. Sujith Dermal.

Finally I thank my parents and I am most grateful to them for giving me an opportunity to pursue my Master's at University of Texas at Arlington. They have supported and motivated with their love in all my endeavors. Thanks to all my friends, well-wishers and former colleagues at Robert Bosch, BlackBerry and Freescale Semiconductors for providing me with much needed moral and financial support to complete this work successfully!!

November 18, 2013

Abstract

A CMOS SWITCHED CAPACITOR BASED AMPEROMETRIC READOUT CIRCUIT FOR MICRONEEDLE GLUCOSE SENSOR

Sunil Govardhan, M.S.

The University of Texas at Arlington, 2013

Supervising Professor: Sungyong Jung

Accurate regulation of glucose metabolism is one of the key factors in keeping a healthy state among mammalians. Increase in failure of this natural blood glucose regulatory mechanism has propelled the research for improvements in blood glucose measurement and its regulation. Also, advancement in the research of internet of things has increased the demand for smart sensors creating a revolution in health care industry and which has inturn led to the improvement in point-of-care testing.

Therefore in this thesis work a microneedle glucose sensor is chosen as it can be fabricated by MEMS process which allows it to be easily integrated with CMOS integrated circuit in a single package creating a smart glucose sensor. This smart glucose sensor can sense glucose concentration and process the data all in one chip called Lab-on-chip(LOC). To meet architectural requirements of smart glucose sensor such as low power and compact area a switched capacitor based trans-impedance amplifier architecture is chosen as amperometric readout circuit, as the existing circuit architectures consume higher power compared to switch capacitor trans-impedance amplifier architecture.

In this work a switched capacitor trans-impedance amplifier is analyzed and designed using an operational amplifier and transmission gates. The integrated circuit layout of the design is prepared for 0.35µm fabrication technology. The total area of the

layout is 160µm x 157µm and the area of a 100pF on chip capacitance is 900µm x 50µm. The design is simulated and tested with on chip gain capacitor of 100pF at 200 kHz and with external gain capacitor of 100nF at 200Hz. The circuit linearly amplifies the input current from 2µA-30µA to an output voltage of 45mV-664mV with a trans-impedance gain of 22kΩ. The measured noise at 200 kHz sampling clock is 3mVrms and system power consumed is 1.67mW, whereas measured noise at 200Hz sampling clock is 1.3mVrms and the power consumed is 1.34mW.

Table of Contents

List of Illustrations

List of Tables

Chapter 1

Introduction

Blood glucose is the fundamental metabolic fuel for aiding in cancer cell progression, cardiovascular disease and inflammation[1]. Accurate regulation of glucose metabolism is one of the essential factor's in keeping a healthy state among mammalians. The natural regulatory function is performed by a hormone called insulin which is released by pancreatic β-cells [2][3]. Incorrectness of insulin release (including total absence) is the primary cause of various forms of diabetes[4]. Thus increase in failure of this natural blood glucose regulatory mechanism has propelled the research of blood glucose measurement and its regulation.

It is pivotal to understand the criteria for classification of diabetic conditions to develop an accurate and intelligent measurement system. Glucose levels in the blood are broadly classified into three states as euglycemia, hypoglycemia and hyperglycemia. If the blood glucose level is between 4mM – 7mM it is considered normal state and is called euglycemia. Below 4mM is hypoglycemia, it can cause fainting, comma and even death. Above 7mM is hyperglycemia, it can cause damages to eyes, kidneys, nerves etc.[5] . Currently measurement of glucose from blood is most widely practised method. But in the yesteryear urine tasting using ants was practised by doctors to determine diabetic condition[6]. Thrust for compact systems is driving the research to shrink glucose measurement system to monitor glucose concentration in a tear drop by placing the system in a contact lens[7][8][9].

The earliest glucose measurement was done in the 1870s using chemical methods such as: polarimetry (rotation of polarized light), reduction of Cu(II) to Cu(I) by reducing sugars, and measurement of CO_2 resulting from the fermentation of a glucose-containing

solution[5]. Then in 1980s electrochemical technique was first used with handheld readout instrument for blood glucose measurement and since then electrochemical based detection of glucose has been the most popular technique. Amperometric electrochemical technique is commonly used over potentiometric technique, as the latter is less sensitive to changes in glucose concentration [10].

Typical amperometric technique based glucose sensing system has two circuit blocks and a glucose sensor as shown in Figure 1-1

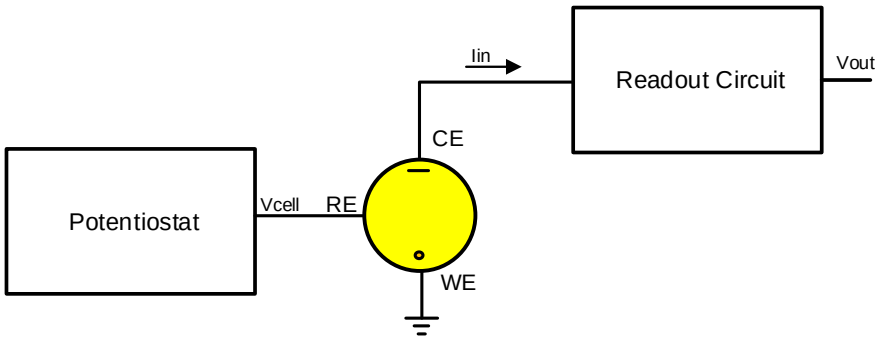

Figure 1-1 Architectural blocks of electrochemical sensor readout system

A potentiostat is required to maintain a constant voltage across the sensor electrodes in order to bias the sensor and kick-start the chemical reaction of interest to produce current proportional to the glucose concentration. The sensor current is converted to a voltage, as voltage can be processed easily to determine the glucose concentration.

Emerging trends in research of internet of things for point-of-care testing (POCT) using intelligent sensor network which can communicate and process data over an internet cloud for health care monitoring as shown in Figure 1-2 is gaining lot of interest among researchers. This evolution in health care monitoring system such as glucose measurement has imposed new architectural challenges for researchers, which are compact architecture and low power along with conventional architectural requirements of

typical glucose measurement system such as: accuracy, sensitivity, range and stability [10] shown in Figure1-3

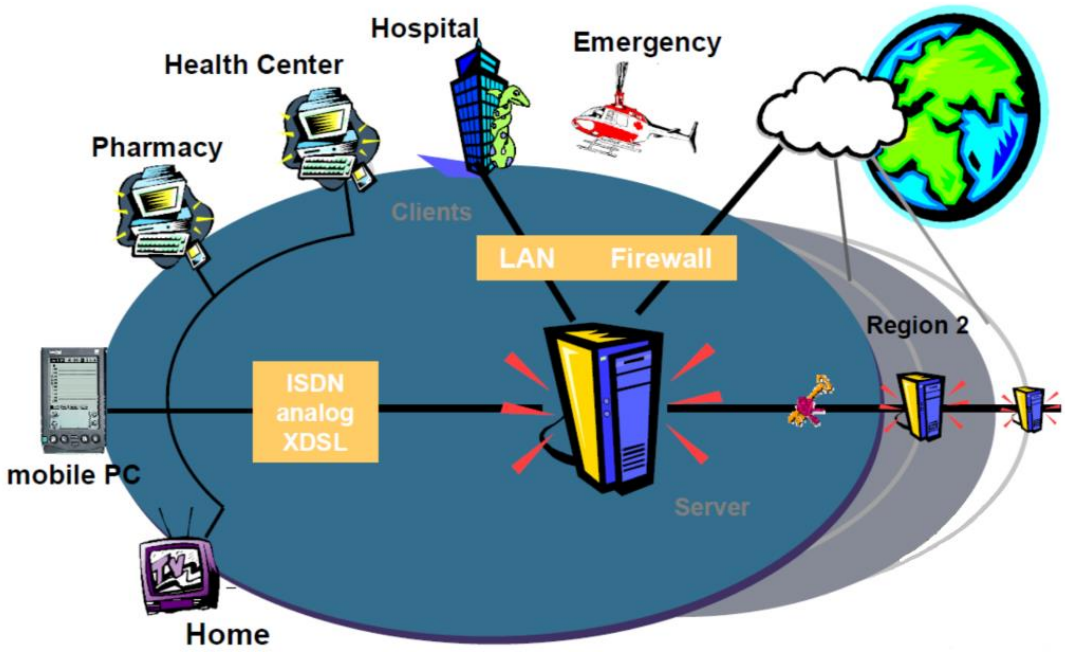

Figure 1-2 Future trends of health care monitoring system [11]

Compact architecture is required to reduce the overall system fabrication cost and low power consumption is a key requirement for integration of this measurement system into battery operated portable computing platforms such as smartphones and tablets. Accuracy, so that glucose level can be measured with minimum errors even in the presence of interfering species. Sensitivity, to be able to detect changes at least less than 1mM in glucose concentration. Range, able to measure all glucose concentrations euglycemia (4mM-7mM), hypoglycemia (below 4mM) and hyperglycemia (above 7mM). Stability, the signal due to glucose must not deviate more than $\pm 5\%$ of its average value during measurement [10]

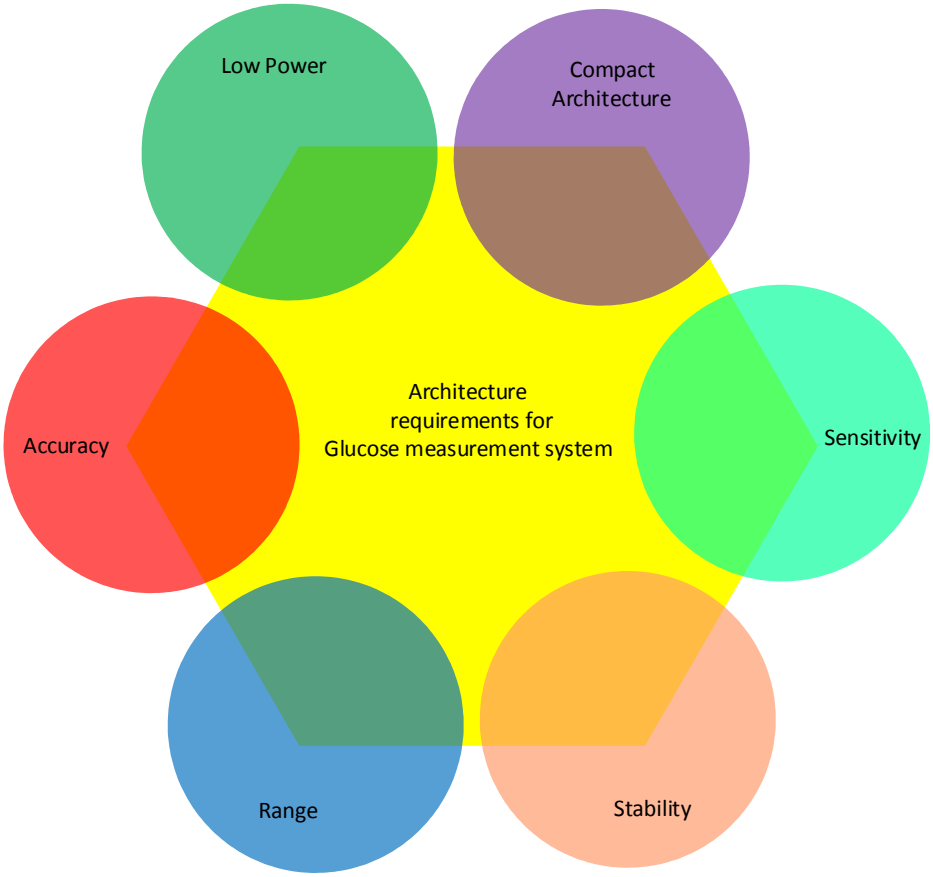

Figure 1-3 Architectural requirements of future glucose measurement system

Glucose sensors are classified as invasive: subcutaneous needle-type sensors, non-invasive: optical techniques and minimally invasive: micropore and microneedle sensors [12]. Minimally invasive microneedle sensors and non-invasive sensors overcome the blood borne infections due to pricking and trypanophobia caused by invasive sensors. However, electrochemical detection is still preferred over non-invasive: optical techniques as these techniques still need to be checked frequently against direct blood glucose measurements (invasive or minimally invasive: microneedle [13].

The most widely used amperometric readout circuit architecture for glucose sensing is trans-impedance amplifier with resistive feedback [10]. This architecture is

simple and suitable for discrete implementation for commercially available handheld glucose meters. But for integrated circuit design it suffers from the drawbacks such as large area, power consumption due to continuous conversion and significant thermal noise contributed by gain resistor [14]. A single ended current measurement architecture [15] uses a resistor inserted between working electrode and ground in the sensor current path, causing a voltage drop which makes it difficult to maintain a constant voltage across reference and working electrode [15]. In a differential current measurement architecture [16] a resistor is inserted in the sensor current path above the counter electrode, the drop across this resistor is measured using a differential amplifier, this architecture requires large area, consumes more power and thus is noisier. Switched capacitor based trans-impedance amplifier architecture provides compatibility with CMOS technology, good accuracy of time constants, good voltage linearity [17] , also capacitive feedback adds lower thermal noise compared to resistive feedback system[18] and switching systems are irreplaceable in the era of digital systems and power conservation.

In this work a microneedle glucose sensor is chosen as it can be fabricated using MEMS technique thus allowing to be integrated with a CMOS readout circuit creating a lab-on-chip (LOC) platform, which will readily fit into the eco system of future health care monitoring.

The switch-capacitor trans-impedance amplifier has never been used along with an amperometric micro-needle glucose sensor. Thus current detection of a microneedle glucose sensor with a switch capacitor trans-impedance amplifier is the novelty of this work. This trans-impedance amplifier architecture is chosen as it provides high linearity, low thermal noise compared to a resistive feedback trans-impedance , satisfies the dynamic range of a microneedle based non- enzymatic glucose sensor [19], readily

discretizes the measurement making signal processing easier and as it is a switching system power can be conserved.

This thesis is organized into four chapters as follows:

Chapter 1 presents the motivation for glucose monitoring system and classification of glucose states, brief history of chemical and electro-chemical glucose sensing, evolution of health care system and new architectural challenges, classification of glucose sensors and amperometric readout circuits for current sensing are reviewed and finally novelty of this work is explained.

Chapter 2 provides a concise review of electrochemistry, electrochemical sensors and techniques, evolution of electrochemical glucose sensors and its evolution. The various current detection circuits used in electrochemical sensing application are presented with their merits and demerits.

Chapter 3 discusses the design specification, microneedle glucose sensor specification, circuit design and analysis of switched-capacitor trans-impedance amplifier circuit to amplify input sensor current to an output voltage. Simulation and measurement results at 200 kHz with 100pF on chip capacitor and 200 Hz with 100nF external capacitor are presented to verify and validate the design.

Chapter 4 concludes this thesis with the contribution of this work and a set of future research objectives that can be conducted to complete the idea of a smart sensor.

Chapter 2

Background

Electrochemical glucose sensing is still by far the most popular and widely used technique over the relatively nascent non-invasive glucose sensing techniques. Thus understanding the theory of electrochemistry is quintessential in this work.

2.1 Electrochemistry

Electrochemistry is a branch of chemistry that is based on Michael Faraday's experimental study published in 1834 that quantifies generation of electricity during a chemical reaction such as electrolysis. The electrode in a solution works as a transducer between the chemical and electrical domains. It induces a electrochemical reactions which causes an electrical response which is monitored to characterize the chemical species in of interest.

Electrochemical reactions occur in a solution containing dissolved ions (electrolyte) which cause the current to flow. Mostly, the solvent-electrolyte combination used in electrochemical experiments are strong electrolytes (fully broken down into ions when dissolved in solvent).Current flowing from the positive electrode to negative electrode in a electrochemical cell is a function of solution resistance of the electrolyte between the electrodes. The value of this resistance depends on the ionic conductivity of the electrolyte, and geometric arrangement of electrodes in the cell [20].

The two basic types of charge transfer reactions take place at an electrode solution interface: oxidation and reduction. During an oxidation reaction, the chemical species transfer electron(s) to the electrode, while in a reduction reaction, the chemical species receive electron(s) from the electrode. The resulting chemical reactions are represented as:

Oxidation:

$$R \rightarrow O + ne^- \tag{1.1}$$

Reduction:

$$O + ne^- \rightarrow R \tag{2.2}$$

where O is the oxidized species, R is the reduced form of species and n is the number of electrons transferred during the reaction.

A classic example of electrochemical reaction is to create silver cations (Ag+) in water, by immersing a silver electrode in pure water as shown in Figure 2-1.

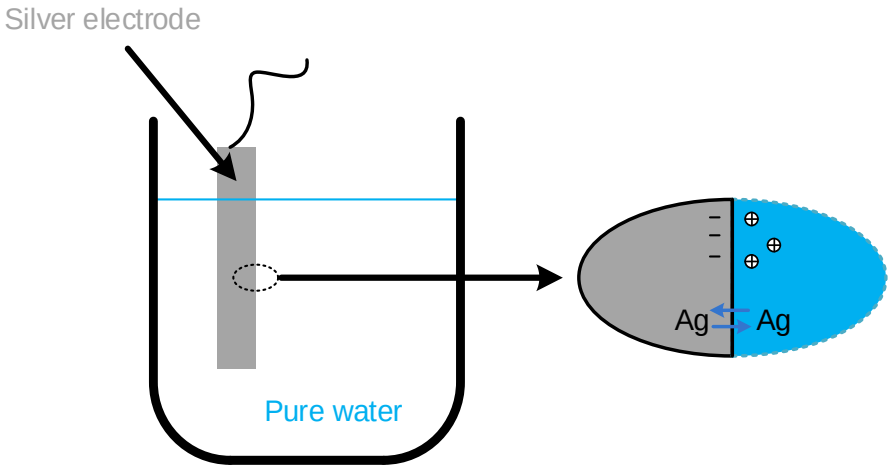

Figure 2-1 Oxidation of a silver electrode immersed in pure water

Some of the silver atoms dissolve in the water as positive ions, leaving their electrons in the electrode as shown in the following equation:

$$Ag \rightarrow Ag^+ + e^- \tag{2.3}$$

This buildup of charge in the electrode and solution causes an interfacial potential difference, which can affect the rate and direction of the reaction. The interfacial potential difference, E, of an electrode can be calculated using the Nernst equation[20]:

$$E = E^0 + \frac{RT}{nF} ln\left(\frac{C_o}{C_R}\right) \tag{2.4}$$

where E^0 is the standard potential of the electrode, R is the molar gas constant, T is temperature, F is Faraday's constant and C_o and C_R are the concentration of the oxidized and reduced forms of the species, respectively[20].

2.2 Electrochemical cell

Electrochemical cells are broadly classified into two sub-types, galvanic and electrolytic. The reaction in galvanic cells start spontaneously when the electrodes are connected using a conductor, while on the other hand an electrolytic cell shown in Figure 2-2 requires a voltage to be applied in excess of its operating cell potential (OCP) in order to start an electrochemical process.

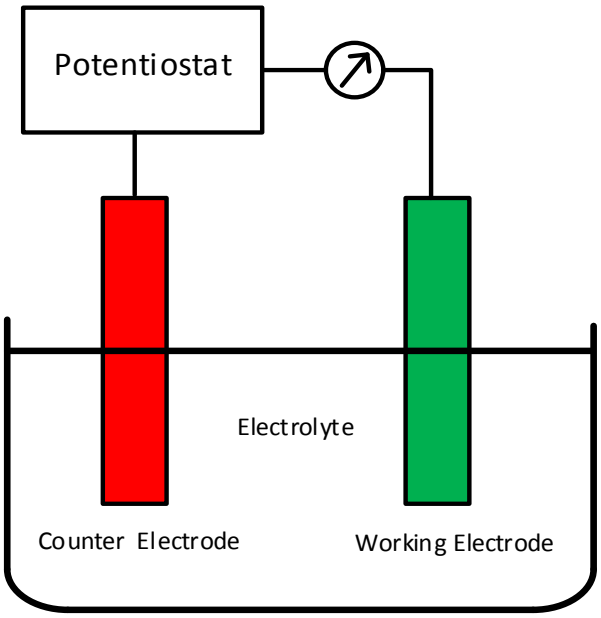

Figure 2-2 Simple two electrode electrochemical cell

The electrodes are identified by the function they perform in the cell: the working electrode (WE) and the reference electrode (RE), [20]. The WE is generally a cathode of an electrochemical cell, it experiences the reaction of interest and can be tailored to

increase its sensitivity to observe a specific species or to decrease the potential required to drive a particular reaction. The RE is an anode, it maintains constant composition and provides a fixed potential across the electrolyte to monitor the reactions occurring at WE reactions can be monitored. Commonly used reference electrode is the silver-silver chloride (Ag/AgCl) electrode. In this work a Saturated calomel electrode (SCE) is used as a reference electrode [19].

2.2.1 Faradaic and Non-faradaic mechanism

The current flow in an electrochemical cell is due to two kinds of mechanisms faradaic and non-faradaic. When charge transfer happens due to oxidation or reduction reactions it is a faradaic mechanism resulting in faradaic current flowing through charge-transfer electrodes. The faradaic current is a function of:

1. The rate at which the material moves from the bulk of the electrolyte to the electrode surface (mass transfer) [20]
2. The rate at which electrons transfer from the electrode to electrolyte and vice versa(charge transfer)[21]

Processes such as adsorption and desorption can cause transient current to flow through the interface when either the potential or electrode area or solution composition changes causing a non-faradaic mechanism [22]. Non-faradaic current is inversely proportional to the size of the electrode. Current in an ideal sensor will only flow due to faradaic mechanism.

Sensitivity of an electrochemical cell is defined as the ratio of faradaic current to non-faradaic current. The peak faradaic current is given by:

$$i_{max} = 2.59 \times 10^5 n^{\frac{3}{2}} (Dv)^{1/2} C_v \qquad (2.2)$$

where v is the constant rate of variation and Cv is the values of ionic activity. Non-faradaic current is given by:

$$i_{ch} = C\frac{dE}{dt} = \pm Cv \quad (2.3)$$

from equations 2.5 and 2.6 it can be observed that increasing scan rate will reduce sensitivity. Thus, lower scan rates are preferred in measurements at solid electrode [23].

2.3 Electrochemical sensors

The principle of all electrochemical sensors is to measure chemical concentration of the reactions taking place in an electrochemical cell by monitoring the change in current, cell potential, resistance or impedance. Electrochemical sensors are broadly classified into three categories [24]:

2.3.1 Voltammetric sensor

In a voltammetric sensor current flows when a constant potential is applied across the electrodes of the electrochemical cell. This current is measured current to the characterize response of chemical species of interest. Voltammetry provides better sensitivity by increasing the ratio of the faradaic current (the current of interest) to non-faradaic current (the background). By applying either a ramp, square or cyclic voltage, improved selectivity and sensitivity maybe obtained.

Cyclic voltammetry is a procedure where a periodic triangular waveform based voltage is applied to the two electrodes of a voltammetric sensor at a scan rate *v*. The varying voltage may enable reactions of various chemical species in the electrolyte. The plot of measured current vs. applied voltage is known as cyclic voltammogram. These plots are studied to obtain stability information of reaction products, the presence of intermediate redox reactions and the reversibility of a reaction.

2.3.2 Amperometric sensor

Amperometric sensor is a special type of voltammetric sensor, which requires a constant voltage to be applied across the electrodes of the electrochemical cell and the current flow caused by the change in resistance due to chemical reaction is measured. The measured current is a function of the concentration of the electroactive species. The response will have high linearity if the current is limited by the rate of the mass transfer and not by the rate of charge transfer[20].

Chronoamperometry is an electrochemical technique in which the potential of the working electrode is stepped, and the resulting faradaic current (caused by the stepped potential) is measured as a function of time[20]. In this technique current is integrated over relatively longer time intervals, thus allowing it to produce a better signal to noise ratio in comparison to other amperometric technique.

2.3.3 Potentiometric sensor

In a potentiometric sensor, the open circuit electrochemical cell potential caused by the chemical reaction is measured, which is given by equation 2.4 it is logarithmically proportional to the concentration of the chemical species of interest. Potentiometric sensors are mostly used when the concentration of chemical specie to be measured changes by several orders of magnitude, such as pH measurements[24].

2.3.4 Conductometric sensor

A conductometric sensor working principle is based on modulation of resistivity of the selected material upon interaction with chemical species and thus is also called chemiresistor. Fabrication cost of conductometric sensor is low compared to other electrochemical sensor. Commonly used as gas sensor and biosensor [25].

A biosensor is a special type of electrochemical sensor made of biological materials, e.g., tissue, micro-organisms, enzymes, antibodies, nucleic acids and so on, to

detect chemical species such as glucose, urea, lactate, etc. [24]. The property of a biosensor to be sensitive and selective to monitor a particular type of biological material makes it attractive. A biosensor comprises of two parts:

- A biological element such as enzymes or antibodies or micro-organisms.
- An optical or a electrochemical detector.

The selectivity of a biosensor is constrained by the biological element, whereas the sensitivity depends on both biological element and the transducer (optical or electrochemical). The property of selecting a particular biological material gives biosensor edge over chemical sensors analogous to sensing mechanisms existing commonly in the nature[24].

2.4 Electrochemical Glucose Sensor

Electrochemical detection of glucose concentration works based on interaction of glucose oxidase (biosensor enzyme) with glucose. In normal conditions, glucose oxidase enzyme reacts with glucose causing redox reaction. First it reacts with the glucose to form gluconic acid and changes into an inactivated reduced state by accepting electrons. This reduced enzyme returns to active oxidized state by giving these electrons to molecular oxygen and thereby producing hydrogen peroxide (H_2O_2) as shown in Figure 2.3 and is represented by the reaction:

$$Glucose + O_2 \xrightarrow{GOx} Gluconice\ Acid + H_2O_2 \tag{2.7}$$

The glucose oxidase enzyme performs the role of catalyzer for the oxidation of glucose and is not consumed in the reaction. From the above reaction, there are only three possible electrochemical techniques for detecting the glucose concentration [10]. The first technique is to use an amperometric sensor to measure the amount of oxygen consumed or to measure the hydrogen peroxide produced in the reaction. Second technique is to use

a potentiometric sensor to detect the change in pH level caused by the release of gluconic acid. Third technique is to use a conductometric sensor to detect the change in electrical resistance due to the reaction.

Potentiometric and conductometric glucose biosensors, are sensitive to the interfering biological species other than glucose and, also the response of potentiometric sensors is logarithmic to detect glucose concentration, which further limits the potentiometric sensors sensitivity [10]. Thus amperometric biosensors are commonly used to measure glucose concentration which is linearly proportional to the current flowing in the electrochemical cell.

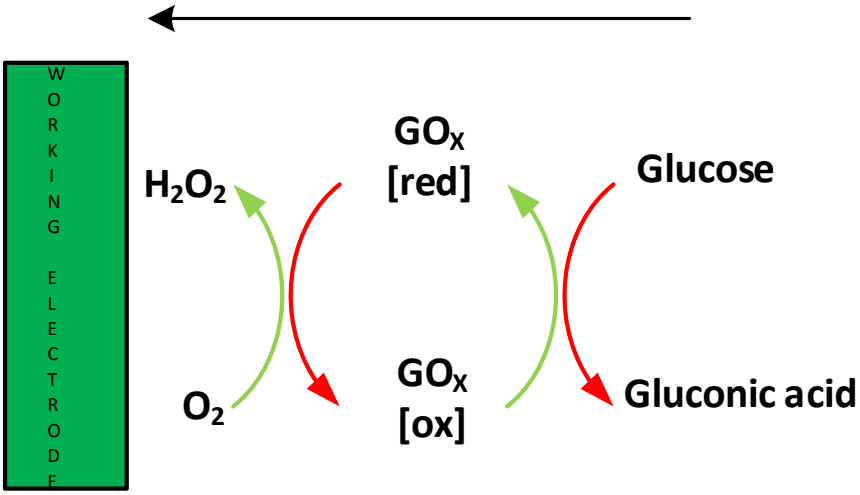

Figure 2-3 Enzymatic reaction between glucose and glucose oxidase

Amperometric biosensors are broadly classified into four generations[10]. In the first generation sensors, the hydrogen peroxide produced or the oxygen consumed in the reaction 2.7 is sensed. In the second generation, a mediator which reduces required cell potential to start the reaction is used to transfer electrons from the reduced enzyme to the electrode. The third generation amperometric glucose biosensor is based on direct electron

transfer between the enzyme and electrode. The fourth generation is based on glucose oxidation at a noble electrode without using enzymes as mediator.

2.4.1 First Generation Sensor

The first generation glucose sensors are of two types: hydrogen peroxide electrode-based (H_2O_2) biosensors and oxygen electrode-based (O_2) biosensors.

A H_2O_2-based sensor responds to hydrogen peroxide produced in the enzymatic glucose reaction. This sensor can be easily fabricated by screen-printing technique. However, these sensors have a few drawbacks [10].

1. Enzymatic reaction is oxygen limited.
2. Hydrogen peroxide produced by the reaction over a period of time makes the glucose oxidase ineffective.
3. High cell voltage is required for oxidizing the hydrogen peroxide, thus may also trigger the interferers such as urea and ascorbate (vitamin-C).

In a O_2 based biosensor, oxygen used in the enzymatic reaction is measured. This method is not limited by oxygen deficit and interference problems. But it still has short life time problem due to release of hydrogen peroxide. The other drawbacks are slow response time, requirement for more complex electronic circuitry, difficulties in miniaturization, and low accuracy and reproducibility[10].

2.4.2 Second Generation Sensor

In the second generation glucose biosensors, a mediator (chemical component) is introduced to aid the transfer of electrons from the reduced enzyme to the electrode. The oxidation cell potential of the mediator would be much lower than that of a hydrogen peroxide based sensor, thus reducing the impact from interferers and also, the signal generation is independent of oxygen. This technique is popularly used to detect, the true glucose concentration in the subcutaneous tissue[10]. Disadvantage of this type of sensor

is that, mediator could leak from the electrode surface and secondly most of the proposed mediators are toxic, which makes their use hazardous for in vivo sensing [10].

2.4.3 Third Generation Sensor

The third generation glucose biosensor is based on the direct electron transfer without any mediator between the enzyme and the electrode made of organic conducting substances [26]. This type of biosensor require low operating potential, and thereby will have reduce the impact of interferers. As there is no soluble compound involved in the construction of this sensor, it is most suited for in vivo sensing [10].

2.4.4 Fourth Generation Sensor

A fourth generation sensor is based on direct glucose oxidation at noble electrode interface without the use of any enzyme [27]. Direct glucose oxidation at a noble electrode with a large surface area offers a substantial improvement in signal to noise ratio. Major drawback of non-enzymatic glucose sensor is its low sensitivity. Although advancements in fabrication methods has improved the selectivity of non-enzymatic glucose sensors based on direct oxidation on the nanoprous electrode [28]. Due to the use of high electro-active surface area based nano-scale electrodes enhancement in electro-catalysis can be achieved [29].

2.5 Two and three electrode glucose sensors

Electrochemical sensors are broadly classified based on the electrodes as, two electrodes and three electrodes. A two electrode electrochemical sensor as shown in Figure 2-4 it has a working electrode and a counter electrode.

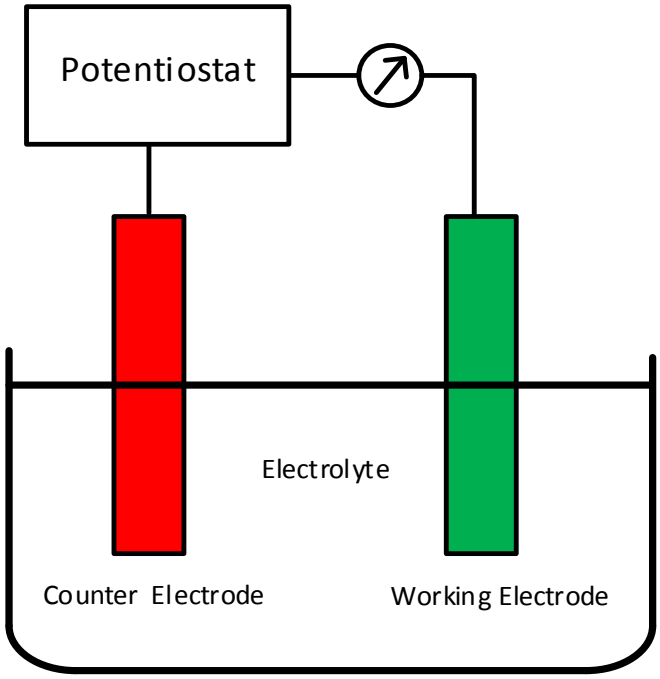

Figure 2-4 Two electrode electrochemical sensor

The reaction of interest occurs at the working electrode and the counter electrode is required to complete the electrical connection for the current to flow in the sensor. As the current flows through the counter electrode due to chemical reaction in the working electrode, it polarizes the counter electrode and also cause a voltage drop across the counter electrode. Thus causing the potential difference across working electrode and the counter electrode to vary. This major drawback of two electrode electrochemical sensor is resolved by a three electrode sensor.

The three electrode electrochemical sensor as shown if Figure 2-5 has three electrodes which are counter electrode, reference electrode and working electrode.

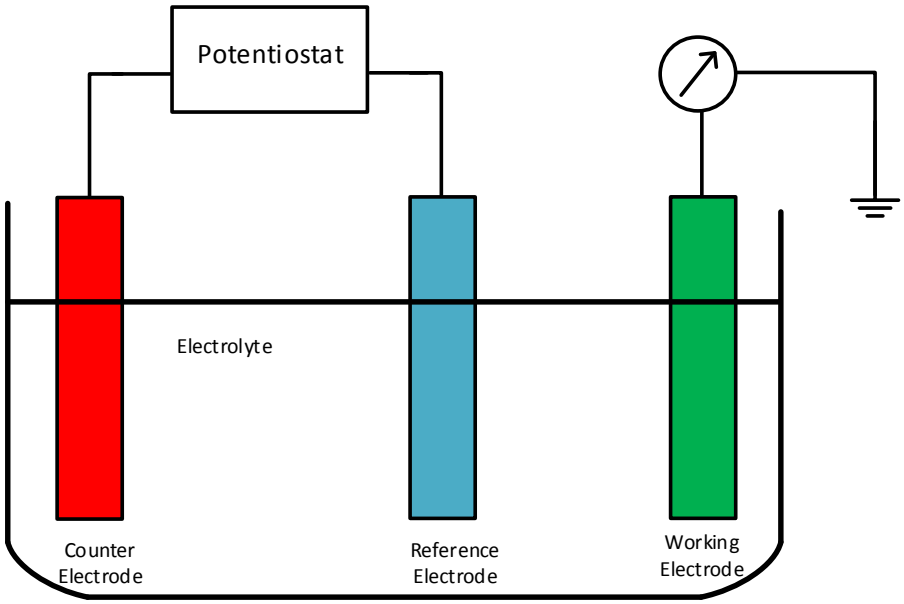

Figure 2-5 Three electrode electrochemical sensor

The role of working electrode is to respond to chemical reaction of interest like it works in a two electrode electrochemical sensor and it is normally coated with an enzyme to improve its sensitivity to a particular chemical or bio-chemical substance for example glucose oxidase is the enzyme commonly used for glucose sensing. Reference electrode maintains a stable voltage across the electrolyte and working electrode, without conducting any current due to chemical reaction, thereby eliminates the problem of varying cell potential seen in a two electrode electrochemical cell. The counter electrode completes the electrical circuit for the current due to reaction at working electrode to flow in the electrochemical sensor as in a two electrode electrochemical sensor. Thus three electrode electrochemical sensor type has been widely used in recent works.

2.5.1 Electrical Model of electrochemical sensor

Glucose electrochemical sensors is a electrochemical cell in which electrical attribute such as current corresponding to the glucose concentration can be measured by an electrical readout circuit and then processed in digital domain. Therefore in order to

design, simulate and test an optimal sensor readout circuit an electrical model of an electrochemical cell is crucial. The electrical model shown in Figure 2-6 is of a three electrode electrochemical cell or sensor.

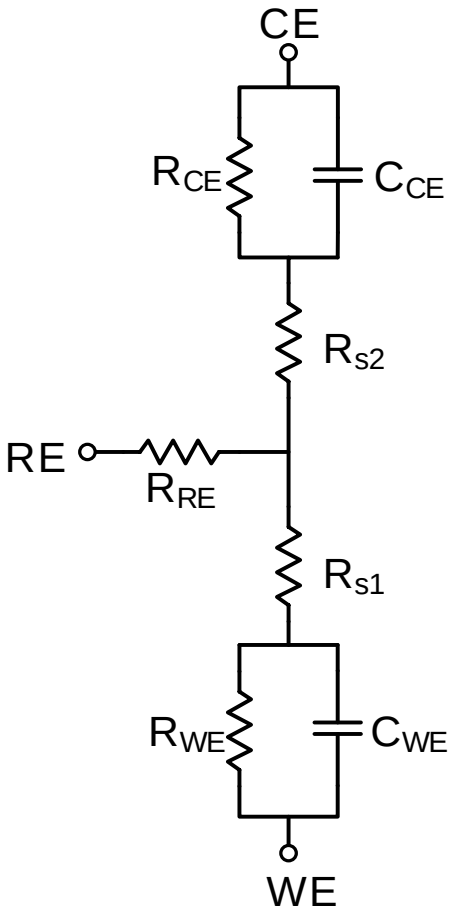

Figure 2-6 Electrical model of a three electrode electrochemical cell

C_{CE} and C_{WE} is the double layer capacitances of CE and WE. R_{CE}, R_{RE} and R_{WE} mimic the charge transfer resistances of the CE, RE, and WE. R_{s1} and R_{s2} function as the solution resistance [15]. Table 2-1 enlists all the components presented above that are required to make an electrical model of an electrochemical sensor.

Table 2-1 Sensor model component description

Component	Description
C_{CE}, Cwe	Double layer capacitances
R_{CE},R_{RE},R_{WE}	Charge transfer resistances
R_{s1},R_{s2}	Solution resistances

2.6 Electrochemical sensor readout circuit architectures

As sensors used for sensing glucose in blood and tear fluid work based on the amperometric electrochemical cell principle, thus readout circuits for amperometric sensing will also be used as glucose sensor readout circuits. Readout system consists of two types of circuit which are potentiostat and an amperometric sensor readout circuit. A potentiostat circuit ensures that a constant potential difference between reference electrode and working electrode is maintained. An amperometric sensor readout circuit amplifies the input reaction current proportional to glucose concentration into output voltage. All architectures presented in this section are made of a potentiostat and an amperometric sensor readout as shown in Figure 2-7.

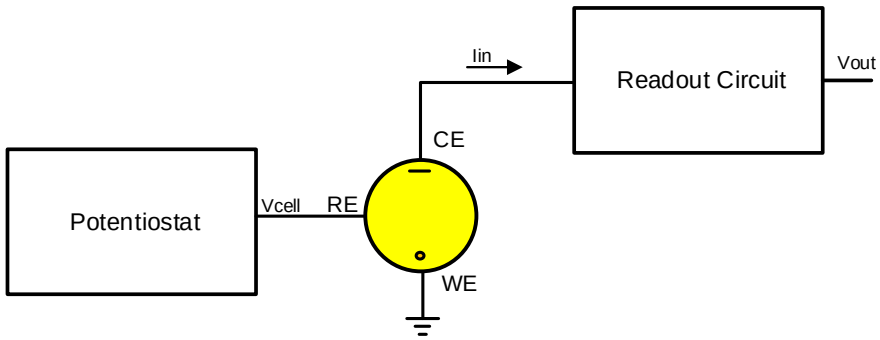

Figure 2-7 Architectural blocks of electrochemical sensor readout system

A transimpedance amplifier architecture shown in Figure 2-8, is most commonly used.

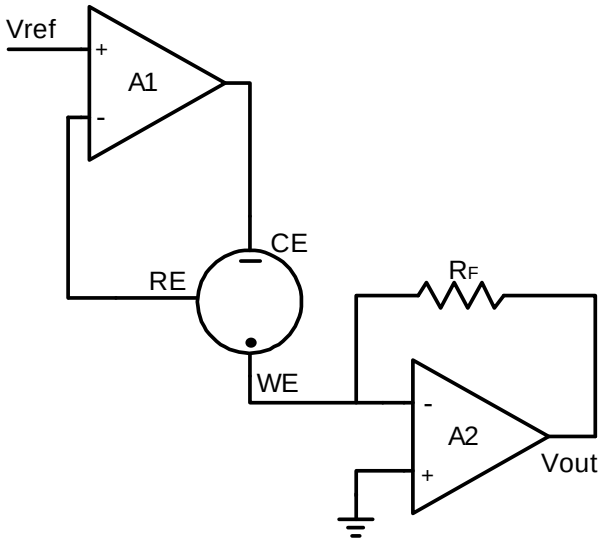

Figure 2-8 Trans-impedance amplifier architecture

Amplifier A1 functions as a potentiostat to maintain constant voltage difference V_{ref} is equal to cell potential between the reference electrode RE and working electrode WE, also completes the electrical circuit by allowing the current due to reaction to flow only through counter electrode. Amplifier A2 functions as a trans-impedance which amplifies the current flowing from working electrode to a gained voltage. Since amplifier A2 is implemented using a high gain operational amplifier forces the WE electrode to ground potential by principle of virtual ground. This architecture is most suited for implementation using commercial off-the-shelf components. But drawbacks such as large area, power and noise restrict this architecture from being implemented using integrated circuit design [30].

A trans-impedance variant architecture is presented in [31] as shown in Figure 2-9.

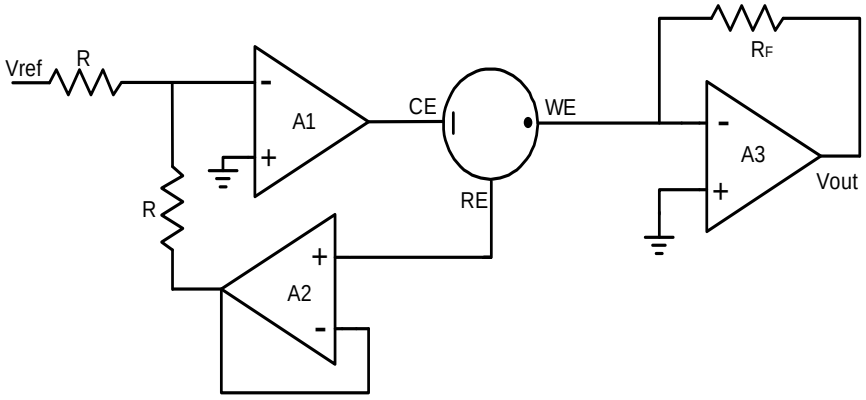

Figure 2-9 Trans-impedance amplifier variant architecture [31]

This architecture has an additional amplifier A2 to buffer the V_{ref} applied to the reference electrode by ensuring that no current is drawn through RE. Thus providing a very high input impedance to reference electrode. The trans-impedance variant provides an accurate potential control, but as in the previous architecture drawbacks such as large area, power and noise restrict this architecture from being implemented using integrated circuit design.

Switched capacitor based architecture shown in Figure 2-10 is a low noise solution [32]. This architecture is implemented using operational amplifier based potentiostat and a switched capacitor trans-impedance amplifier.

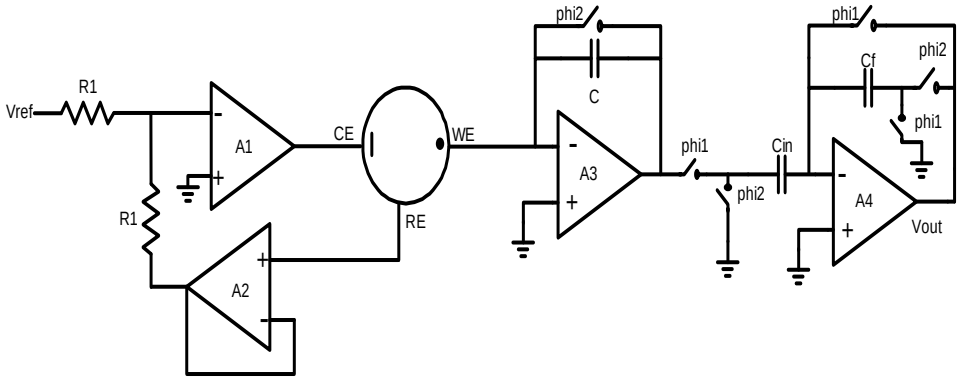

Figure 2-10 Switched capacitor trans-impedance architecture [32]

Operational amplifier A3 and C are used to implement a switched capacitor trans-impedance amplifier. Switched capacitor trans-impedance amplifier works based on charge integration over a fixed time to amplify input current to output voltage. Operational amplifier along with capacitors Cf and Cin work as inverting amplifier to invert the polarity of output voltage amplified by switched capacitor trans-impedance amplifier. Switched capacitor circuits discretize the system, thereby making them fundamental block for circuit based signal processing such as analog to digital conversion.

Fully differential current measurement architecture is as shown in Figure 2-11 [16]. This architecture requires three operational amplifiers A2, A3, A4 for current measurement.

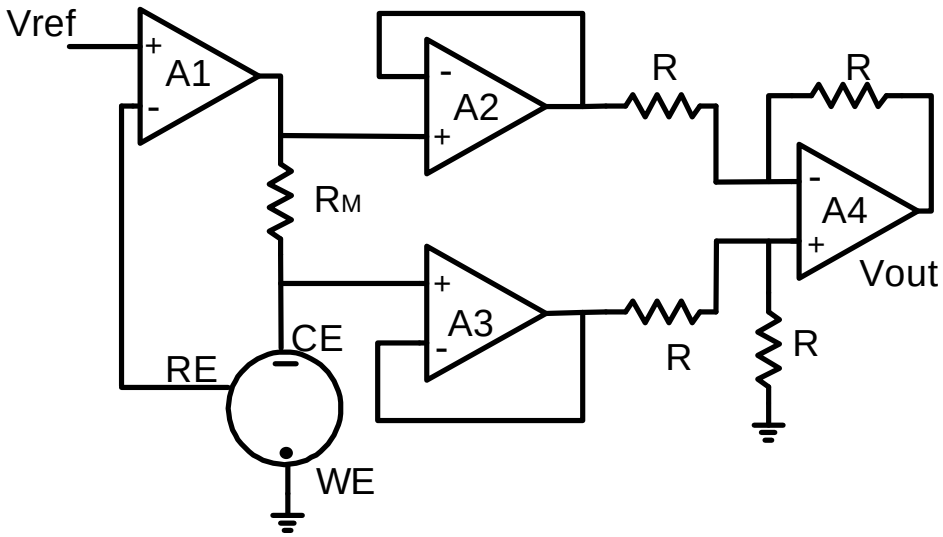

Figure 2-11 Fully differential current measurement architecture [16]

In this architecture the working electrode is connected to circuit ground immunizing it from environmental noise unlike other architectures where it is connected to virtual ground. The resistor R_M is placed in the current path and the drop across it is measured using operational amplifier A2, A3 and A4. A2 and A3 are voltage buffers to prevent the amplifier A4 from drawing any sensor current.

A single ended sensor current measurement architecture is as shown in Figure 2-12 [15].

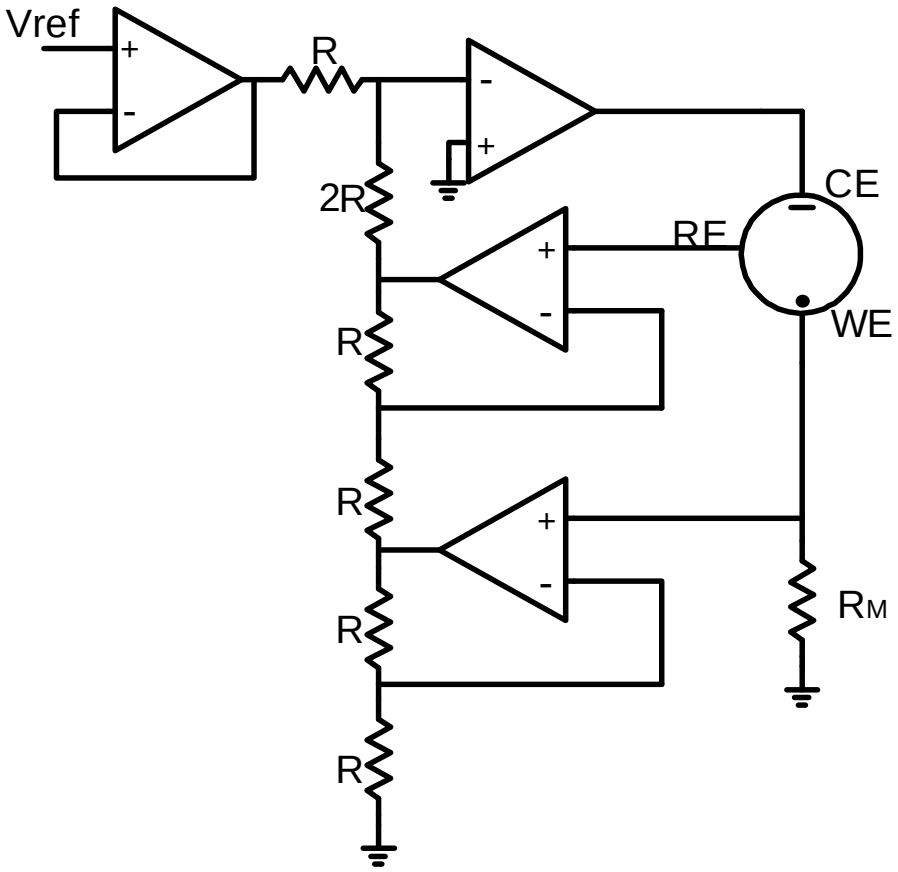

Figure 2-12 Single ended current measurement architecture [15]

R_M is placed between working electrode and ground such that current output from the sensor flows through this resistor causing a voltage drop proportional to the sensor current. This approach changes the potential of working electrode depending on the sensor current flowing through R_M, hence it is difficult to maintain constant potential difference between the reference electrode and working electrode.

Table below shows the comparison of different architectures

Table 2-2 Comparison of different architectures

Architecture	Power consumption	Noise	Complexity
Trans-impedance [33]	≈4.3mW	N/A	Less
Fully differential architecture [31]	15.84mW	N/A	More
Switched capacitor [32]	1.1mW	≈2mVrms	Moderate

Chapter 3

CMOS Switched Capacitor Based Microneedle Glucose Sensor Readout Circuit

As presented in the previous chapter the salient features of a switched capacitor amplifiers such as compatibility with CMOS technology, good accuracy of time constants, good voltage linearity, good temperature characteristics make them most preferred type of circuit for a compact and accurate Lab-on-chip type electrochemical analysis system. In this ubiquitous digital and power conservation era switching systems are irreplaceable. Thus a switched capacitor type trans-impedance amplifier is chosen for this work to read and discretize the response of micro-needle glucose sensor. Lastly, capacitive feedback adds lower thermal noise compared to resistive feedback system [18].

3.1 Design specification

This work is fabricated in 0.35µM CMOS process technology. Technology specification are listed below in Table 3-1:

Table 3-1 Process specifications

Parameter	**Value**
VDD	3.3V
Minimum L	0.35µm
PAD size	81.4µm*81.4µm
Resistance	1KΩ/square
Metal Layers	4

The CMOS device in this process can handle up to 3.3V and the minimum feature size of the CMOS device is 0.35µm. In this technology there are four metal layers available

to lay the interconnections and the bond pad size is 81.4µm*81.4µm to wire bond the pad on the die to the QFPP package leads.

3.1.1 Microneedle Glucose Sensor

This work uses a microneedle array based non-enzymatic electrochemical glucose sensor developed by Yoon et.al [19] as shown in Figure 3-2.

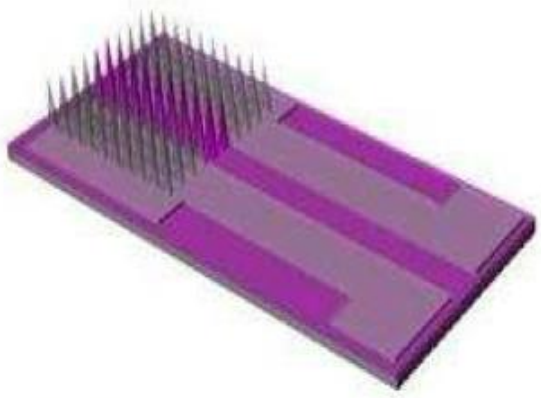

Figure 3-1 Microneedle-integrated non-enzymatic glucose sensor structure [19]

The microneedle array is made of 15x15 sharp silicon microneedle each 380 µm long and tip diameter is 1 µm. As carbon nanotubes have an intrinsically high active surface area that is preferred for kinetically controlled, surface bound reaction such as glucose oxidation. Thus to increase the surface area the multi-walled carbon nanotubes (MWCNTs) are grown directly on non-planar sharp silicon microneedle array, followed by platinum nanoparticle catalyst electroplating on the MWCNT forest. Then a miniaturized silver/silver chloride third electrode is fabricated as reference electrode.

The amperometric sensor response shown in Figure 3-2 is obtained using phosphate buffered saline solution in the presence of relevant physiological species such as acetaminophen and ascorbic acid to mimic interfering agents in blood.

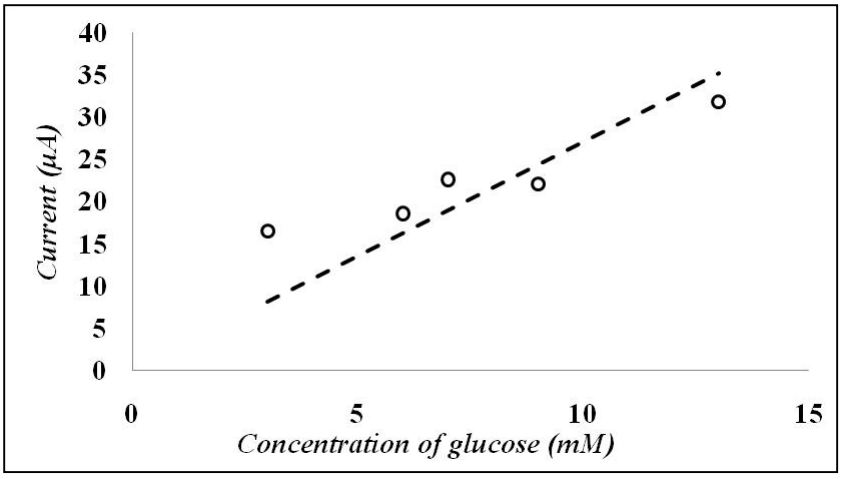

Figure 3-2 Amperometric response vs. glucose concentration [19]

The sensor sensitivity is in the range of 8.10 ~ 13.67 μA/mM-cm^2 for a physiological level of 0 ~ 15 mM glucose concentration [19].

Thus, the microneedle sensor response shown in Figure 3-2 is used in this work as input current specification for simulation and measurement of the proposed switch capacitor based trans-impedance amplifier.

Circuit design specifications for this work are listed in table 3-2:

Table 3-2 Circuit design specifications

Parameter	**Value**
Glucose level	2.5 mM -15 mM
Sensor current	2 μA - 30 μA
Power Supply	±1.65 V
Output Voltage	44mV - 660mV
Switching frequency	200 Hz, 200k Hz
Trans-impedance gain	22kΩ
Power, noise, area	minimize

3.2 Proposed CMOS switched capacitor trans-impedance amplifier design

The proposed switch capacitor trans-impedance amplifier based readout circuit is designed and implemented in 0.35µm CMOS fabrication technology, using operational amplifier for I-V and transmission gates are realized as shunt and series switch.

3.2.1 Theory of operation

The proposed switched capacitor trans-impedance amplifier shown in Figure 3-3 is required to convert the current produced by the micro-needle glucose sensor in three different boundary scenarios, which are Hypoglycemia (below 4mM), Euglycemia (4mM-7mM) and hyperglycemia (above 7mM) to corresponding voltage. The output voltage is a function of the amplifier gain.

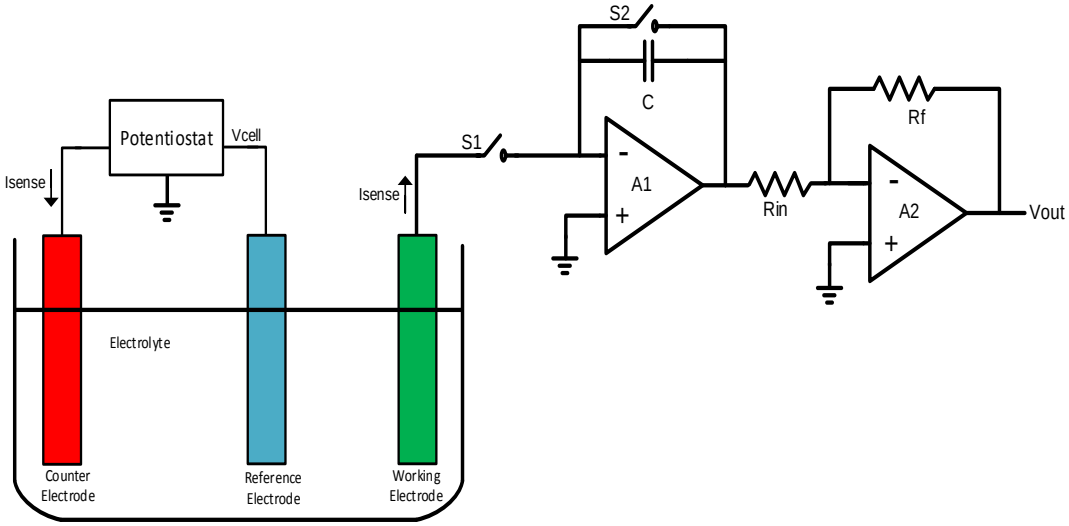

Figure 3-3 Switch capacitor based trans-impedance amplifier system

It works based on charge integration principle. As presented in the previous chapters the reference electrode (RE) and counter electrode (CE) are connected to the potentiostat. The reaction to sense glucose concentration occurs at working electrode (WE) causing a current I_{sense} to flow from potentiostat from counter electrode and out of the

working electrode. Then the sensor current I_{sense} is converted to corresponding output voltage V_{out} which is a function of gain of the switched capacitor trans-impedance amplifier. The voltage output from the switched capacitor has inverse phase dependence to the direction of current I_{sense}, therefore an inverting amplifier of gain 1 is implemented in the second stage to correct the phase.

Working principle:

The switched capacitor trans-impedance amplifier shown in Figure 3-4 operates in two phases. Phase 1 samples the input current onto a holding capacitor and in phase 2 the charge accumulated due to the sampled current is reset or cleared.

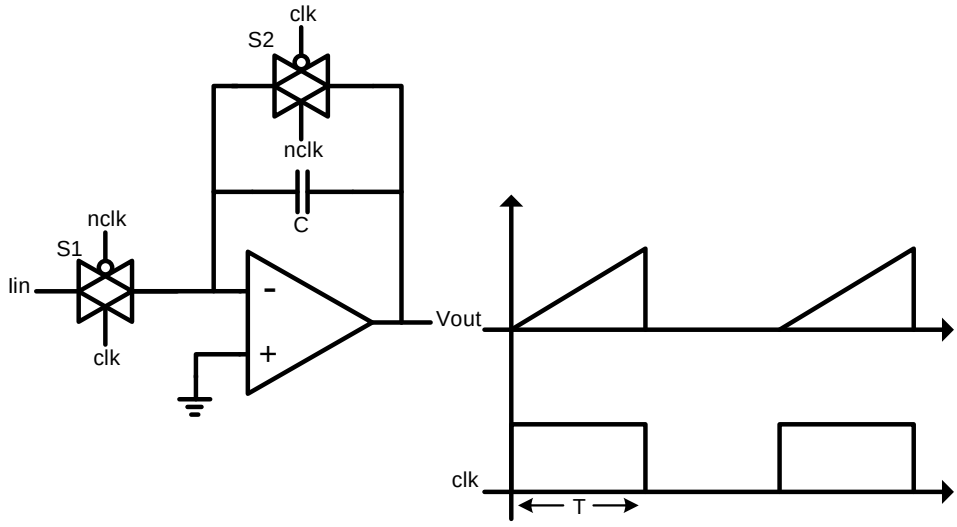

Figure 3-4 Switch capacitor based trans-impedance amplifier

The governing equations for switched capacitor amplifiers that define Q charge stored by the sampling capacitor C to obtain a voltage V is given by:

$$V = \frac{Q}{C} \tag{3.1}$$

And from the conservation of electric charge, as expressed by the charge-continuity equation. The charge transferred between initial time t_i and final time t_f is given by:

$$Q = \int_{t_i}^{t_f} I \, dt \tag{3.2}$$

In steady state, equation 3.2 can be re-written as:

$$Q = I \, . T \tag{3.3}$$

Thus from equations 3.1 & 3.3, the golden equation for switched capacitor trans-impedance amplifier is obtained and is given by:

$$V_{out} = -\frac{I_{in}.T}{C} \tag{3.4}$$

Where V_{out} is the amplifier output voltage, I_{sense} is the glucose sensor current, T is the sampling time and C is holding or gain capacitor.

The series switch S_1 control signal samples the sensor current I_{sense}, and allows it to charge the gain or holding capacitor, C to the output voltage given by equation 3.4. Then the shunt switch S2 resets the charged gain capacitor, C to its initial condition by shunting the capacitor. This prepares the capacitor to sample the sensor current I_{sense} during the sampling phase.

Also, equation 3.4 readily shows that gain of the switched capacitor amplifier can be dynamically controlled by varying the width of switch timing signal.

3.2.2 Operational amplifier design & analysis

The operational amplifier should have high gain to reduce the gain error due to feedback. In this work a folded cascode op-amp architectire as shown in Figure 3-5, as it provides relatively larger output swing while providing equally large gain as the telescopic

op-amps [34]. Large output swing is required to measure the full current range of the micro-needle glucose sensor.

This op-amp is a differential-to-single ended type with NMOS devices at the input. Due to the fact that their higher mobility the NMOS devices at the input offer higher gain and lower noise. The gain expression of this folded cascode op-amp is given by:

$$A_v \approx g_{m1}\left(\left[(g_{m6}+g_{mb6})r_{o6}(r_{o2} \parallel r_{o4})\right] \parallel \left[(g_{m8}+g_{mb8})r_{o8}.r_{o10}\right]\right) \tag{3.5}$$

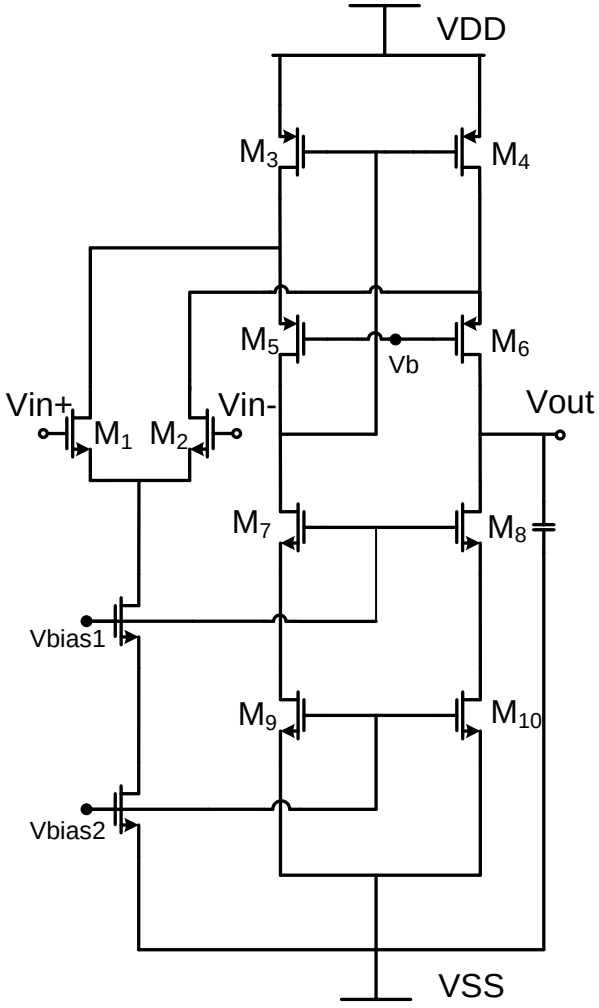

Figure 3-5 Folded cascode operational amplifier schematic

A strong biasing scheme is holds the key to the attractive properties the operational amplifier has to offer. Thus a high swing cascode current mirror shown in Figure 3-6 is implemented in this work.

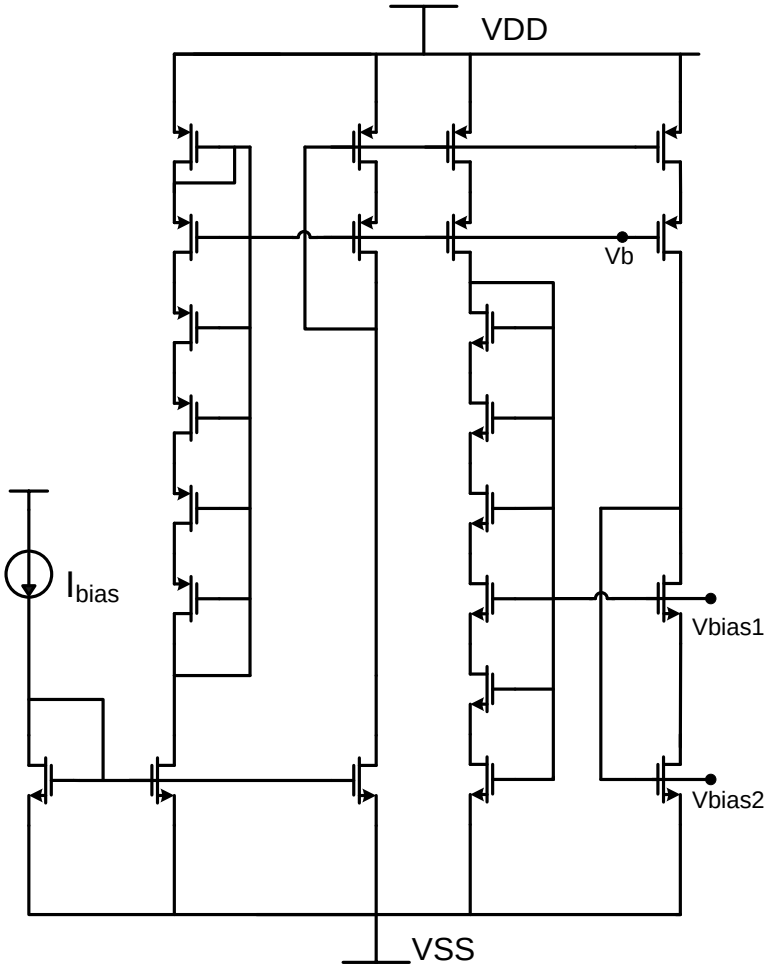

Figure 3-6 High swing casode current mirror for biasing

This is a modified Sooch cascode current mirror. The MOS transistors sourcing or sinking current are minimally biased to operate them at the edge of active region while the cascode MOS transistors are in saturation [35]. Thereby reducing the voltage headroom consumption by at least one threshold voltage. The minimum output voltage required to keep the device in saturation is given by:

$$V_{out(\min)} = 2V_{ov} = 2\sqrt{\frac{2.I_D}{\mu C_{ox} W/L}} \tag{3.6}$$

In order to minimize mismatch due to process variation, the device dimensions of MOS transistors in the high swing cascode current mirror and those of the operational amplifier are identical.

To obtain full output swing with a load, a large current-driving output stage is required. The output stage shown in Figure 3-7 is implemented in this work. This is a buffer amplifier with a typical two-stage differential-to-single ended circuit at its core [36]. This amplifier uses a negative feedback by connecting the output of the amplifier to its negative input. Therefore this output stage configuration has a very low output resistance and thereby allowing it to drive large loads. The output resistance of this amplifier is given by:

$$R_{out} = \left(\frac{1}{(g_{ds6} + g_{ds7})\left[1 + \left(\frac{g_{m2}}{2g_{m4}}\right)\left(\frac{g_{m6} + g_{m7}}{g_{ds6} + g_{ds7}}\right)\right]} \right) \tag{3.7}$$

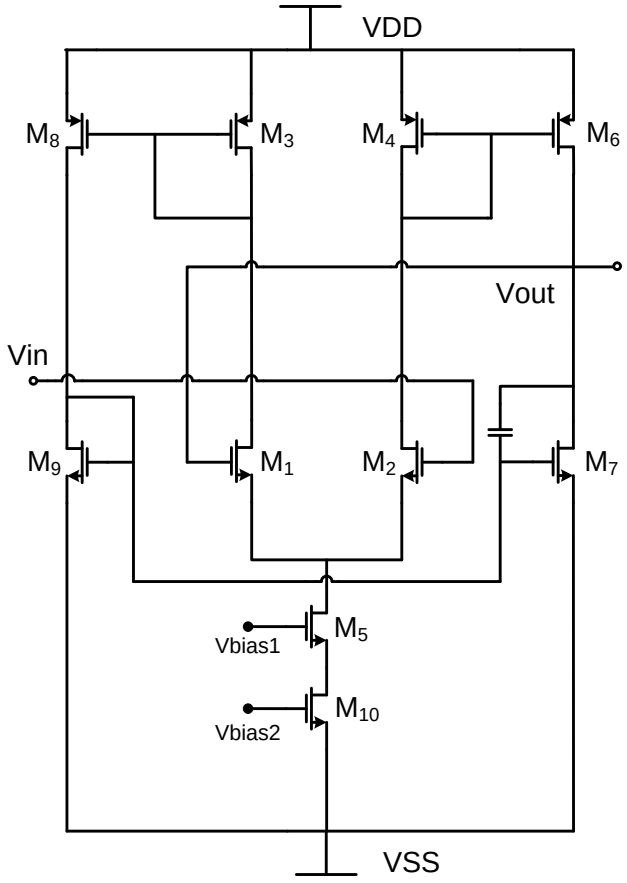

Figure 3-7 Output stage as buffer

Operational amplifier noise analysis

The main contributors of noise in an op-amp are due to the devices in the signal path. Thus, the noise contributed by the cascode devices can be neglected. Also, the noise generated by the tail current source devices is cancelled by the differential property of an op-amp. The resulting input referred noise spectrum of the op-amp can be expressed as:

$$\overline{v_{n,tot}^2} = 2\left[\overline{v_{n1}^2}(f) + \left(\frac{g_{m3}}{g_{m1}}\right)^2 \overline{v_n^3}(f) + \left(\frac{g_{m9}}{g_{m1}}\right)^2 \overline{v_9^2}(f)\right] \qquad (3.8)$$

where $\overline{v_{ni}^2}(f)$ is the noise spectral corresponding to the i[th] transistor due to both thermal and 1/f noise and g_{mi} is the transconductance of transistor M_i. Thus by substituting the thermal noise and 1/f noise of M1, M3, and M9 into the input voltage, yields noise spectral.

$$\overline{v_{n,tot}^2} = \frac{16kT}{3\sqrt{2\mu_n C_{ox}\left(W/L\right)_1 I_{DS1}}}\left(1+\sqrt{\frac{2\mu_p\left(W/L\right)_3}{\mu_n\left(W/L\right)_1}}+\sqrt{\frac{\left(W/L\right)_9}{\left(W/L\right)_1}}\right) + \frac{2k_{fn}}{C_{ox}(WL)_1}\frac{\Delta f}{f}\left[1+\frac{2\mu_p k_{fp}}{\mu_n k_{fn}}\left(\frac{L_1}{L_3}\right)^2+\left(\frac{L_1}{L_9}\right)^2\right] \quad (3.9)$$

From equation 3.9, by increasing W/L for the input devices and increasing the tail current will decrease the thermal noise. As $\mu_n > \mu_p$, the amplifier with NMOS inputs has lower thermal noise than the one with PMOS input devices. The noise contributed by the output stage is:

$$\overline{\mathrm{v_{n,tot}^2}} = \frac{16\mathrm{kT}}{3}\frac{1}{\mathrm{g_{m1}^2}}\left[\mathrm{g_{m1}}+\mathrm{g_{m3}}+\frac{\mathrm{g_{m8}}+\mathrm{g_{m9}}}{\mathrm{g_{m8}^2}\left(\mathrm{r_{01}}\|\,\mathrm{r_{03}}\right)^2}\right] \quad (3.10)$$

$$\approx \frac{16\mathrm{kT}}{3\sqrt{2\mu_\mathrm{n}\mathrm{C_{ox}}\left(\frac{\mathrm{W}}{\mathrm{L}}\right)_1\frac{\mathrm{I_{ss}}}{2}}}\left\{1+\sqrt{\frac{\mu_\mathrm{p}\left(\frac{\mathrm{W}}{\mathrm{L}}\right)_3}{\mu_\mathrm{n}\left(\frac{\mathrm{W}}{\mathrm{L}}\right)_1}}\right\} + \frac{2\mathrm{k_{fn}}}{\mathrm{C_{ox}(WL)_1}}\frac{1}{\mathrm{f}}\left[1+\frac{\mu_\mathrm{p}\mathrm{k_{fp}}}{\mu_\mathrm{n}\mathrm{k_{fn}}}\left(\frac{\mathrm{L_1}}{\mathrm{L_3}}\right)^2\right] \quad (3.11)$$

From equation 3.11, the noise decreases by decreasing the PMOS transistor width to length ratio and also by increasing the NMOS transistor width to length ratio.

The complete implementation of the operational amplifier is shown in Figure 3-8.

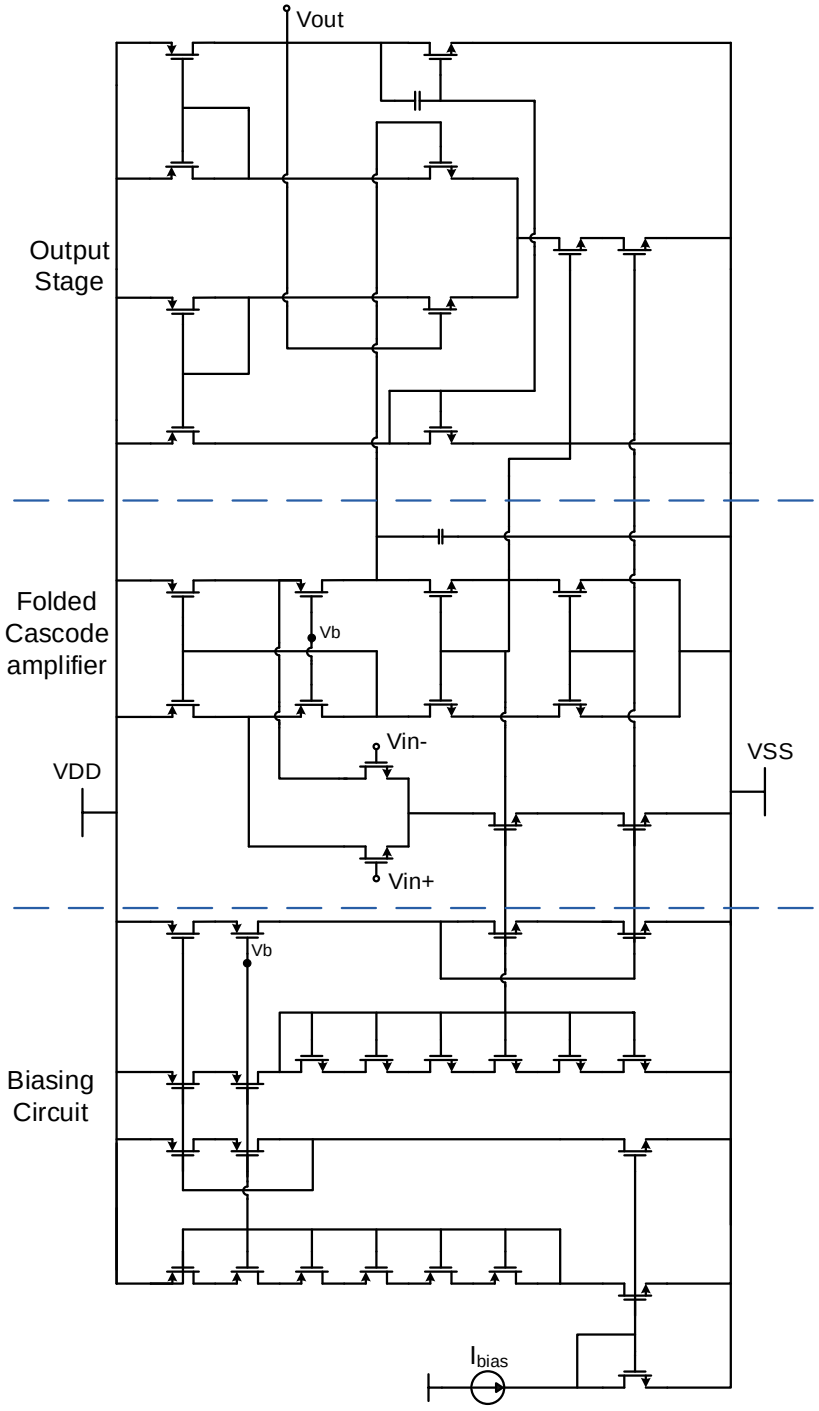

Figure 3-8 Complete op-amp schematic

Operational amplifier gain, phase margin and DC response simulations

The operational amplifier shown in Figure 3-8 achieves a gain of 118.3 dB and phase margin of 47.3 degrees with a load capacitance of 100fF. The plots of this simulation is shown in Figure 3-9.

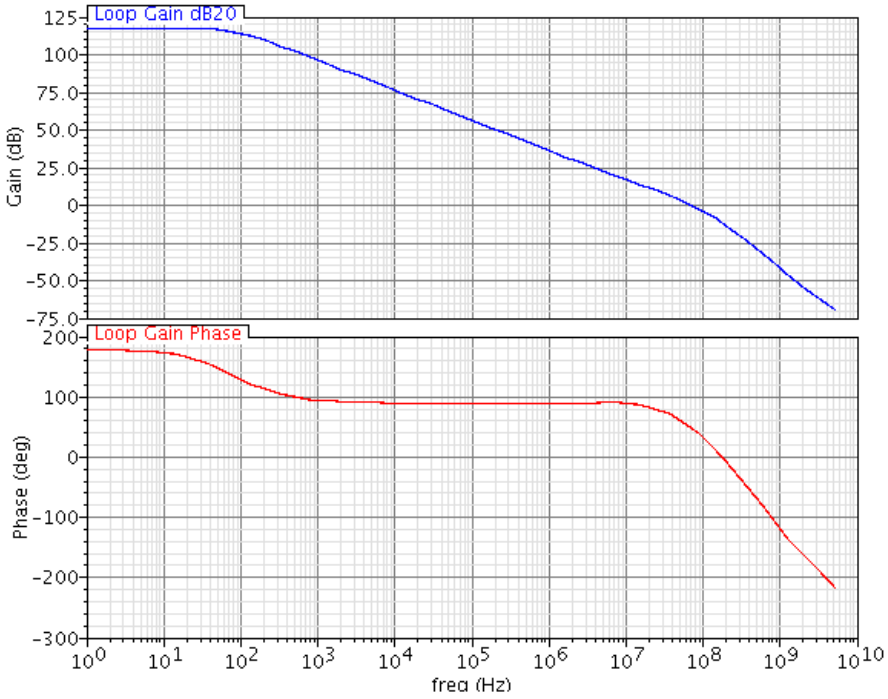

Figure 3-9 Operational amplifier gain and phase plots

In order to measure the output and input swing, the operational amplifier is simulated in a unity-gain buffer configuration, by connecting the output to inverting terminal. The non-inverting terminal is connected to a DC power supply which is swept from V_{DD} to V_{SS}. The output vs. input curve is shown in Figure 3-10. The output swing of 1.56 to -1.52V is achieved.

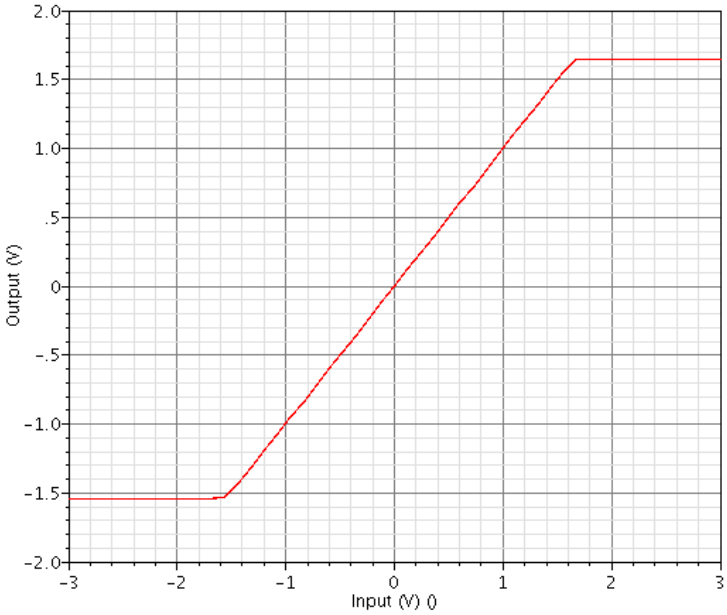

Figure 3-10 Operational amplifier DC response

3.2.3 Transmission gate design & analysis

The series switch S1 and shunt switch S2 in Figure 3-4 is implemented using a transmission gate. The schematic of transmission gate is as shown in Figure 3-11.

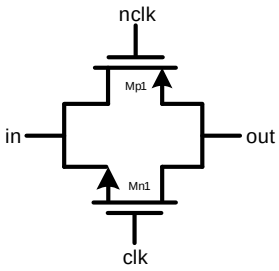

Figure 3-11 Transmission gate schematic

The philosophy for using a parallel combination of an NMOS and a PMOS device is due to the fact that an NMOS cannot pass a strong logic 1 voltage, while a PMOS cannot pass a strong logic 0 voltage. Thus by paralleling the two devices, the full voltage range

from V_{SS} to V_{DD} can be transmitted. The equivalent transmission gate resistance R_{TG} can be defined by [37]:

$$R_{TG} = \frac{V_{TG}}{I_{Dn} + I_{Dp}} \tag{3.12}$$

Since the devices are connected in parallel as shown in Figure 3-11, R_{TG} can also be obtained by:

$$R_{TG} = r_n || r_p \tag{3.13}$$

where, r_n is NMOS device resistance and r_p is PMOS device resistance.

Thus, R_{TG} is approximated obtained as PMOS device resistance while charging the capacitor [37]:

$$R_{TG} = \frac{2}{\mu_p C_{ox} \left(\frac{W}{L}\right)_p \left[2\left(V_{DD} - |V_{Tp}|\right) + V_{Tn}\right]} \tag{3.14}$$

where, μ_p is the mobility of charge carriers in PMOS device, C_{ox} is oxide capacitance of PMOS device, W and L are device dimensions of PMOS device, V_{Tp} is threshold voltage of PMOS device and V_{Tn} is the threshold voltage of NMOS device. R_{on} is in the range of 2.5kΩ - 870Ω and is strongly dependent on [34].

Transmission gate noise analysis

The two important intrinsic noise effects in MOS transistors are: thermal and flicker noise. Thermal motion of the charge carriers in the channel of the device causes random fluctuation in the drain current by a small amount. The thermal noise of a device operating in triode region is given by [38]:

$$S_I = \frac{4kT}{R_{on}} \left[A^2/Hz\right] \tag{3.15}$$

where, k is the Boltzmann constant , $k = 1.38 * 10^{-23} J/K$, T is absolute temperature of the device in degrees Kelvin, and R_{on} is its on-resistance in ohms of a transmission gate and it is given by equation 3.14.

Flicker noise or $1/f$ noise is caused when charge carriers get trapped and later released as they move through the channel of the transistor. The power spectral density $S_{Id}(f)$ is derived from "*Hooge's bulk mobility fluctuation model"* [39]and is given by:

$$S_{Id}(f) = \frac{I_d^2 \alpha_H}{fWLN} \ [A^2/Hz] \tag{3.16}$$

where,α_H is Hooge's empirical parameter universal value of about $2 * 10^{-3}$, N is the total number of free carriers in the sample.

Transmission gate transient simulation

Transient analysis is performed on the transmission gate to ascertain its functionality at sampling frequencies of 200 Hz and 200 kHz is as shown in Figure 3-12 and Figure 3-13. A +1.25 V DC power supply is connected at the input and a 15kΩ resistive load is connected at the output. A 200 Hz sampling clock is applied to NMOS gate and an inverted phase clock is connected to PMOS gate of transmission gate in Figure 3-11. The output toggles between +1.16V and 0V at 200 Hz as shown in Figure 3-12. Similarly the transient analysis is performed at 200 kHz as shown in Figure 3-13 output toggles between +1.16V and 0V at 200 kHz. The transient analysis at both 200 Hz and 200 kHz are performed on post layout extracted netlist.

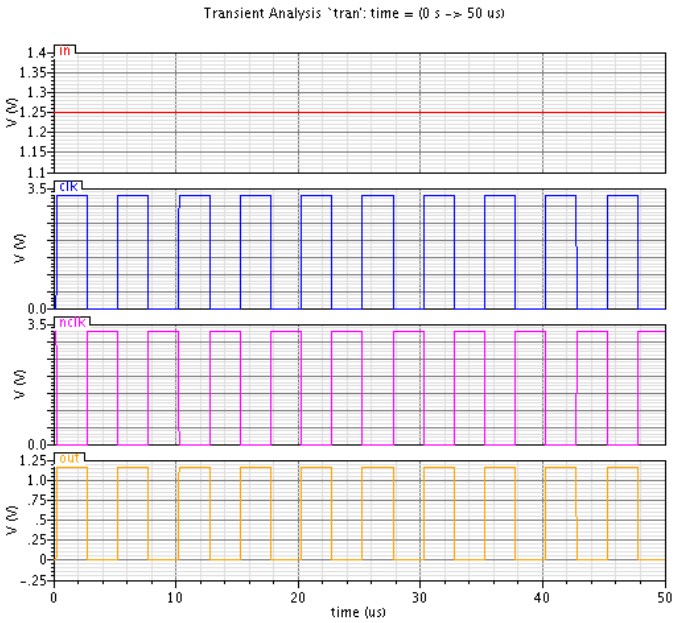

Figure 3-12 Transient response with 200 Hz clock and 15kΩ load

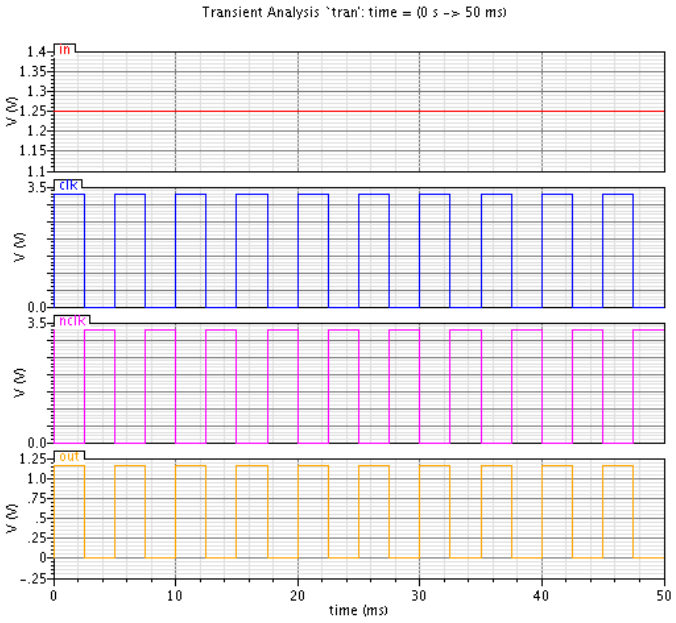

Figure 3-13 Transient response with 200 kHz clock and 15kΩ load

3.2.4 Switched capacitor trans-impedance amplifier analysis

Gain Analysis

The gain analysis of a switched capacitor trans-impedance is divided into two phases (a) sampling phase (b) reset phase as shown in Figure 3-14.

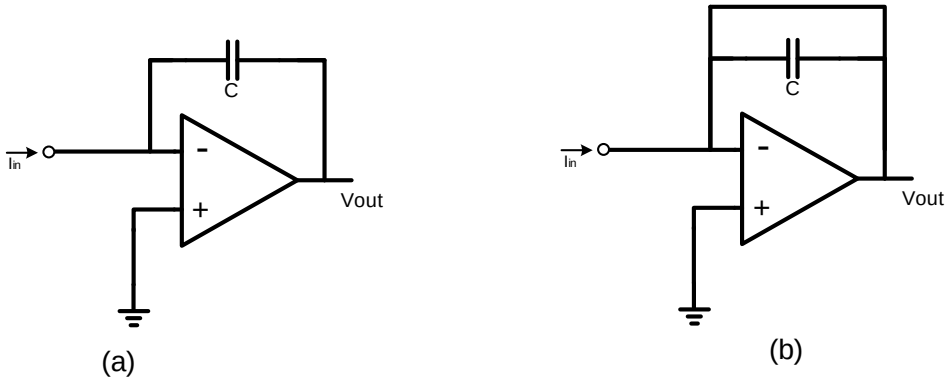

Figure 3-14 Gain analysis (a) sampling phase (b) reset phase

Reset phase

During the reset phase, operational amplifier functions as a non-inverting voltage follower and its gain is given by

$$\frac{Vout}{Vin} = 1 \tag{3.17}$$

where Vin is the voltage at non-inverting terminal and since it is connected to ground, Vin = 0V. Thus, Vout of this voltage follower is 0V.

Sampling phase

During the sampling phase, the operational amplifier functions as a charge integrator. Thus, integrated output voltage $V_{out}(t)$ during sampling time T can be represented as the convolution of the glucose sensor current and a rectangular time pulse given by equation 3.17:

$$V_{out}(t) = \frac{1}{C} \cdot I_{in}(t) * (u(t) - u(t-T)) \tag{3.18}$$

Laplace transform of equation 3.18 can be obtained as:

$$v_{out}(s) = \frac{1}{Cs} \cdot i_{in}(s).(1 - e^{-Ts}) \tag{3.19}$$

Thus, gain of switched capacitor trans-impedance amplifier in frequency domain is:

$$\frac{v_{out}(s)}{i_{in}(s)} = \frac{1}{Cs} \cdot (1 - e^{-Ts}) \tag{3.20}$$

By applying inverse Laplace transform to equation 3.20, gain in time domain is

$$\frac{V_{out}(t)}{I_{in}(t)} = \frac{T}{C} \tag{3.21}$$

Thus, from equation 3.21 the DC value of Vout for DC input Iin is:

$$V_{out} = I_{in} \cdot \frac{T}{C} \tag{3.22}$$

where I_{in} is the sensor current, T is sampling time and C is value of holding capacitor.

Noise Analysis

The flicker and thermal noise, are dominant noise mechanisms in a switched capacitor contributed by operational amplifier noise e_M^2 is given by:

$$e_M^2\,[V^2/Hz] \approx \frac{16kT}{3\sqrt{2\mu_n C_{ox}\left(\frac{W}{L}\right)_1 \frac{I_{ss}}{2}}}\left\{1 + \sqrt{\frac{\mu_p\left(\frac{W}{L}\right)_3}{\mu_n\left(\frac{W}{L}\right)_1}}\right\} + \frac{2k_{fn}}{C_{ox}(WL)_1}\frac{1}{f}\left[1 + \frac{\mu_p k_{fp}}{\mu_n k_{fn}}\left(\frac{L_1}{L_3}\right)^2\right] \tag{3.23}$$

and the thermal noise and flicker noise due to transmission gate is given by:

$$S_{thermal\_TG} = \frac{4kT}{R_{on}} \ [A^2/Hz] \tag{3.24}$$

$$S_{Id\_flicker\_TG}(f) = \frac{I_d^2 \alpha_H}{fWLN} \ [A^2/Hz] \tag{3.25}$$

The noise analysis of switched capacitor system is different from a continuous time system because the integration time is not infinite. Thus noise analysis of the system has to be done separately for each of the operating phases namely sampling and reset. The noise contribution of the first stage is the most dominant source of noise in a multi-stage amplification system.

In the reset phase as shown in Figure 3-15, the holding capacitor's terminals are shunted, configuring the op-amp as a voltage follower.

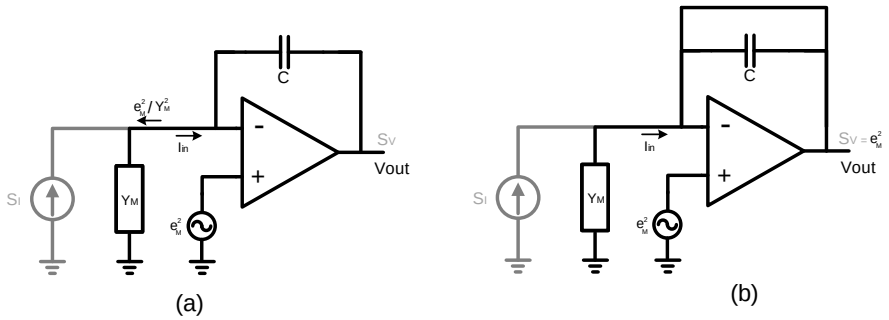

Figure 3-15 Noise model (a) sampling phase (b) reset phase.

Thus, the only noise if from the op-amp and the voltage power spectral density of the output equivalent voltage noise, $S_{V,rst}$ is

$$S_{V,rst} = e_M^2 \ [V^2/Hz] \tag{3.26}$$

where e_M is the input referred noise of the op-amp. The equivalent input referred current noise, $S_{I,rst}$ in terms of the feedback capacitance C and the sampling time T is

$$S_{I,rst} = S_{V,rst} \cdot \left(\frac{C}{T}\right)^2 \tag{3.27}$$

$$S_{I,rst} = e_M^2 \cdot \left(\frac{C}{T}\right)^2 \ [A^2/Hz] \tag{3.28}$$

Post reset phase, the holding capacitor has an initial charge of zero. During the sampling phase, the holding capacitor samples the input current, and the integrated output voltage during sampling time T can be represented as the convolution of the glucose sensor current and a rectangular time pulse, following from [40]

$$V_{out}(t) = \frac{1}{C} \cdot i(t) * (u(t) - u(t-T)) \tag{3.29}$$

where i(t) is an input current and u(t) is the unit step function. The Laplace transform of the expression of equation 3.29 can be obtained as

$$L\left(\frac{1}{C} \cdot i(t) * \big(u(t) - u(t-T)\big)\right) = \frac{1}{Cs} \cdot i(s).(1 - e^{-Ts}) \tag{3.30}$$

where L(i(t)) = i(s).

From equation 3.29, the power spectral density of the output, S_V is calculated as

$$S_{V,sample} = e_M^2 \left(\frac{Y_M}{C.s} \cdot (1 - e^{-T.s})\right)^2 \ [V^2/Hz] \tag{3.31}$$

where Y_M is the admittance of the equivalent input circuit, which includes the inverse of resistance of the series switch given by equation 3.32:

$$R_{on} = \frac{1}{\mu C_{ox} \frac{W}{L} (V_{DD} - V_{in} - V_{TH})} \tag{3.32}$$

where, μ is the mobility of charge carriers, C_{ox} is oxide capacitance, W and L are device dimensions. R_{on} is in the range of 2.5kΩ - 870Ω and is strongly dependent on [34].

Thus, from the above equations, the input referred current noise during sampling is $S_{I,sample}$ is:

$$S_{I,sample} = S_{V,sample} \cdot \left(\frac{C}{T}\right)^2 \tag{3.33}$$

$$S_{I,sample} = e_M^2 \cdot \left(\frac{Y_M}{T.s} \cdot (1 - e^{-T.s})\right)^2 \ [A^2/Hz] \tag{3.34}$$

The total input referred noise, S_T, in a capacitive feedback measurement system is the sum of the noise current power spectral densities of the rest phase and the sampling phase including the noise of the input equivalent circuit [18]:

$$S_T = S_M + S_{I,rst} + S_{I,sample} \tag{3.35}$$

where S_M is the noise of equivalent input circuit

The main source of S_M is from MOSFET based sampling switch due to thermal motion of the charge carriers in the channel of the device causing random fluctuations in the drain current. When operated as switch the MOS transistor operates in triode region, thus noise can be represented by a current source in parallel to the channel current [38]. The power spectral density (PSD) of this current source is white and is given by equation 3.36:

$$S_I = \frac{4kT}{R_{on}} \ [A^2/Hz] \tag{3.36}$$

where, k is the Boltzmann constant, , T is absolute temperature of the device in degrees Kelvin, and R_{on} is on-resistance in ohms of a MOS transistor and is given by equation 3.32.

In the low frequencies the noise from the input equivalent circuit has a large effect while at higher frequencies the contribution from the sampling phase is dominant [18].

3.3 Simulation results

The post layout extracted netlist is simulated at 200 kHz clock with only on chip capacitor of 100pF and at 200 Hz clock with external capacitor of 100nF for the input current range of 2µA-30µA obtained from the output current vs. glucose concentration plot of the microneedle glucose sensor as shown in Figure 3-2.

3.3.1 CMOS IC layout of proposed circuit

The circuit for the proposed architecture is fabricated in 0.35µm CMOS technology process. Circuit design and custom layout is done using Cadence tool suite. Assura is used to complete the custom design flow by doing design rule check, layout versus schematic check and parasitic RC extraction of the layout. The PAD size provided for this design along with the seal ring is 81.4µm x 81.4 µm. Figure 3-16 shows the full chip layout with the layout of proposed architecture marked in red. The area of the proposed architecture is 160 µm x 157 µm. The area of 100pF on chip capacitance is 900 µm x 50 µm.

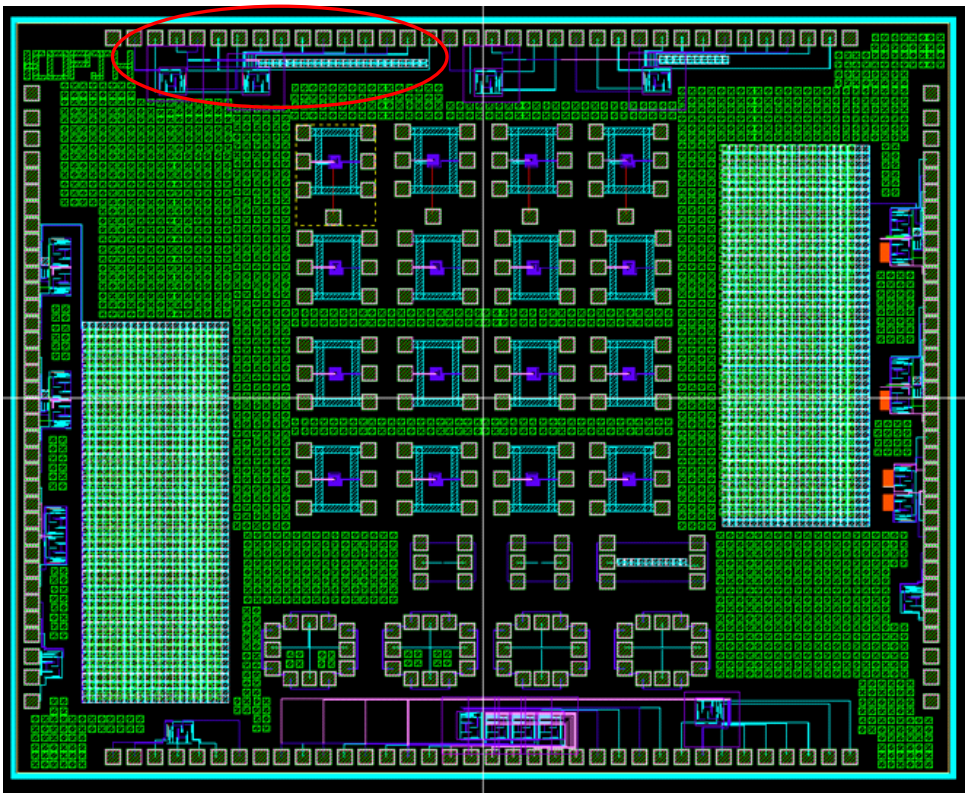

Figure 3-16 Full chip layout

Figure 3-17 shows the zoomed layout capture of the proposed architecture.

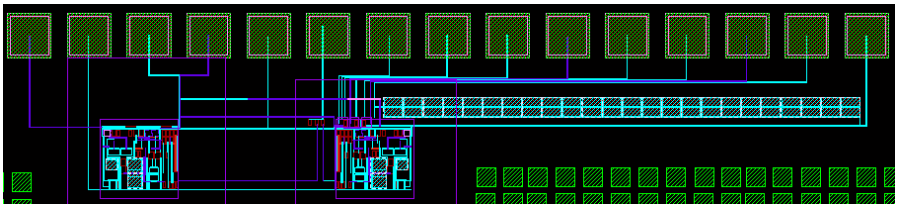

Figure 3-17 Zoomed layout of proposed architecture

3.3.2 Simulation results with 100pF on chip capacitor and 200 kHz sampling clock

The post extracted simulated response of proposed circuit for input current range from 2µA to 30µA is shown in Figure 3-19 to Figure 3-30 and the corresponding output varies from 45mV to 664mV.

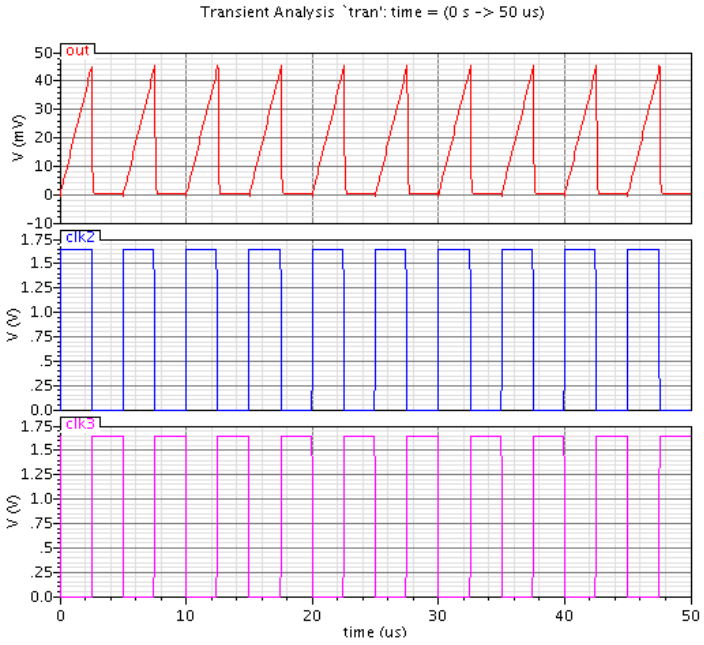

Figure 3-18 Post extraction netlist simulation with 200 kHz clock @ Iin = 2µA

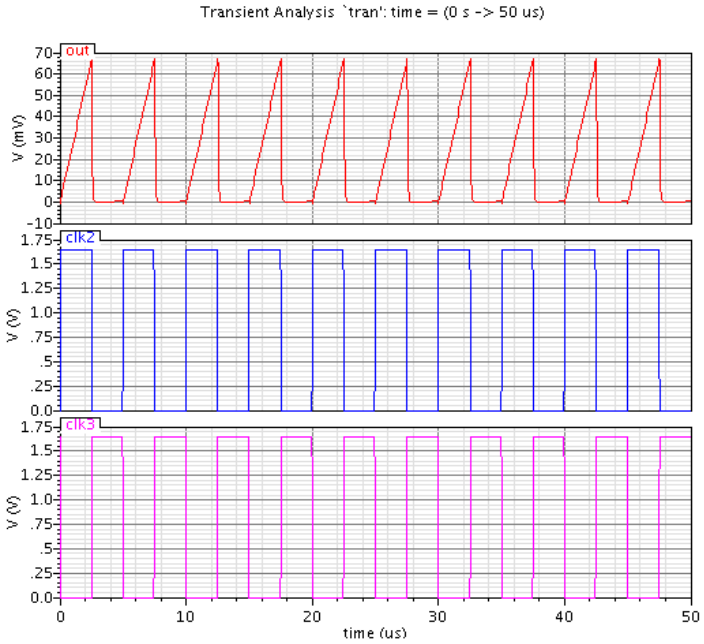

Figure 3-19 Post extraction netlist simulation with 200 kHz clock @ Iin = 3µA

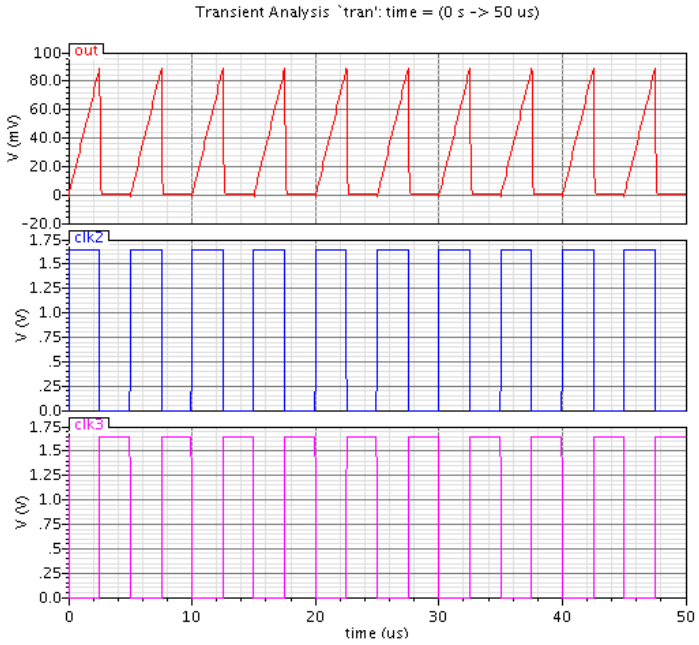

Figure 3-20 Post extraction netlist simulation with 200 kHz clock @ Iin = 4µA

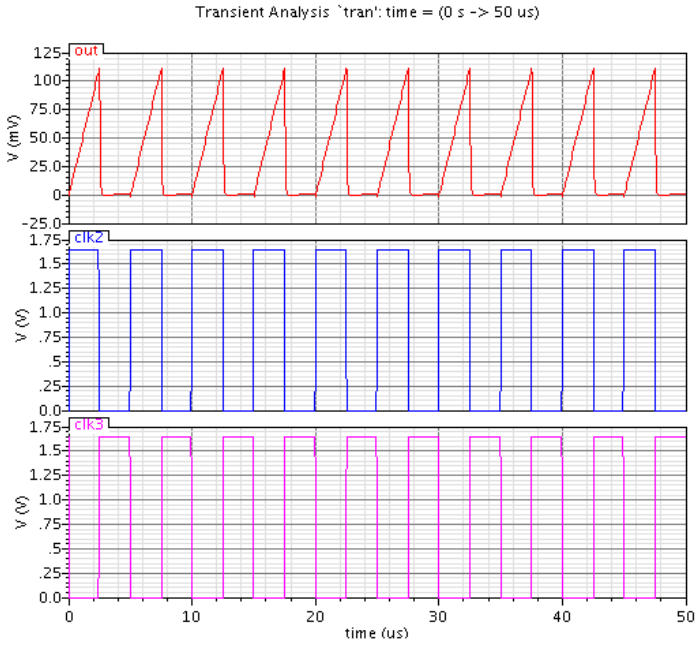

Figure 3-21 Post extraction netlist simulation with 200 kHz clock @ Iin = 5µA

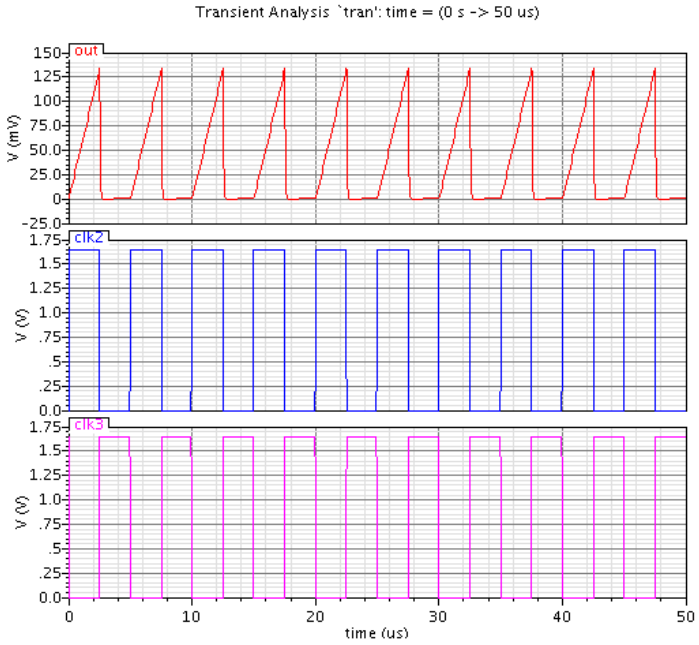

Figure 3-22 Post extraction netlist simulation with 200 kHz clock @ Iin = 6µA

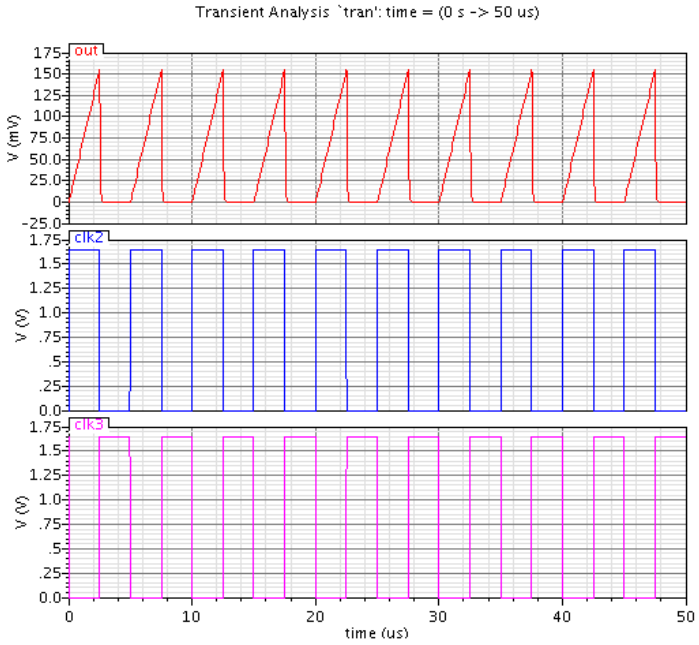

Figure 3-23 Post extraction netlist simulation with 200 kHz clock @ Iin = 7µA

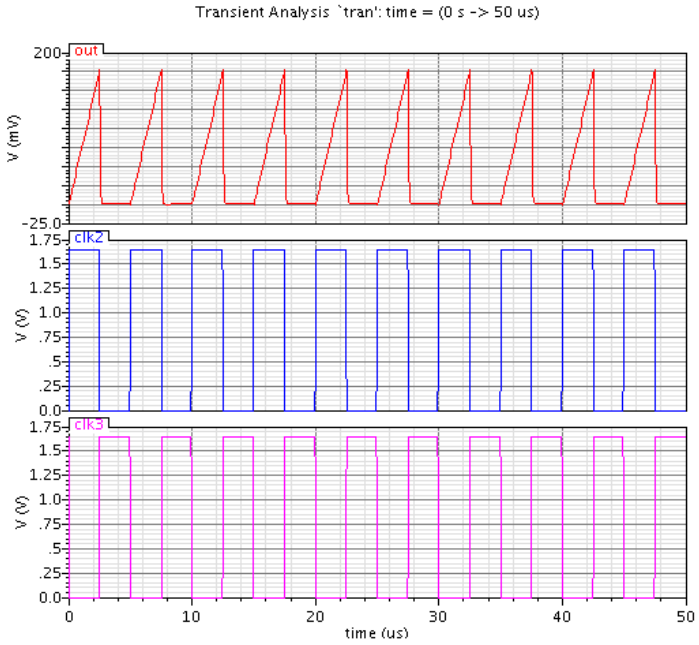

Figure 3-24 Post extraction netlist simulation with 200 kHz clock @ Iin = 8µA

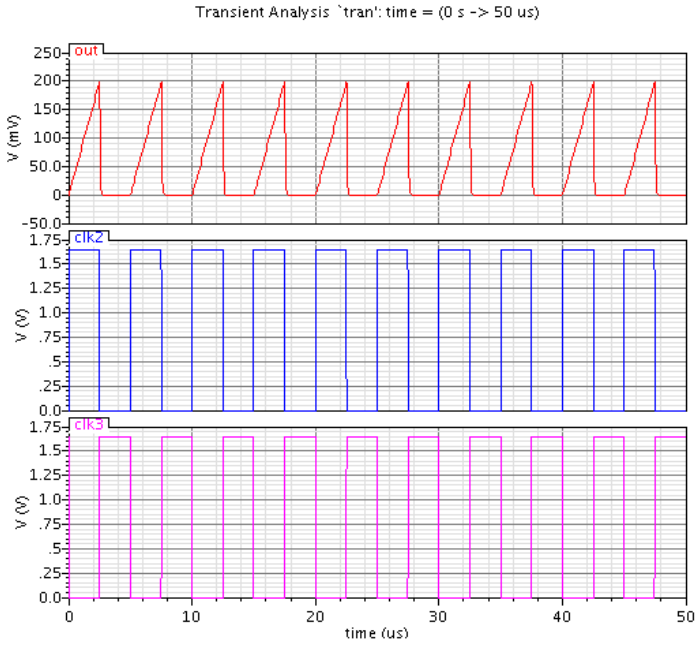

Figure 3-25 Post extraction netlist simulation with 200 kHz clock @ Iin = 9µA

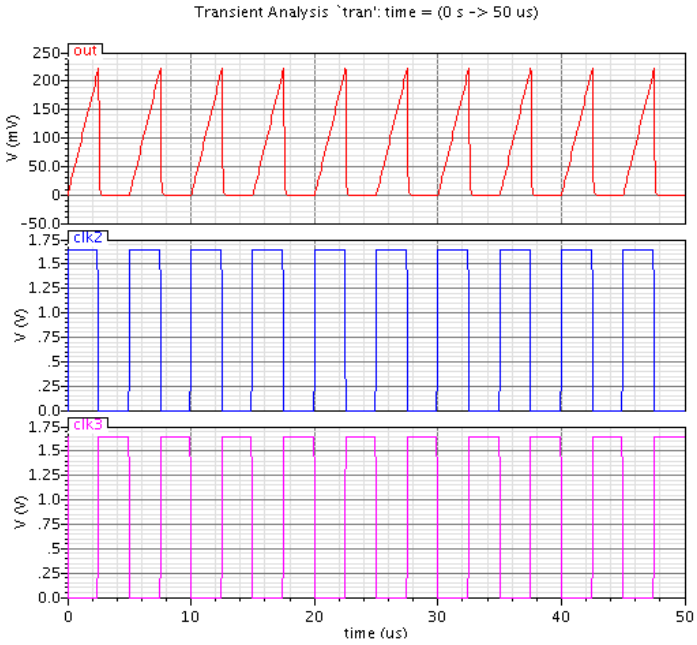

Figure 3-26 Post extraction netlist simulation with 200 kHz clock @ Iin = 10µA

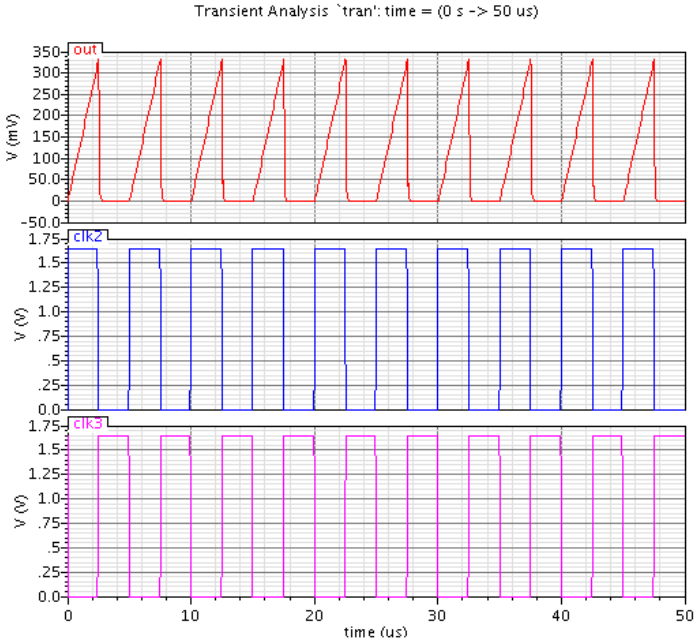

Figure 3-27 Post extraction netlist simulation with 200 kHz clock @ Iin = 15µA

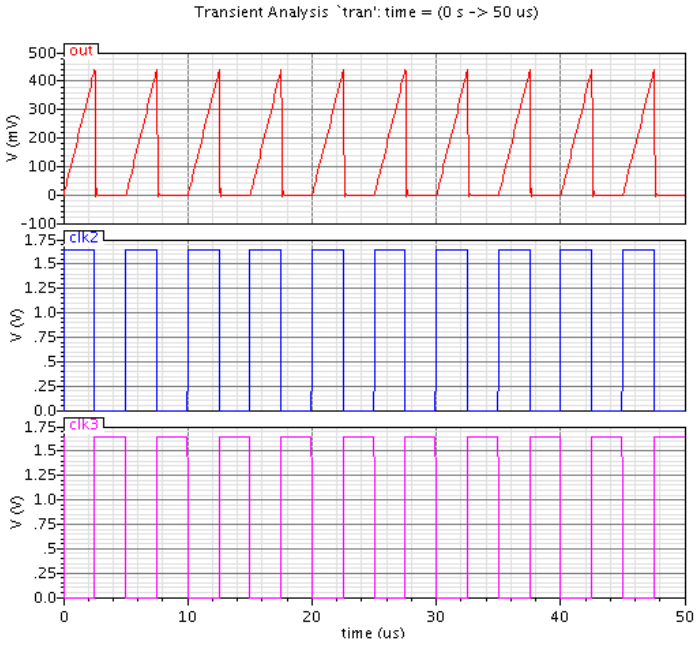

Figure 3-28 Post extraction netlist simulation with 200 kHz clock @ Iin = 20µA

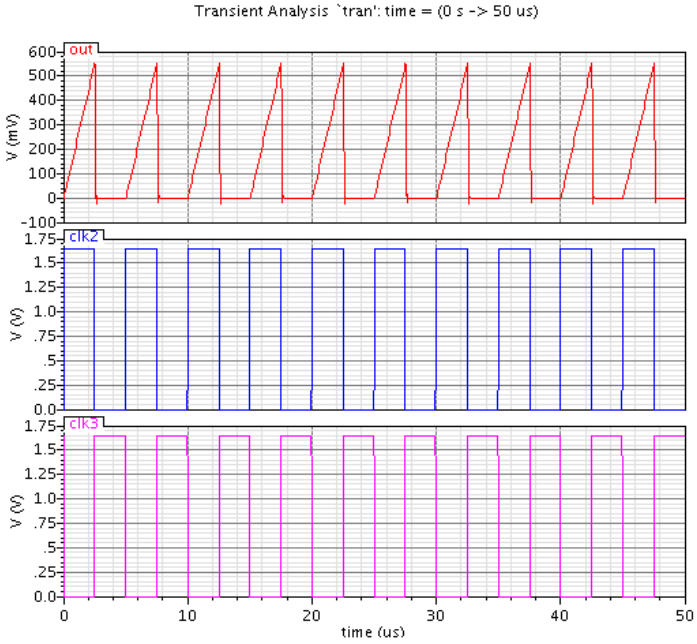

Figure 3-29 Post extraction netlist simulation with 200 kHz clock @ Iin = 25µA

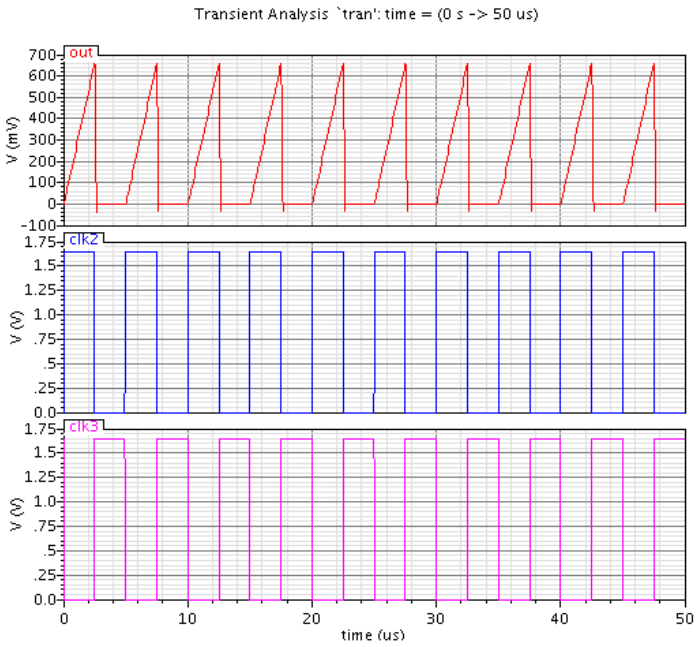

Figure 3-30 Post extraction netlist simulation with 200 kHz clock @ Iin = 30µA

The readings of all the measurements shown from Figure 3-19 to 3-20 is tabulated in Table 3-3. The minimum glucose level that can be measured is 1mM, the corresponding sensor current is 2µA and maximum is 15mM corresponding sensor current is 30 µA.

Table 3-3 Post extraction simulation results with 200 kHz clock

Glucose concentration (mM)	Electrode Resistance (kΩ)	Iin (µA)	Simulated Output (mV)	Gain (kΩ)
1	250	2	45.05	22
1.5	166.6	3	66.98	22
2	125	4	88.491	22
2.5	100	5	110.79	22
3	83.33	6	132.69	22

Table 3.3—*Continued*

Glucose concentration (mM)	Electrode Resistance (kΩ)	Iin (μA)	Simulated Output (mV)	Gain (kΩ)
3.5	71.428	7	156.04	22
4	62.5	8	177.93	22
4.5	55.5	9	199.1	22
5	50	10	222.39	22
7.5	33.3	15	331.4	22
10	25	20	441.56	22
12.5	20	25	553.59	22
15	16.66	30	663.43	22

Output voltage vs. sensor current at sampling frequency of 200 kHz is plotted in Figure 3-31. The resolution of the proposed circuit is 22mV/ μA which indicates that for every 1 μA change in input current the output voltage changes by 22mV.

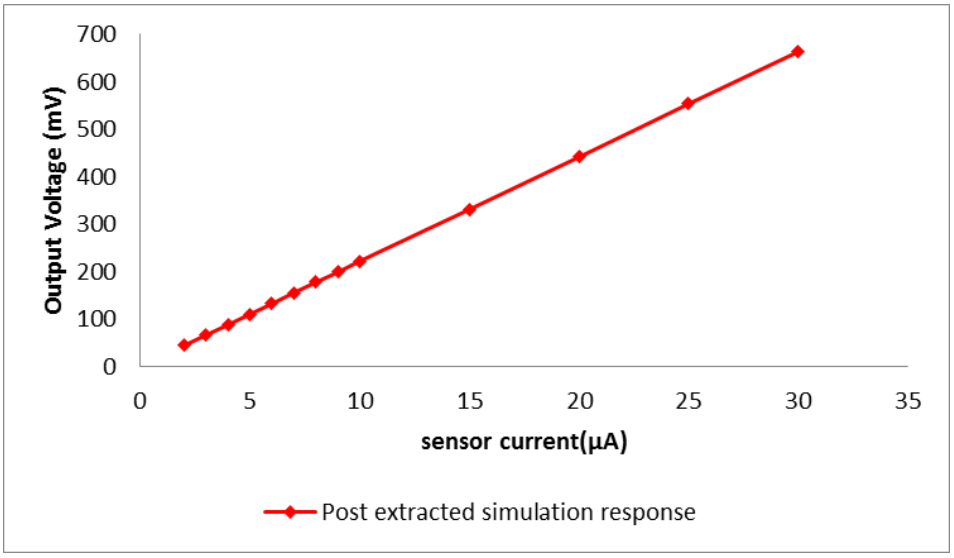

Figure 3-31 Sensor current vs. output voltage with 200 kHz clock

Output voltage vs. glucose concentration at sampling frequency of 200 kHz is plotted in Figure 3-32. The simulated trans-impedance gain of the proposed switched capacitor trans-impedance amplifier circuits is 22 kΩ. Thus at 1mM glucose concentration output voltage is 45.05mV and at 15mM glucose concentration output voltage is 663.43mV.

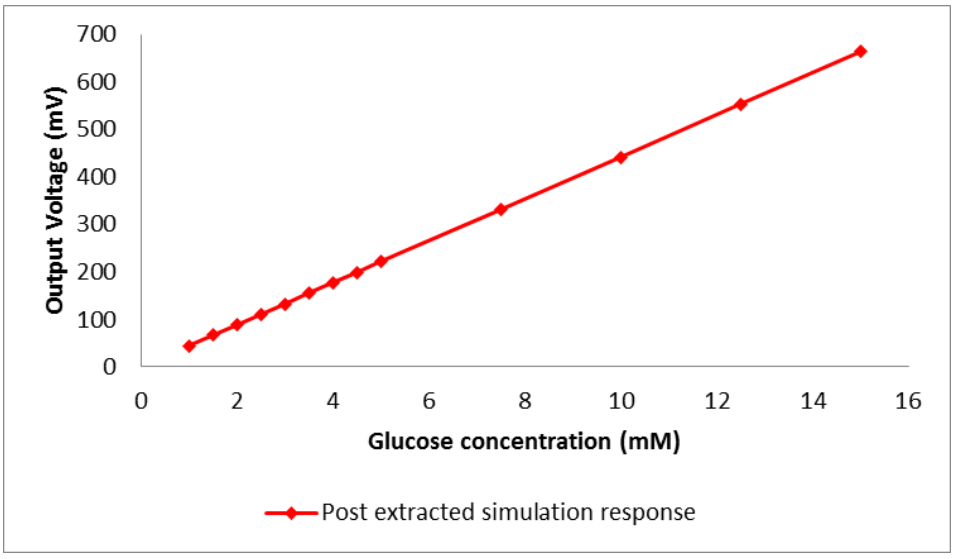

Figure 3-32 Glucose concentration vs. output voltage with 200 kHz clock

The noise simulation response of the proposed circuit with 200 kHz clock is obtained from 10Hz to 100MHz is shown in Figure 3-32. The total output integrated rms noise in the 10Hz to 100MHz bandwidth is 953.442µVrms. The power consumed by the system at 200 kHz is 3.05mW. Table 3-4 is the summary of post extracted simulation results with 200 kHz sampling clock.

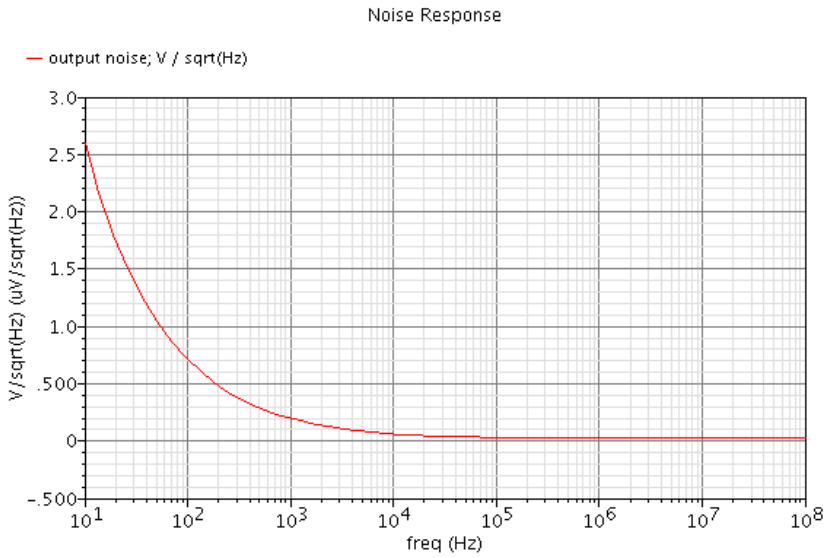

Figure 3-33 Proposed circuit noise simulation with 200 kHz clock

Table 3-4 Summary of post extraction simulation results with 200 kHz clock

Parameter	**Post extraction simulation**
Input current	2µA – 30µA
Output voltage	45mV - 664mV
Total integrated noise	953.442µVrms
System power dissipation	3.05mW

3.3.3 Simulation results with 100nF external capacitor and 200 Hz sampling clock

The post extracted simulated response of proposed circuit for input current range from 2µA to 30µA is shown in Figure 3-34 to Figure 3-46 and the corresponding output varies from 45mV to 664mV.

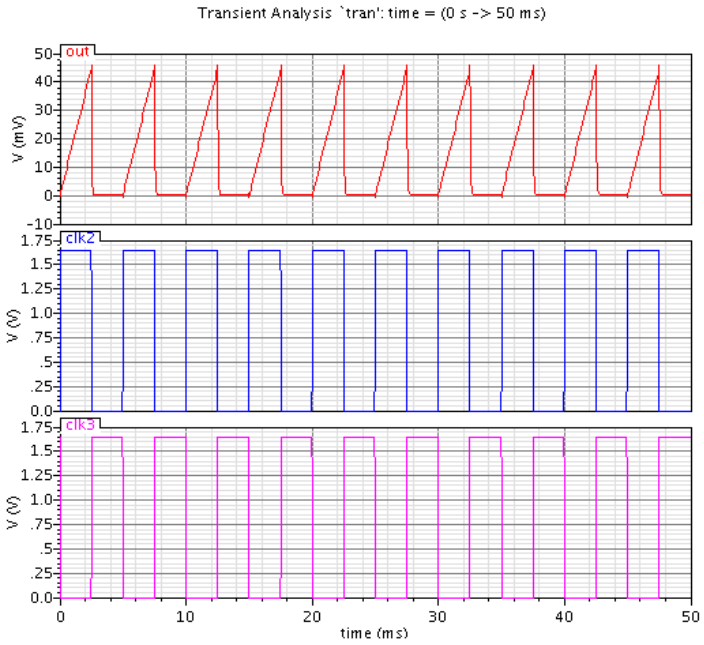

Figure 3-34 Post extraction netlist simulation with 200 Hz clock @ Iin = 2µA

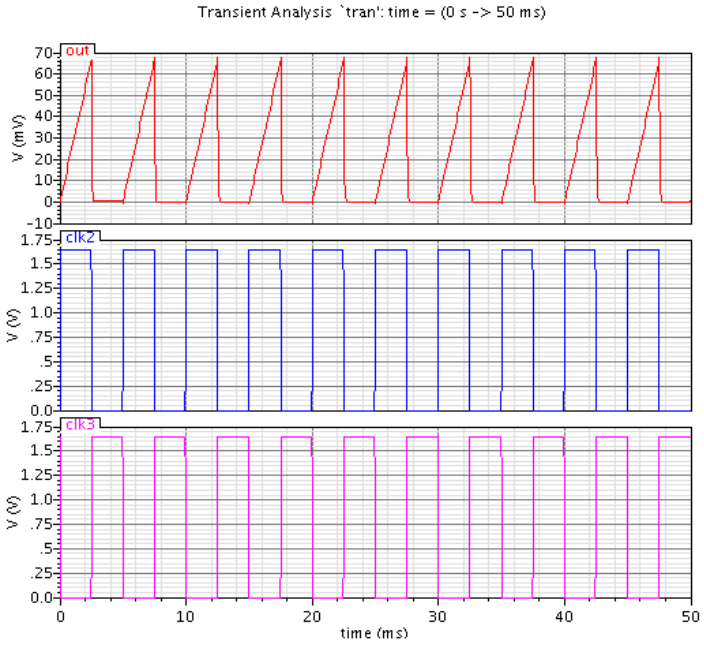

Figure 3-35 Post extraction netlist simulation with 200 Hz clock @ Iin = 3µA

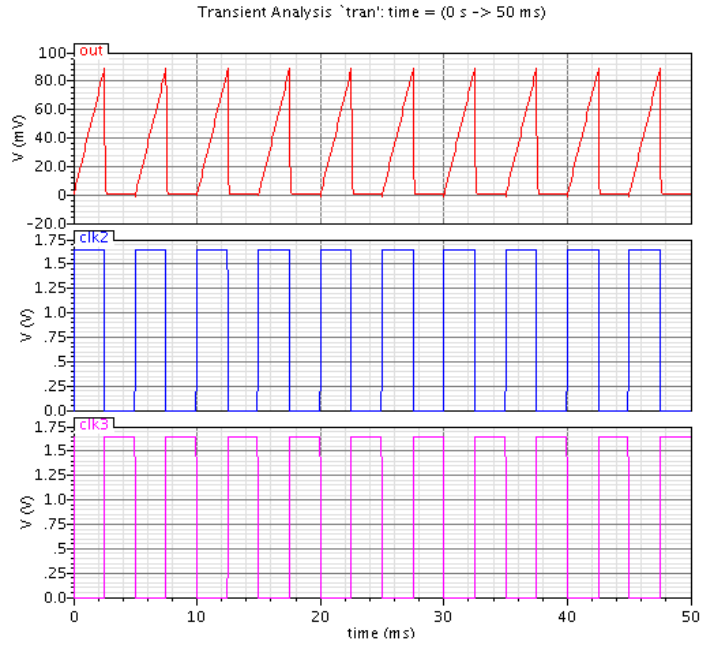

Figure 3-36 Post extraction netlist simulation with 200 Hz clock @ Iin = 4µA

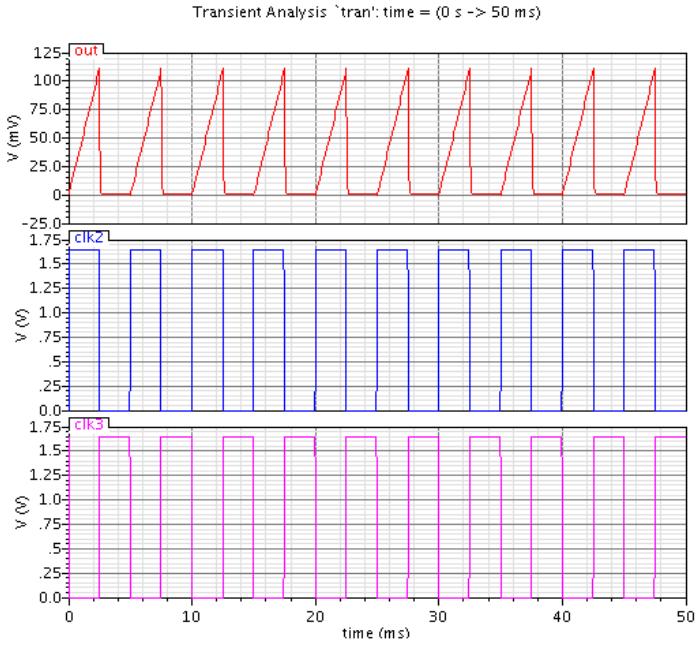

Figure 3-37 Post extraction netlist simulation with 200 Hz clock @ Iin = 5µA

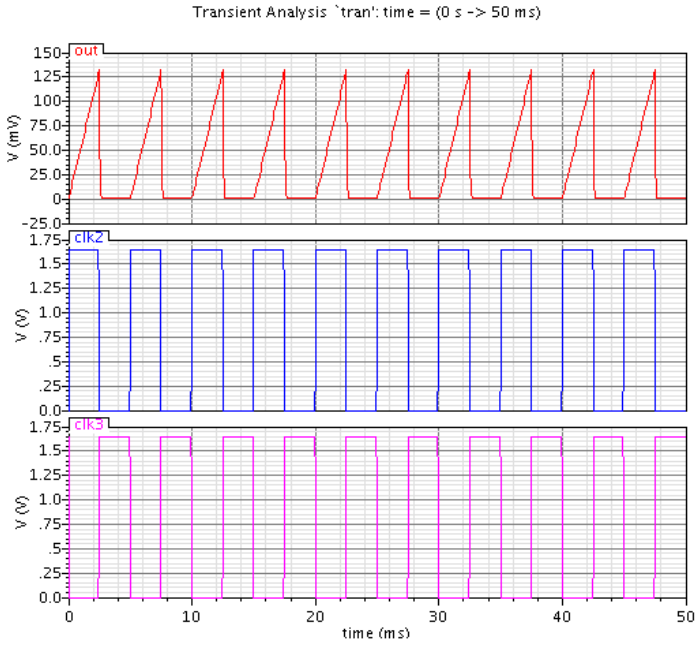

Figure 3-38 Post extraction netlist simulation with 200 Hz clock @ Iin = 6µA

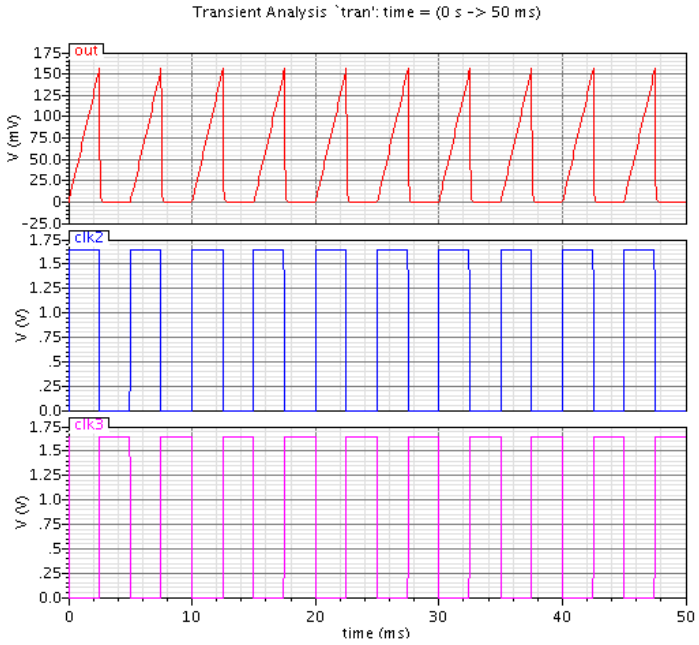

Figure 3-39 Post extraction netlist simulation with 200 Hz clock @ Iin = 7µA

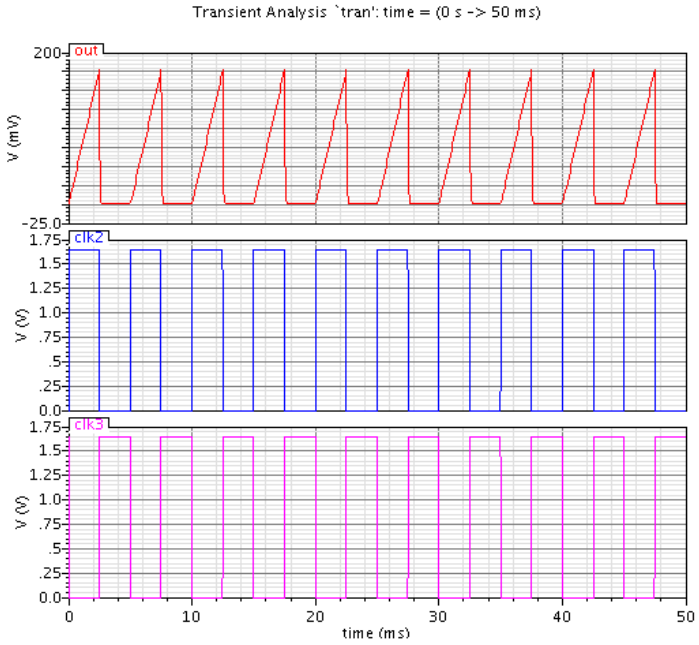

Figure 3-40 Post extraction netlist simulation with 200 Hz clock @ Iin = 8µA

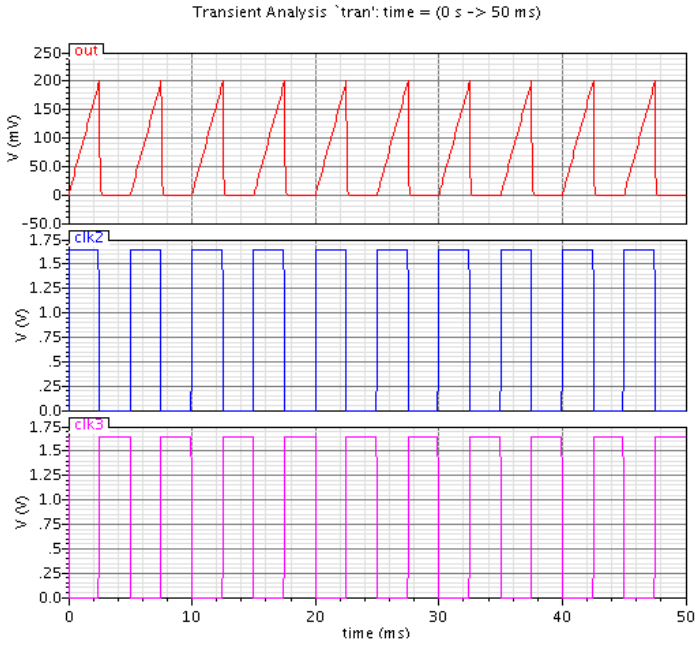

Figure 3-41 Post extraction netlist simulation with 200 Hz clock @ Iin = 9µA

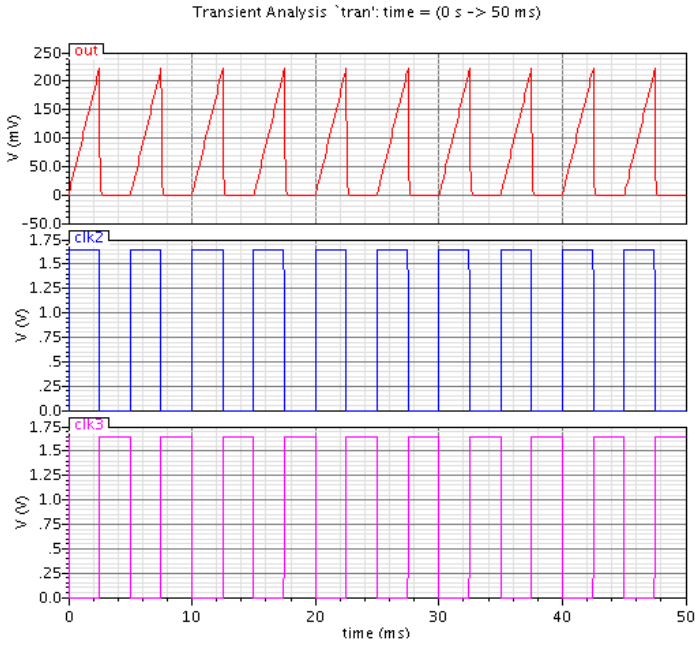

Figure 3-42 Post extraction netlist simulation with 200 Hz clock @ Iin = 10µA

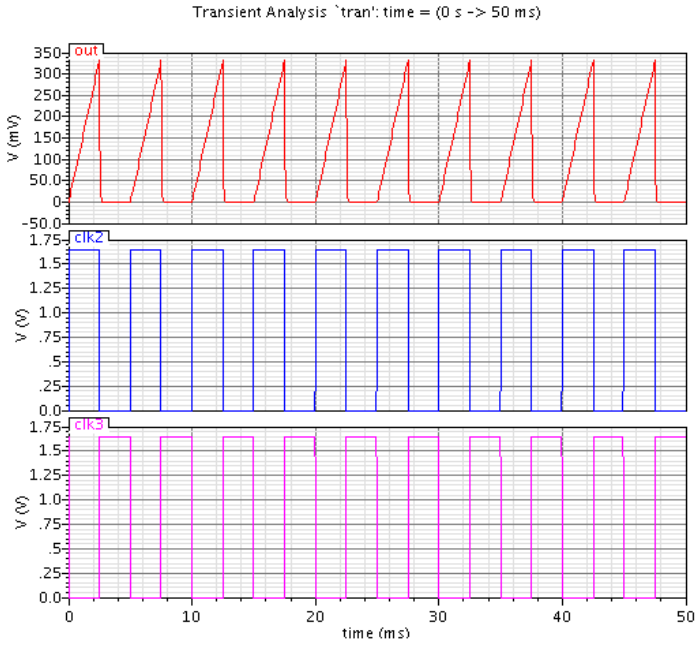

Figure 3-43 Post extraction netlist simulation with 200 Hz clock @ Iin = 15µA

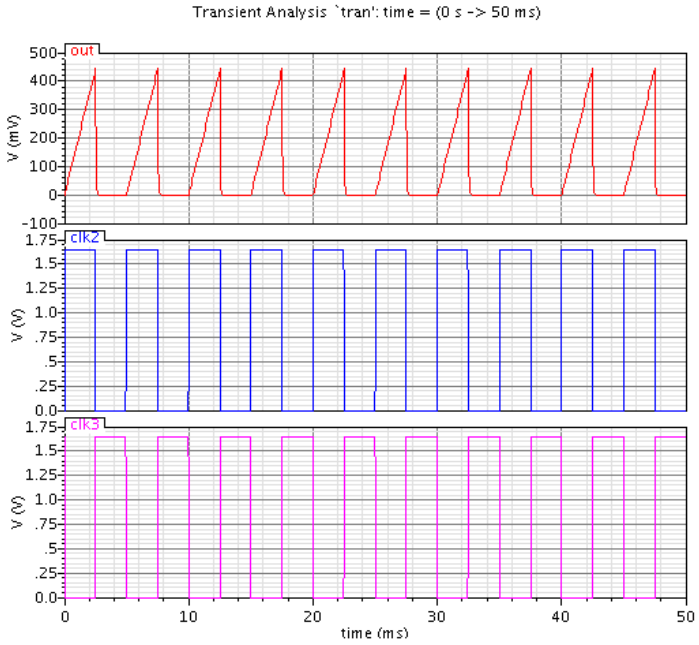

Figure 3-44 Post extraction netlist simulation with 200 Hz clock @ Iin = 20µA

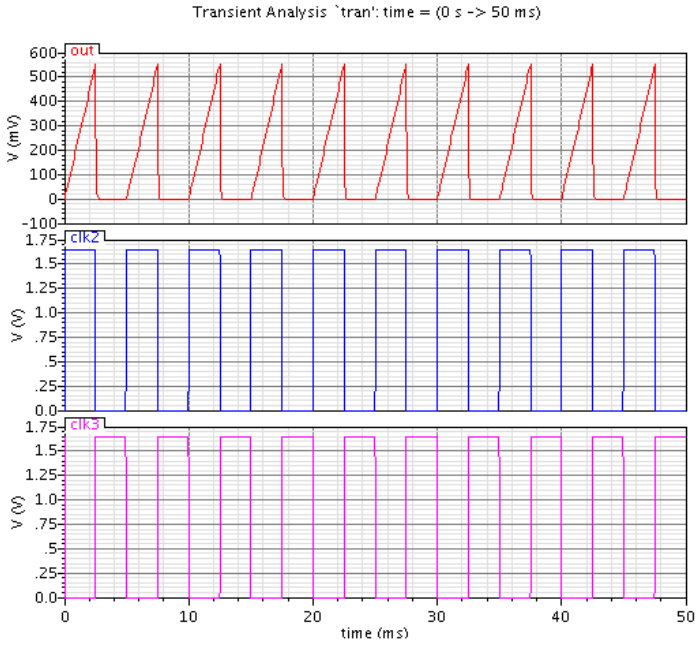

Figure 3-45 Post extraction netlist simulation with 200 Hz clock @ Iin = 25µA

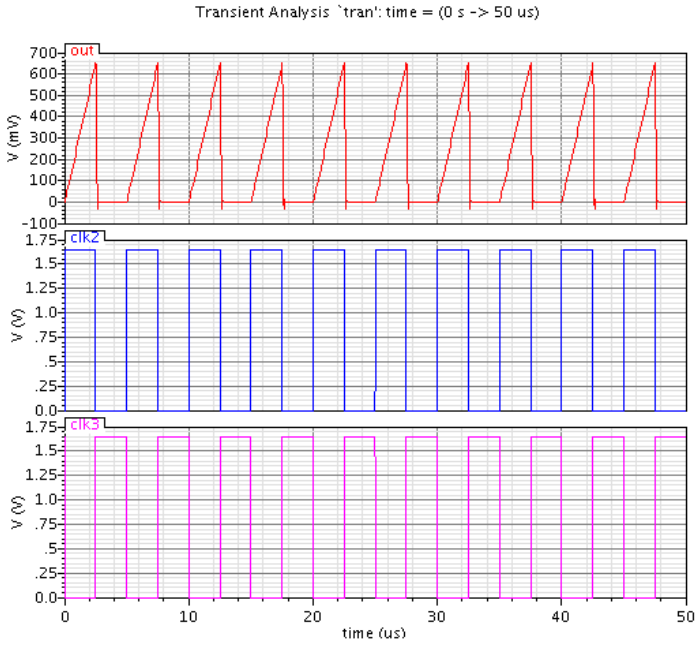

Figure 3-46 Post extraction netlist simulation with 200 Hz clock @ Iin = 30µA

The readings of all the measurements shown from Figure 3-34 to 3-46 is tabulated in Table 3-5. The minimum glucose level that can be measured is 1mM, the corresponding sensor current is 2μA and maximum is 15mM corresponding sensor current is 30 μA.

Table 3-5 Post extraction simulation results with 200 Hz clock

Glucose concentration (mM)	Electrode Resistance (kΩ)	Iin (μA)	Simulated Output (mV)	Gain (kΩ)
1	250	2	44.89	22
1.5	166.6	3	66.86	22
2	125	4	89.806	22
2.5	100	5	110.89	22
3	83.33	6	132.89	22
3.5	71.428	7	157.11	22
4	62.5	8	178.2	22
4.5	55.5	9	200.97	22
5	50	10	224.34	22
7.5	33.3	15	332.99	22
10	25	20	443	22
12.5	20	25	554.24	22
15	16.66	30	664	22

Output voltage vs. sensor current at sampling frequency of 200 kHz is plotted in Figure 3-47. The resolution of the proposed circuit is 22mV/ μA which indicates that for every 1 μA change in input current the output voltage changes by 22mV.

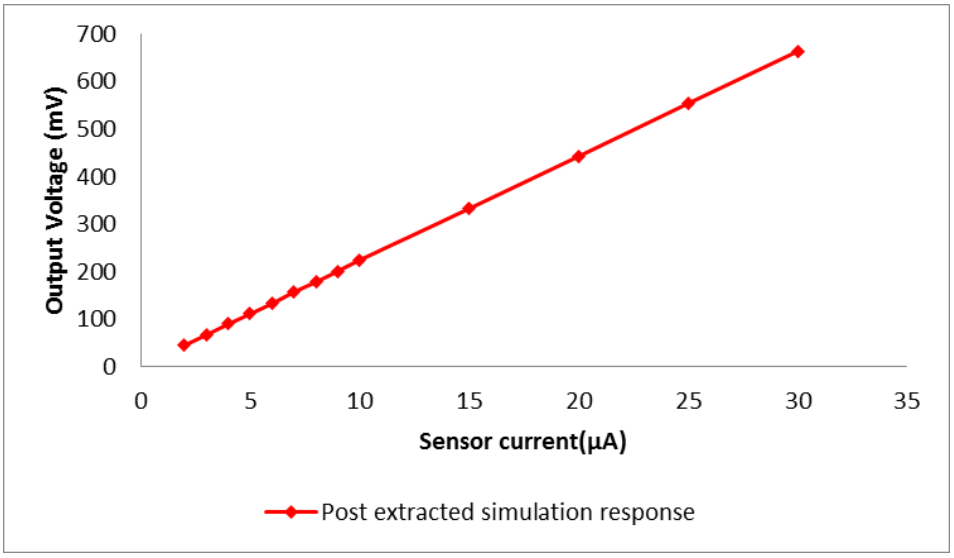

Figure 3-47 Sensor current vs. output voltage with 200 Hz clock

Output voltage vs. glucose concentration at sampling frequency of 200 kHz is plotted in Figure 3-32. The simulated trans-impedance gain of the proposed switched capacitor trans-impedance amplifier circuits is 22 kΩ. Thus at 1mM glucose concentration output voltage is 44.89mV and at 15mM glucose concentration output voltage is 664mV.

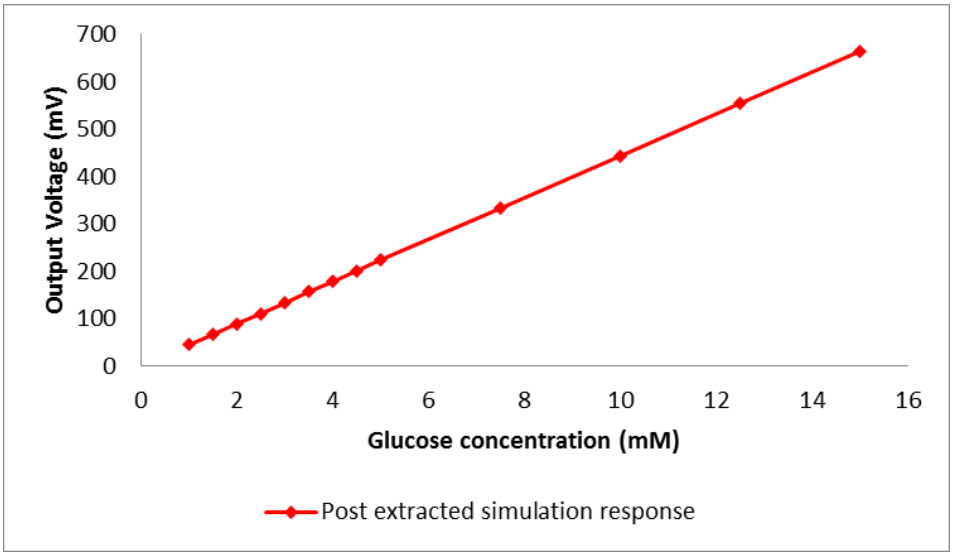

Figure 3-48 Glucose concentration vs. output voltage with 200 Hz clock

The noise simulation response of the proposed circuit with 200 Hz clock is obtained from 10Hz to 100MHz is shown in Figure 3-49. The total output integrated rms noise in the 10Hz to 100MHz bandwidth is 803.442µVrms. The power consumed by the system at 200 Hz is 2.49mW. Table 3-6 is the summary of post extracted simulation results with 200 Hz sampling clock.

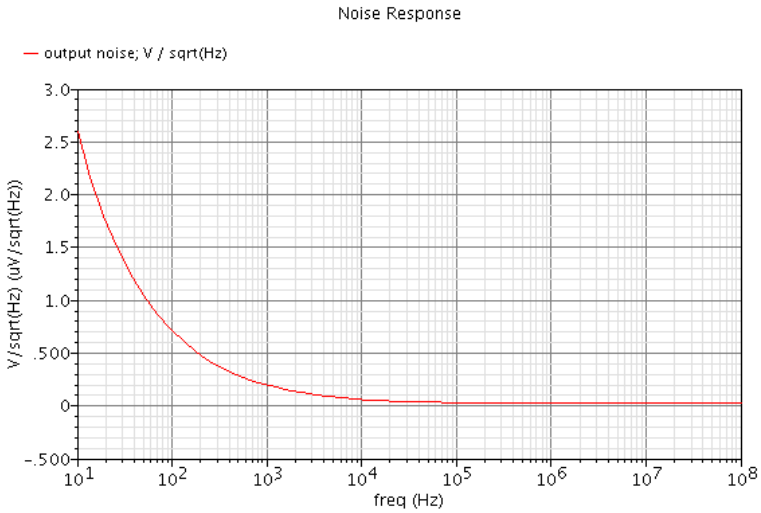

Figure 3-49 Proposed circuit noise simulation with 200 Hz clock

Table 3-6 Summary of post extraction simulation results with 200 Hz clock

Parameter	Post extraction simulation
Input current	2μA – 30μA
Output voltage	45mV - 664mV
Total integrated noise	803.442μVrms (100MHz BW)
System power dissipation	2.49mW

3.4 Measurement results

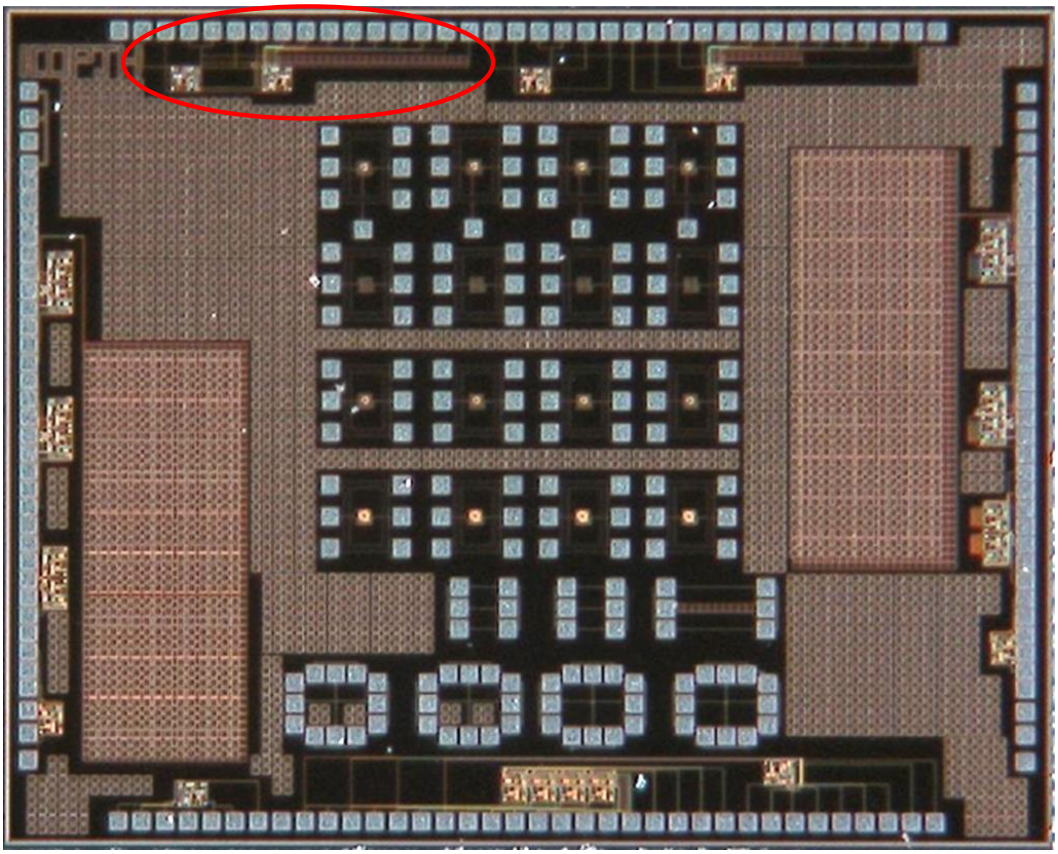

Figure 3-50 Die photograph of complete chip

Figure 3-51 shows the die photograph of complete chip. Location of the proposed circuit in Figure 3-51 is marked in red. Figure 3-52 is the zoomed area of the die showing the proposed circuit.

Figure 3-51 Zoomed die photograph of proposed circuit

The die shown in Figure 3-51 is wire bonded and packaged into a 208 pin quad flat package case and Figure 3-53 shows the photograph of a packaged chip.

Figure 3-52 Photograph of packaged chip

3.4.1 Measurement setup

The block diagram of measurement setup is as shown in Figure 3-54, equipment used and their respective function is listed in Table 3-7. The glucose sensor model as shown in Figure 2-6 is connected on the breadboard. The sampling and reset clocks are generated using a 16bit microcontroller from Microchip dsPIC33FJ128GP on a Microstick II evaluation board.

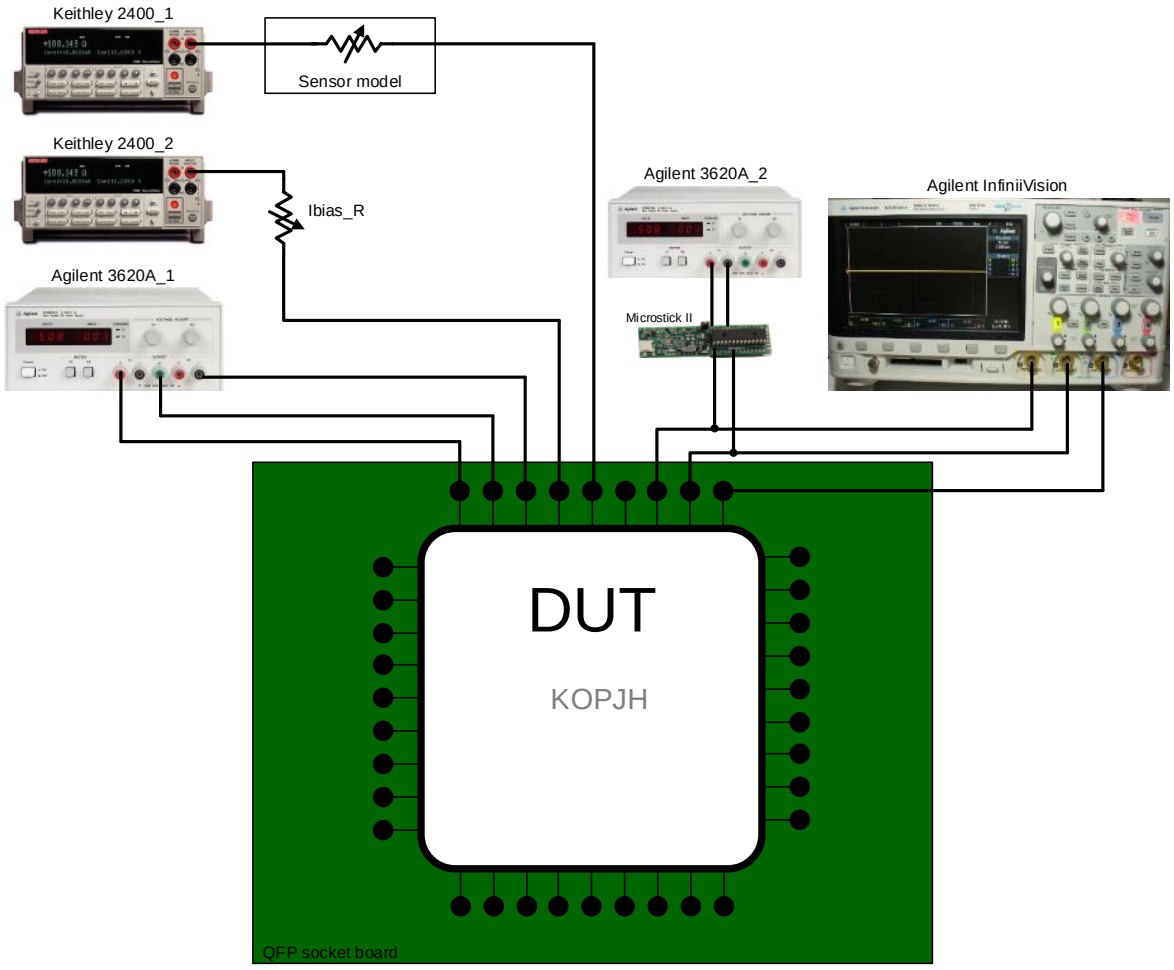

Figure 3-53 Block diagram of measurement setup

A 200 pin quad flat package socket is soldered on to the adapter board as shown in Figure 3-55 to test the chip.

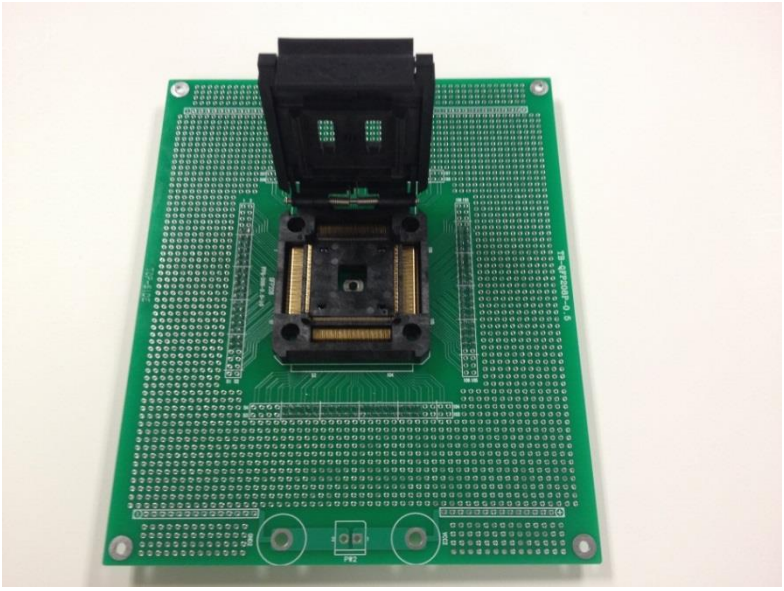

Figure 3-54 Adapter board with QFPP socket

The packaged chip is put into this socket for testing. Sensor model is wired on the bread board and connections are made from adapter board to bread board. The complete measurement setup is shown in Figure 3-56.

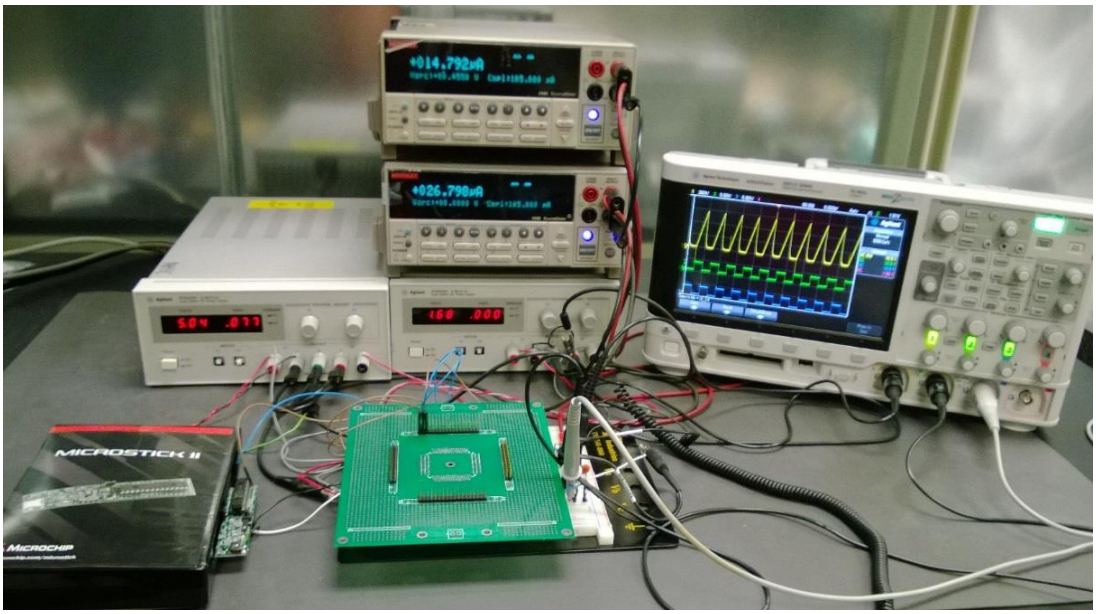

Figure 3-55 Measurement setup

Keithley 2400 source meter is used to bias the glucose sensor model and operational amplifier, Agilent power supply is used to power on the chip and microcontroller for generating switch control signals. Agilent InfiniiVision digital storage oscilloscope to measure the output of proposed circuit. Agilent multi-meter is used to measure the power consumption.

Table 3-7 Equipment list and functions

Equipment	**Function**
Keithley 2400_1	Sensor bias
Keithley 2400_2	Opamp bias current
Agilent 3620A_1	Opamp power supply
Agilent 3620A_2	Microstick II power supply
Microstick II PIC eval board	Sampling and reset clocks
Agilent InfiniiVision	Digital storage oscilloscope

3.4.2 Measurement results with 100pF on chip capacitor and 200 kHz sampling clock

The post extracted simulated response of proposed circuit for input current range from 2µA to 30µA is shown in Figure 3-57 to Figure 3-69 and the corresponding output varies from 20mV to 749mV.

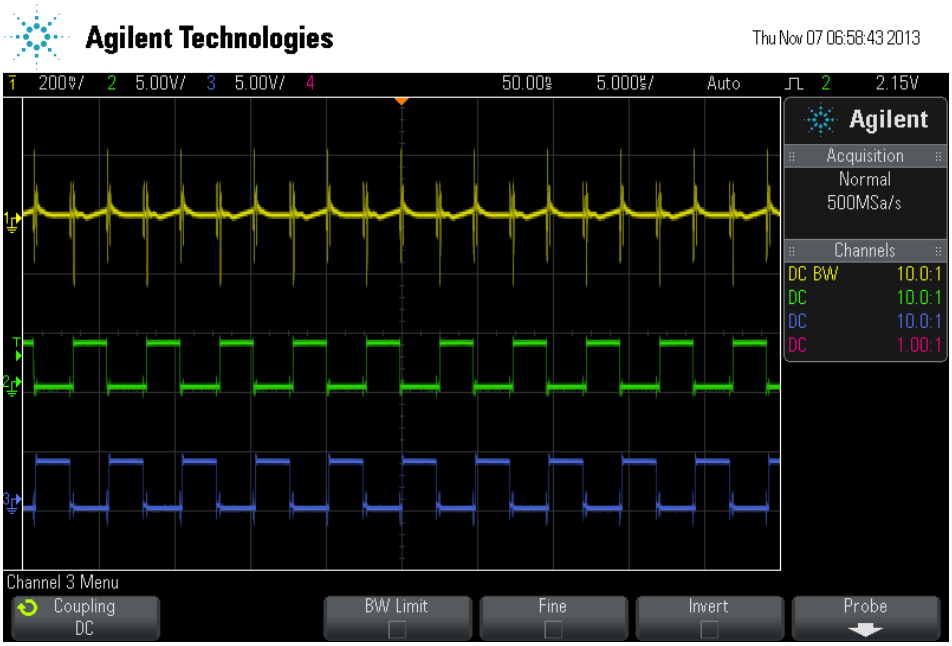

Figure 3-56 Measured output with 200 kHz clock @ Iin = 2µA

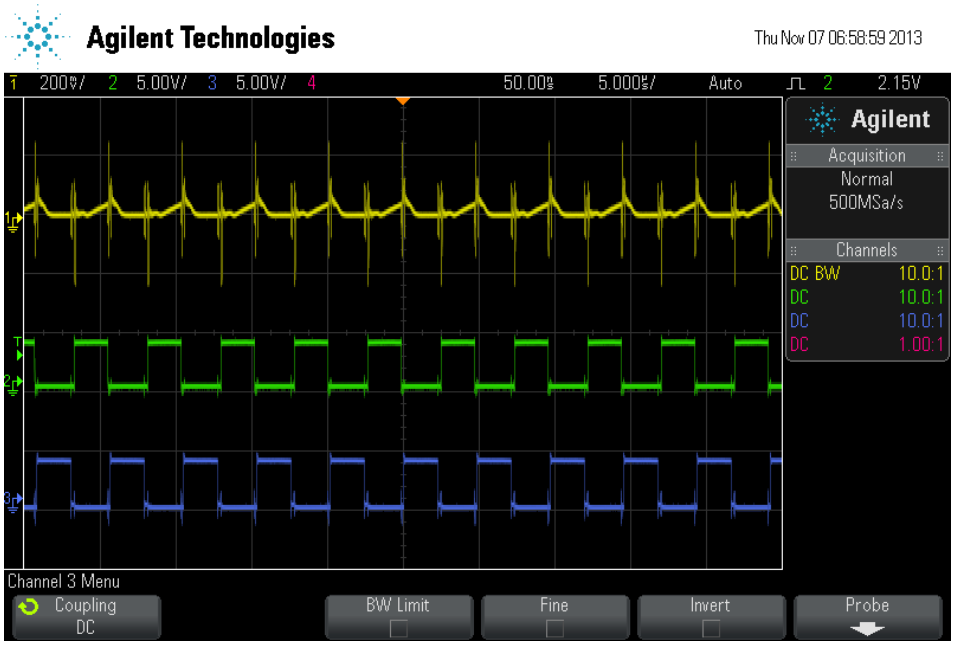

Figure 3-57 Measured output with 200 kHz clock @ Iin = 3µA

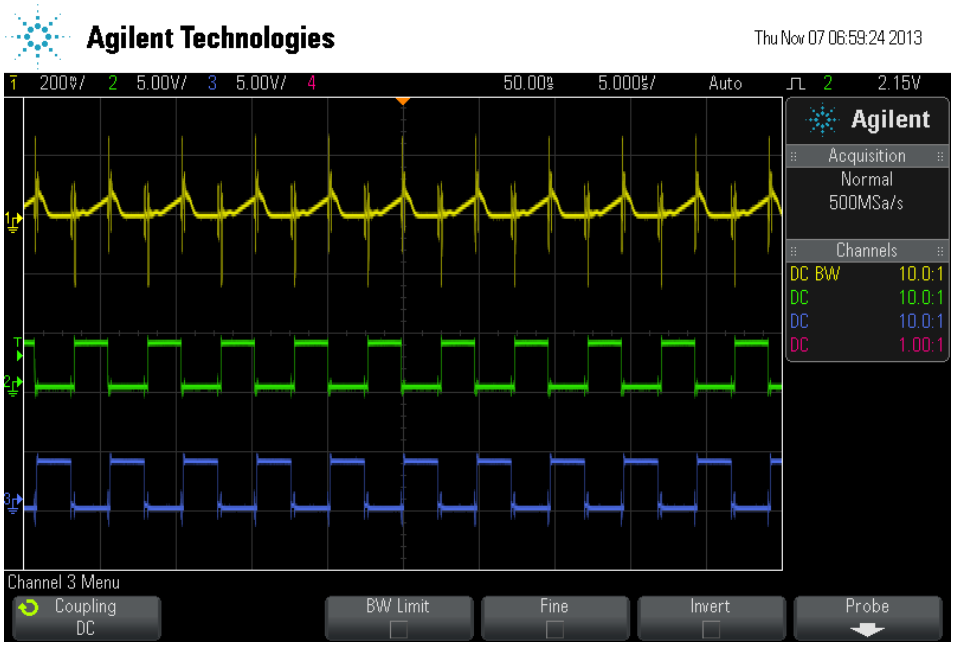

Figure 3-58 Measured output with 200 kHz clock @ Iin = 4µA

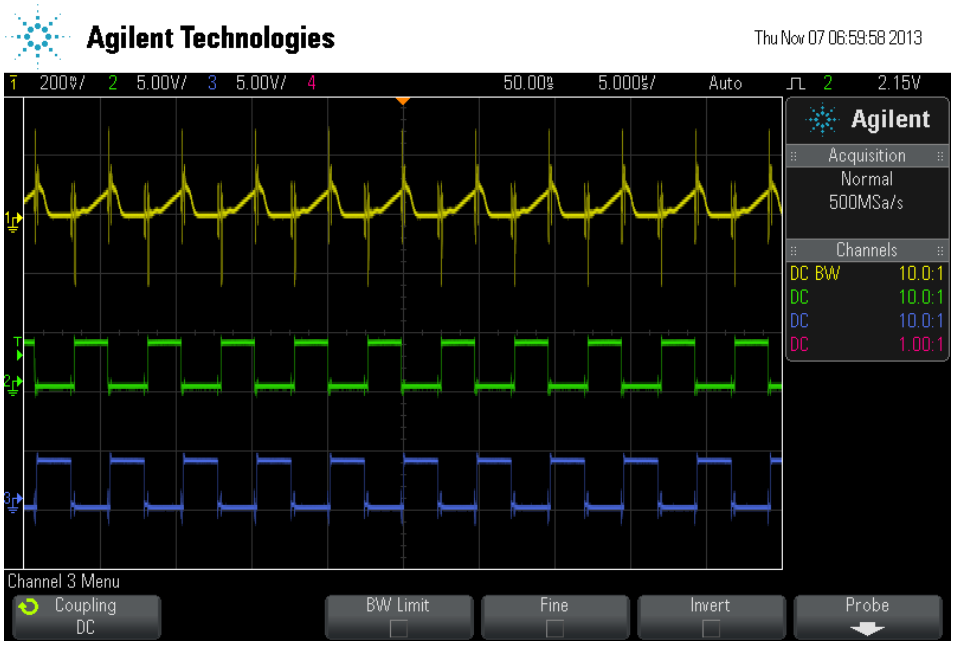

Figure 3-59 Measured output with 200 kHz clock @ Iin = 5µA

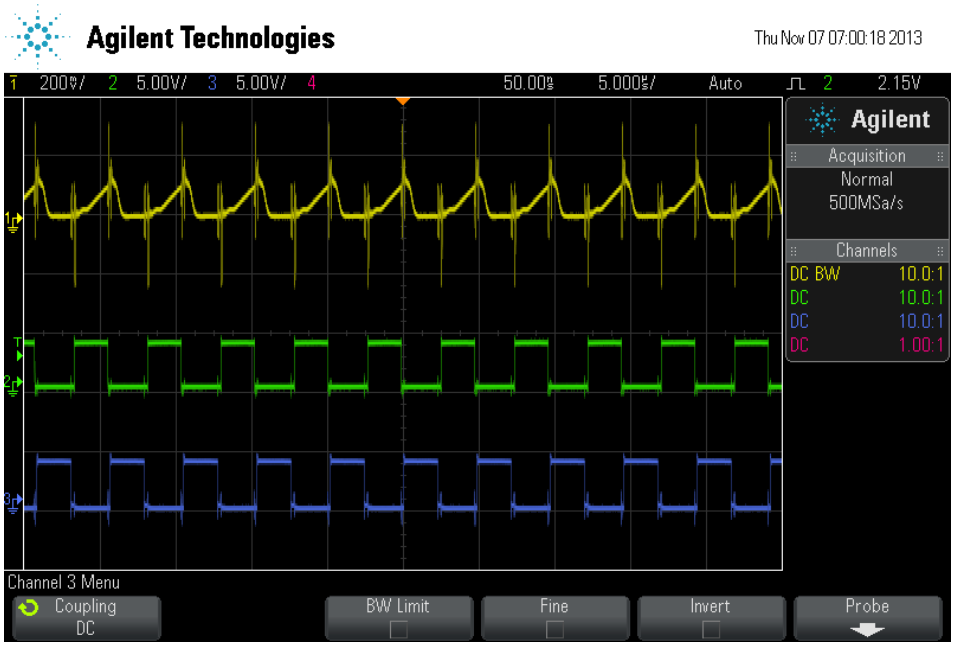

Figure 3-60 Measured output with 200 kHz clock @ Iin = 6µA

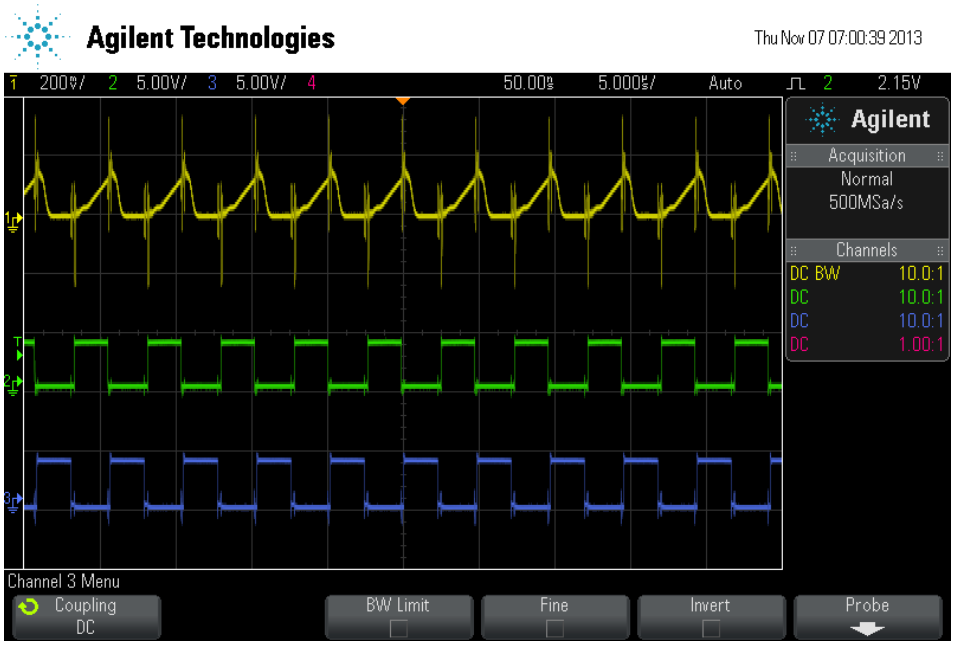

Figure 3-61 Measured output with 200 kHz clock @ Iin = 7µA

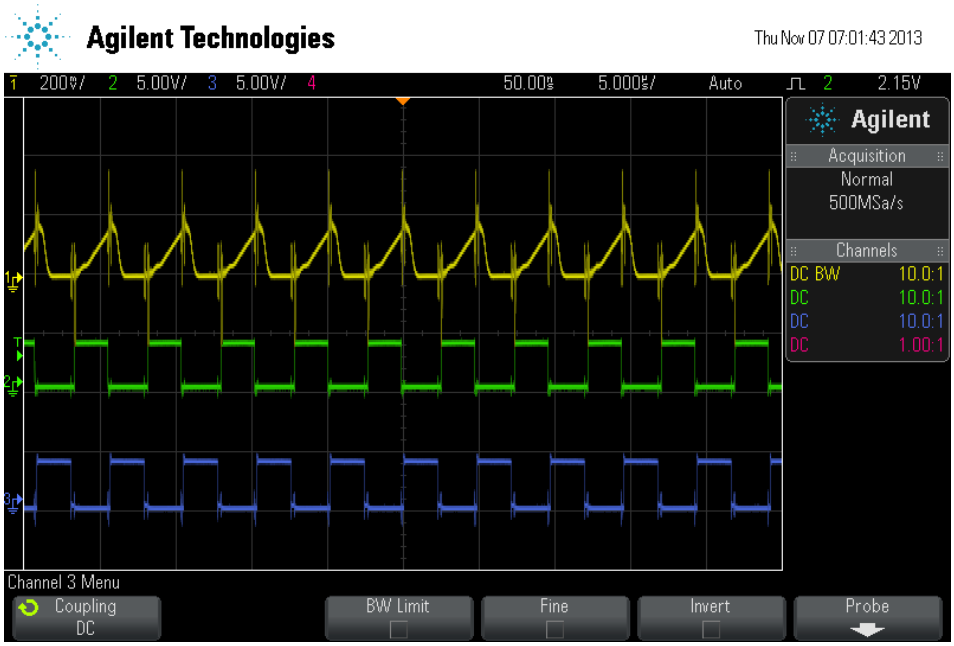

Figure 3-62 Measured output with 200 kHz clock @ Iin = 8µA

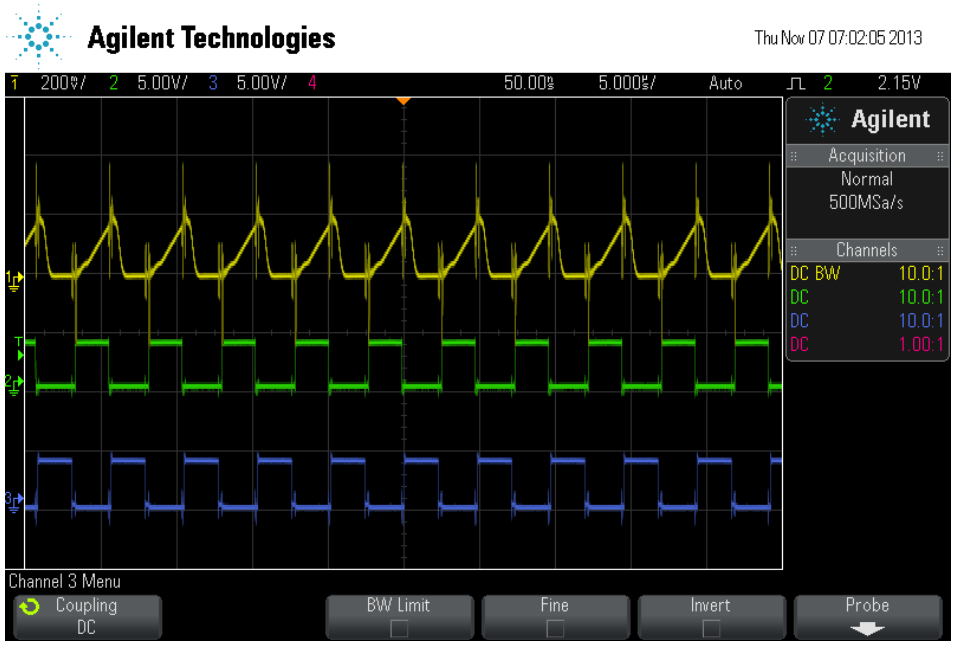

Figure 3-63 Measured output with 200 kHz clock @ Iin = 9µA

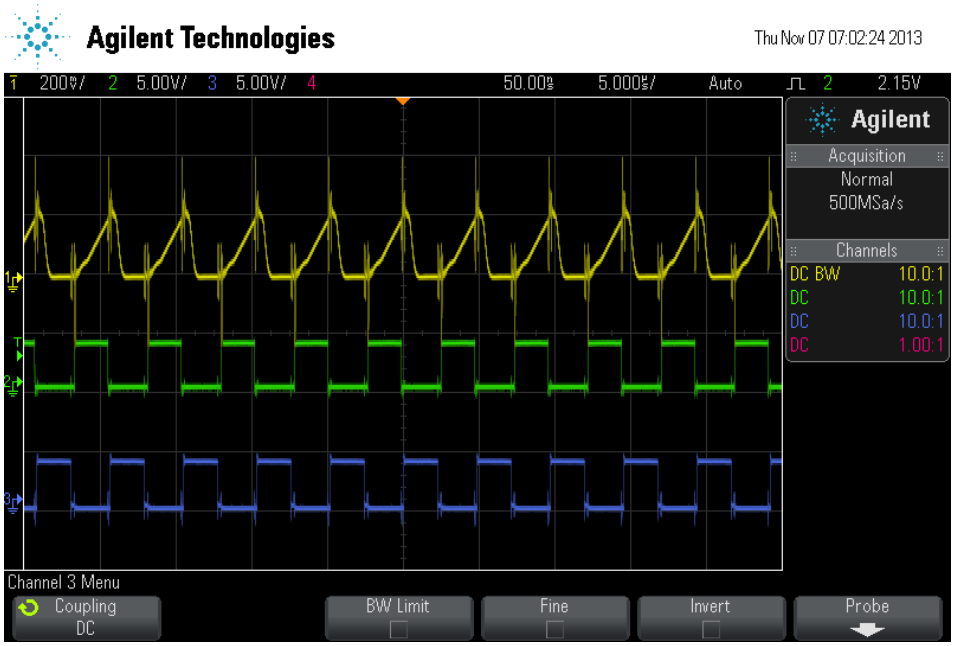

Figure 3-64 Measured output with 200 kHz clock @ Iin = 10µA

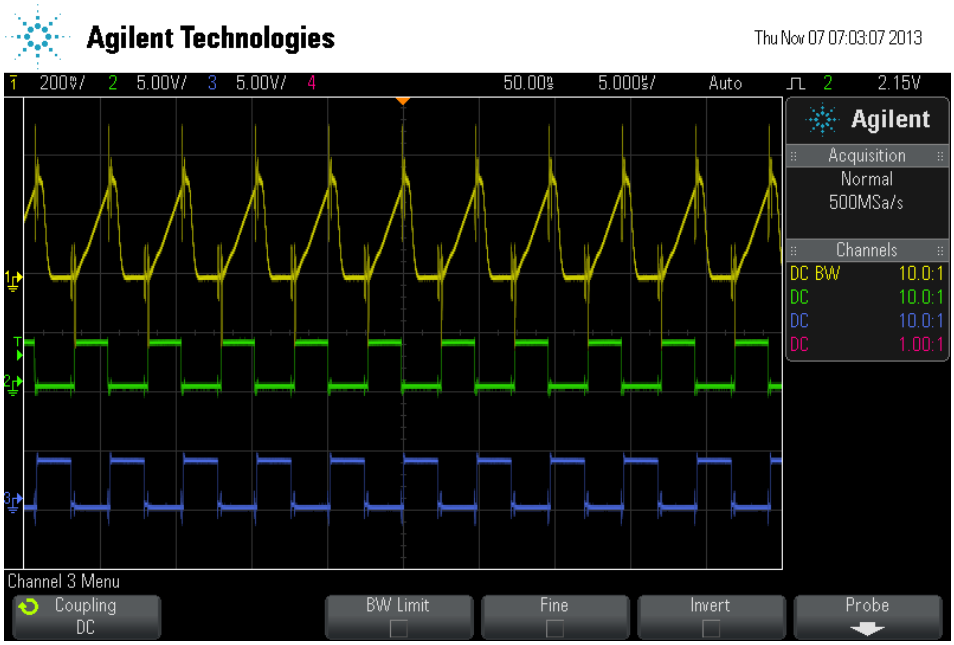

Figure 3-65 Measured output with 200 kHz clock @ Iin = 15µA

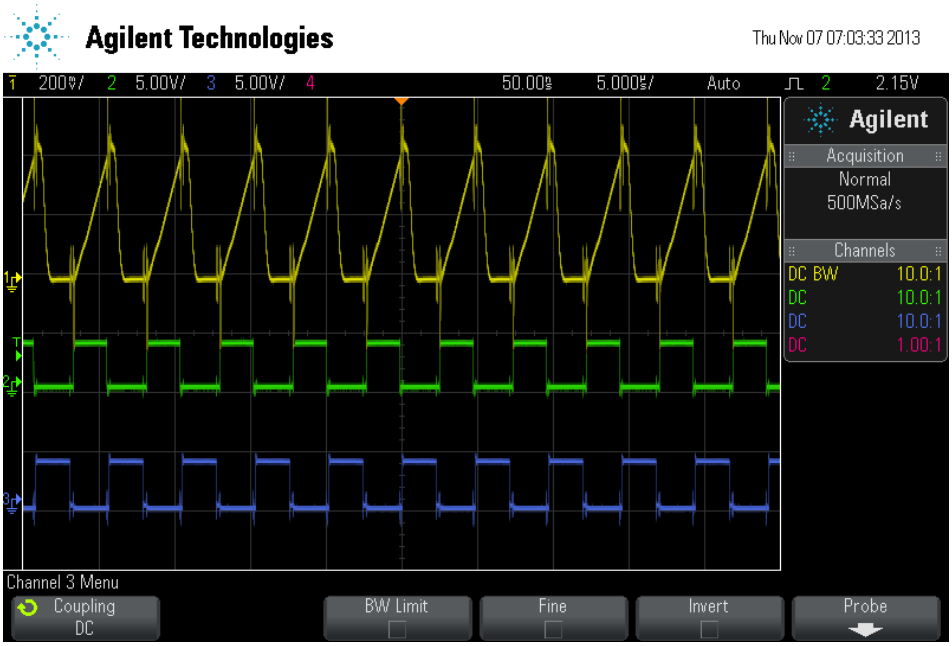

Figure 3-66 Measured output with 200 kHz clock @ Iin = 20µA

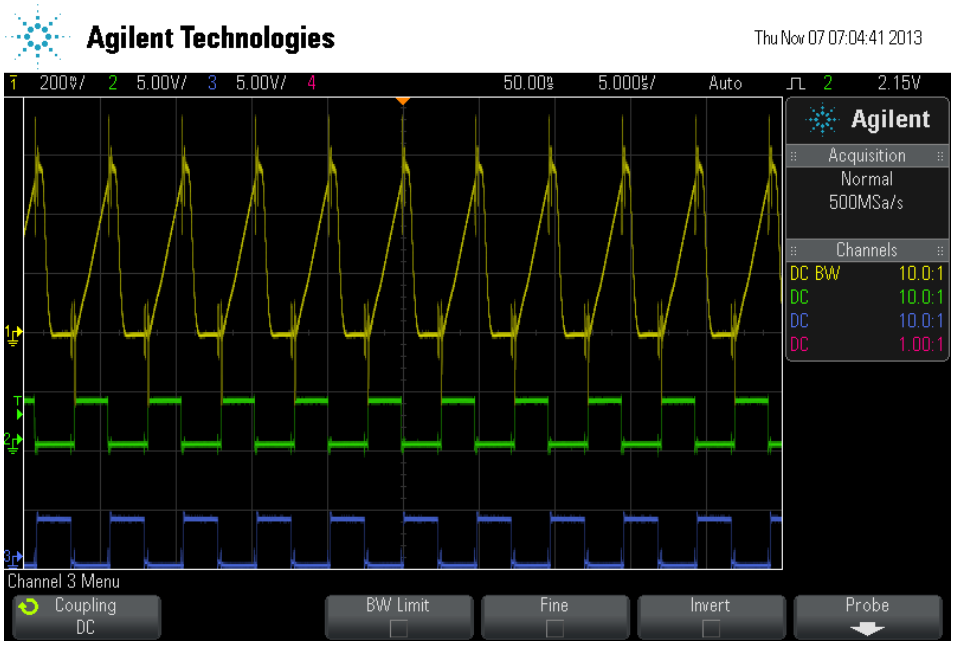

Figure 3-67 Measured output with 200 kHz clock @ Iin = 25µA

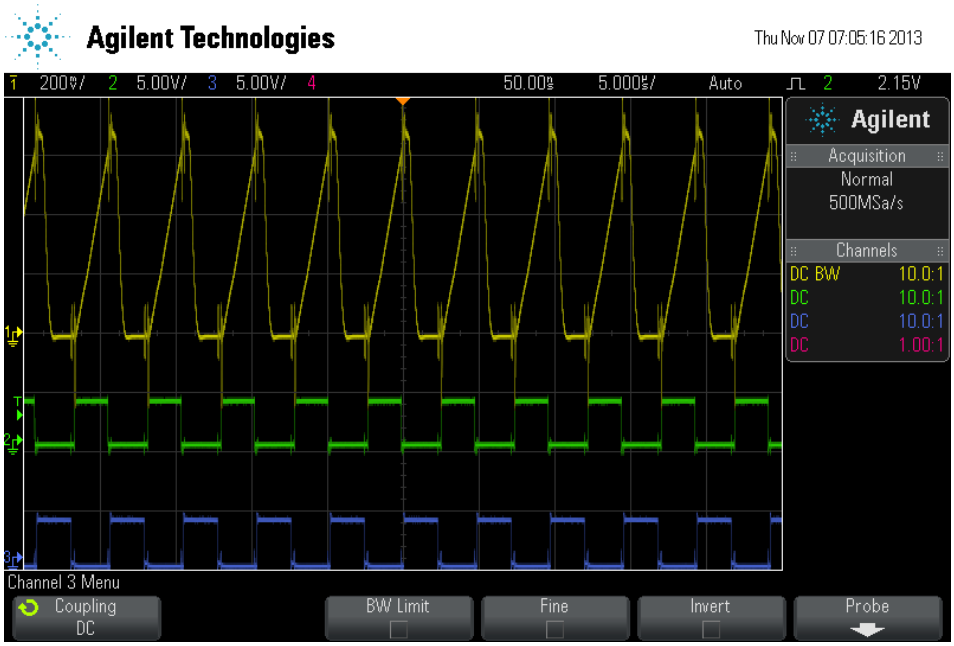

Figure 3-68 Measured output with 200 kHz clock @ Iin = 30µA

The readings of all the measurements shown from Figure 3-57 to 3-69 is tabulated in Table 3-8. The minimum glucose level that can be measured is 1mM, the corresponding sensor current is 2µA and maximum is 15mM corresponding sensor current is 30 µA.

Table 3-8 Measured results with 200 kHz clock

Glucose concentration (mM)	Electrode Resistance (kΩ)	Iin (µA)	Measured Output (mV)
1	250	2	20
1.5	166.6	3	50
2	125	4	73.25
2.5	100	5	97
3	83.33	6	122.5

Table 3.8—*Continued*

Glucose concentration (mM)	Electrode Resistance (kΩ)	Iin (µA)	Measured Output (mV)
3.5	71.428	7	150
4	62.5	8	172.5
4.5	55.5	9	198.7
5	50	10	222.5
7.5	33.3	15	355
10	25	20	492.5
12.5	20	25	615
15	16.66	30	749

Output voltage vs. sensor current at sampling frequency of 200 kHz is plotted in Figure 3-70. The resolution of the proposed circuit is 22.5mV/ µA which indicates that for every 1 µA change in input current the output voltage changes by 25mV.

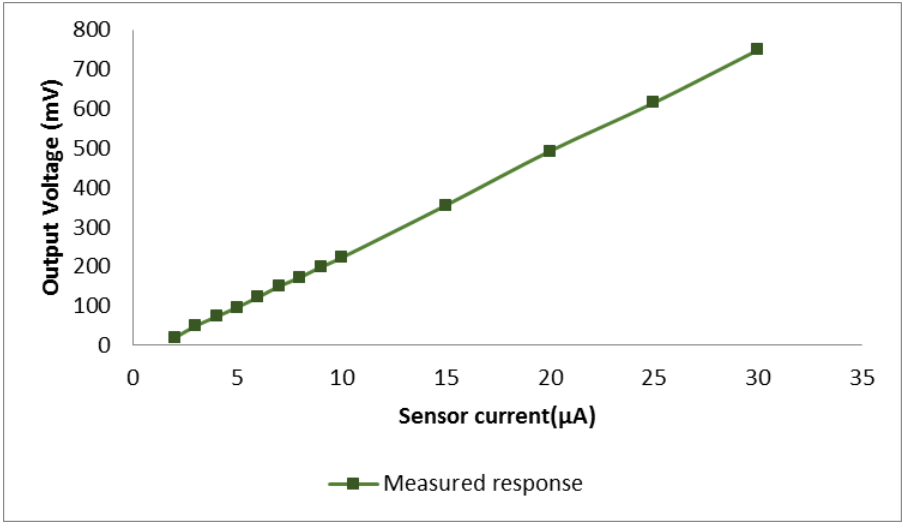

Figure 3-69 Sensor current vs. measured output voltage

Output voltage vs. glucose concentration at sampling frequency of 200 kHz is plotted in Figure 3-72. The measured trans-impedance gain of the proposed switched capacitor trans-impedance amplifier circuits is 22.8 kΩ. Thus at 1mM glucose concentration output voltage is 20mV and at 15mM glucose concentration output voltage is 749mV.

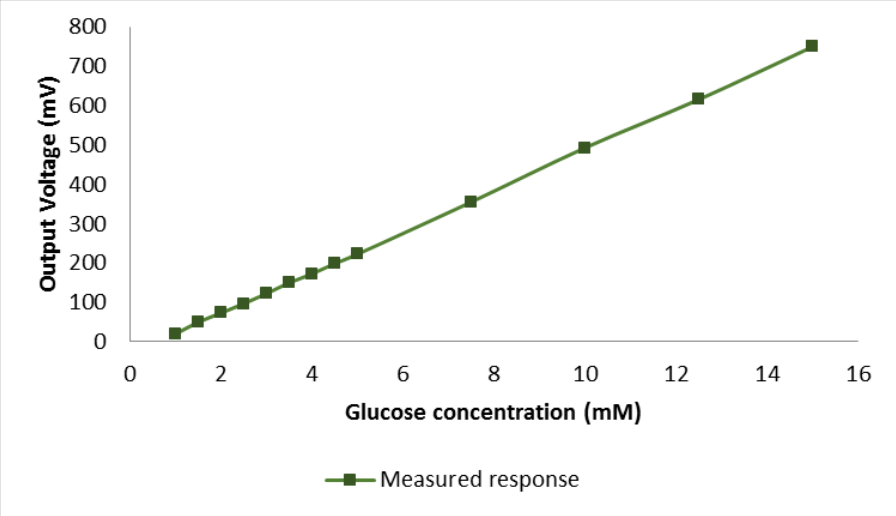

Figure 3-70 Glucose concentration vs. measured output voltage

3.4.3 Measurement results with 100nF external capacitor and 200 Hz sampling clock

The post extracted simulated response of proposed circuit for input current range from 2µA to 30µA is shown in Figure 3-72 to Figure 3-83 and the corresponding output varies from 19.25mV to 624mV.

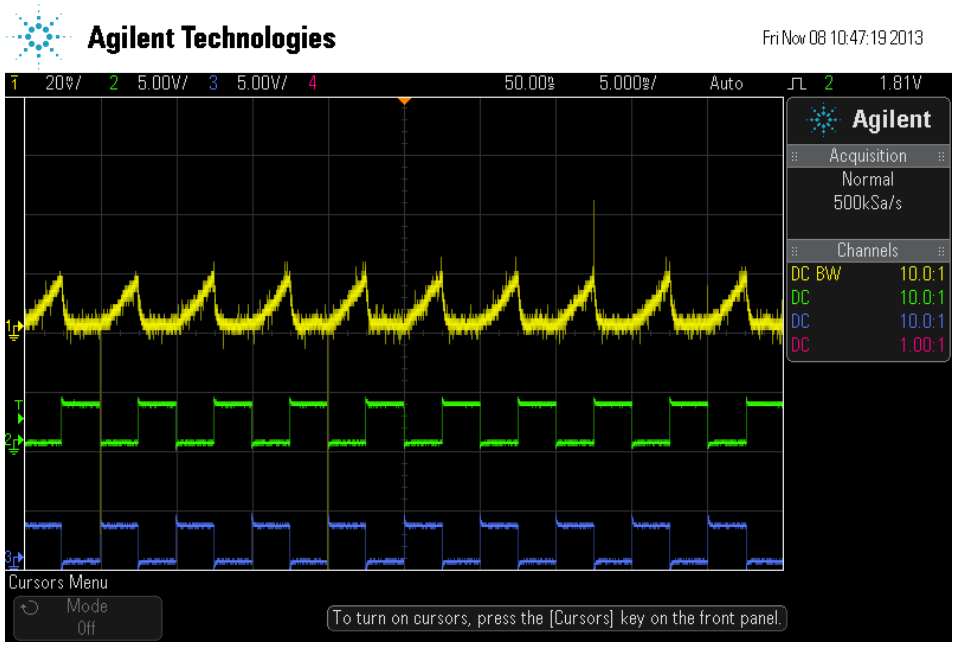

Figure 3-71 Measured output with 200 Hz clock @ Iin = 2µA

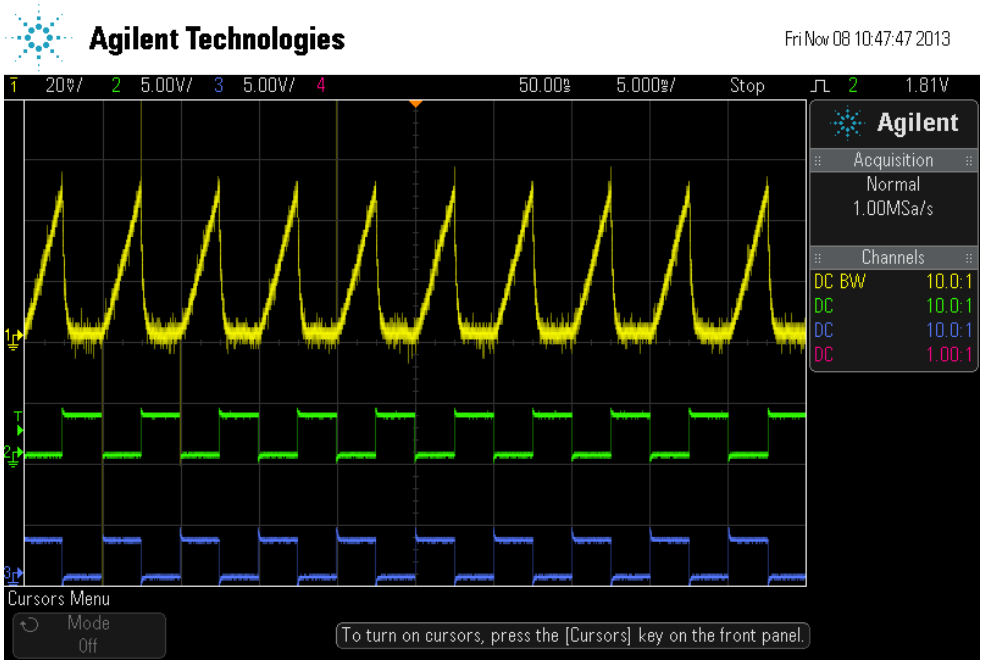

Figure 3-72 Measured output with 200 Hz clock @ Iin = 3µA

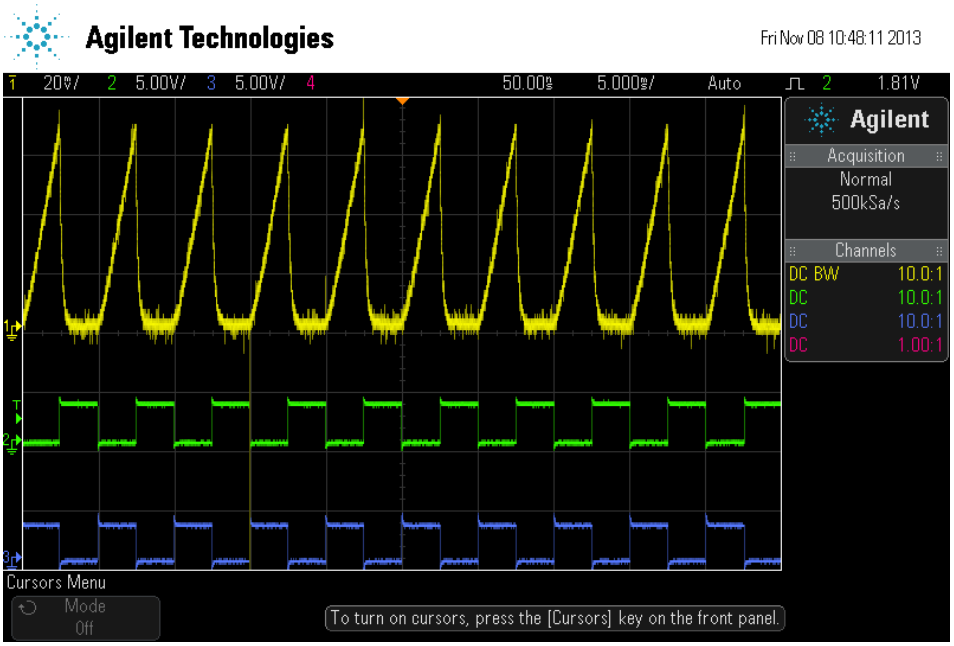

Figure 3-73 Measured output with 200 Hz clock @ Iin = 4µA

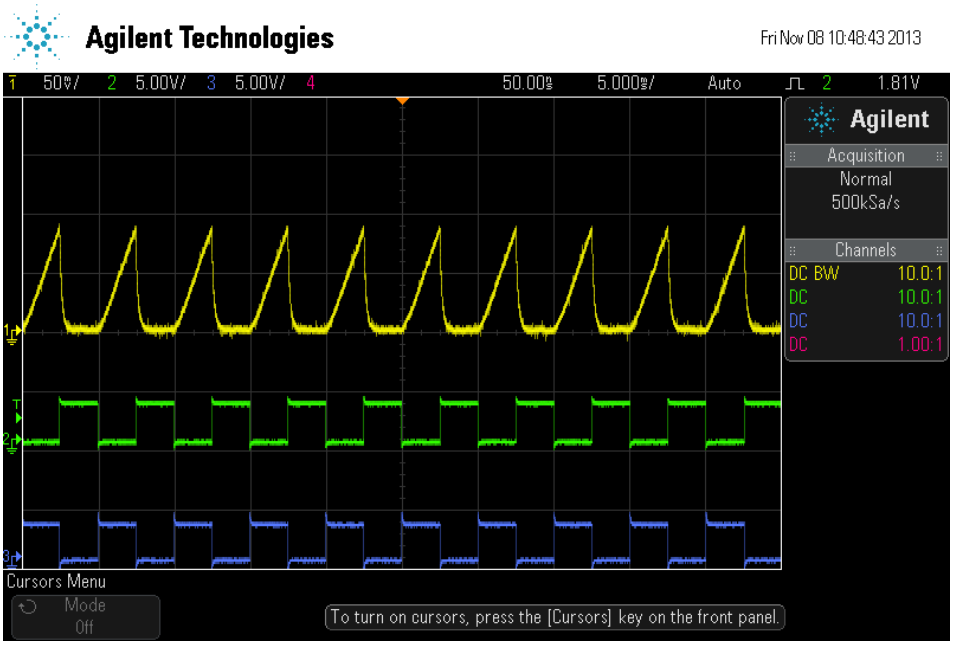

Figure 3-74 Measured output with 200 Hz clock @ Iin = 5µA

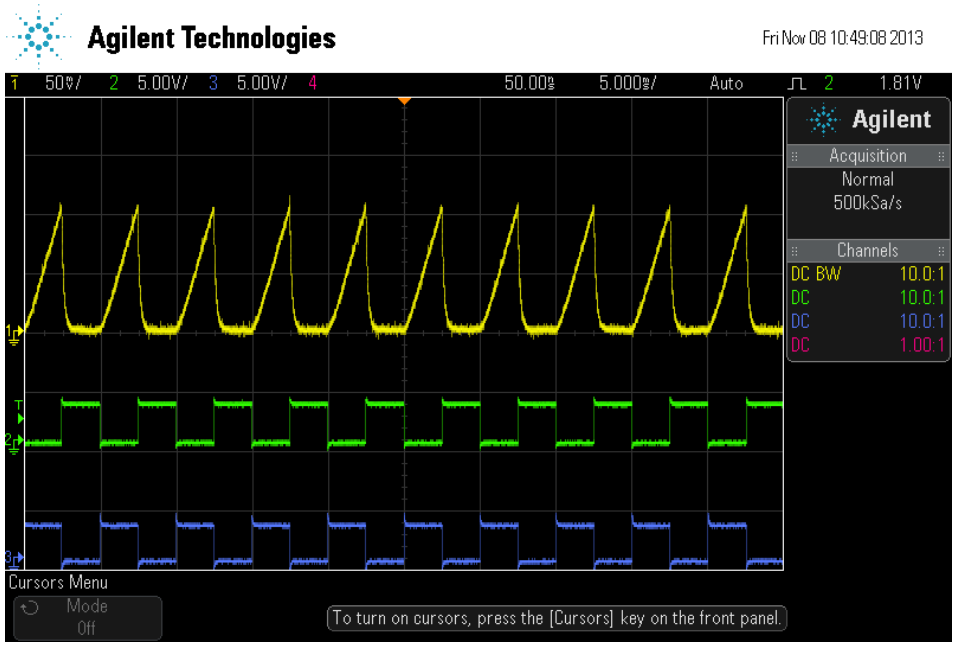

Figure 3-75 Measured output with 200 Hz clock @ Iin = 6µA

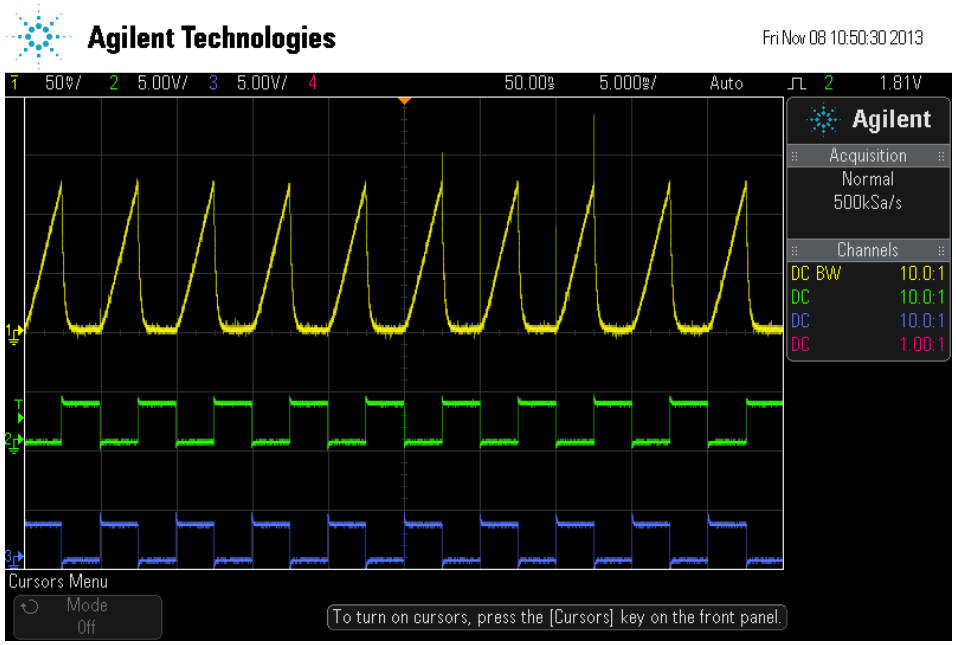

Figure 3-76 Measured output with 200 Hz clock @ Iin = 7µA

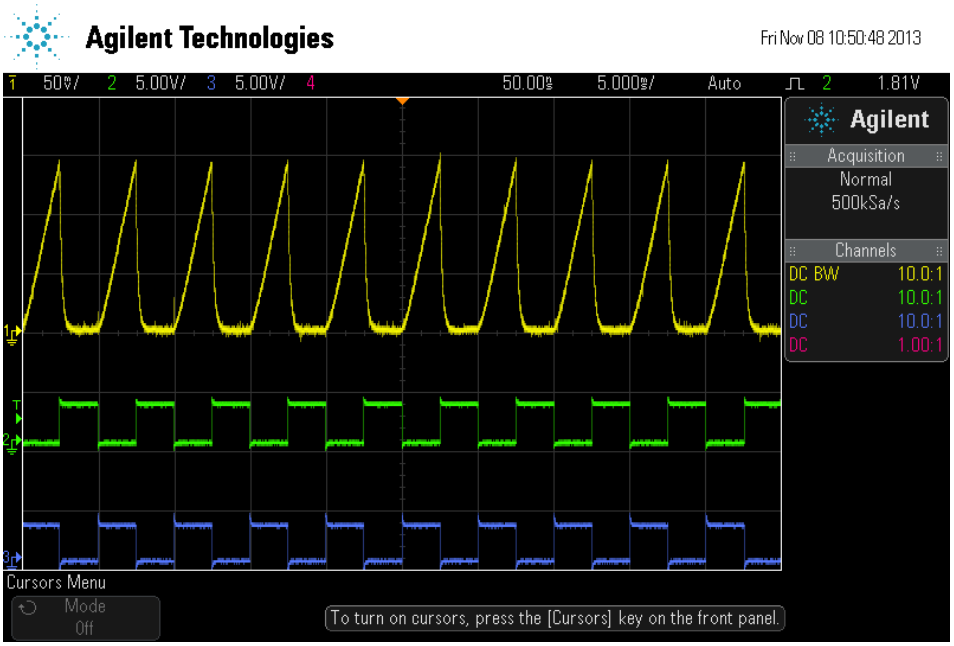

Figure 3-77 Measured output with 200 Hz clock @ Iin = 8µA

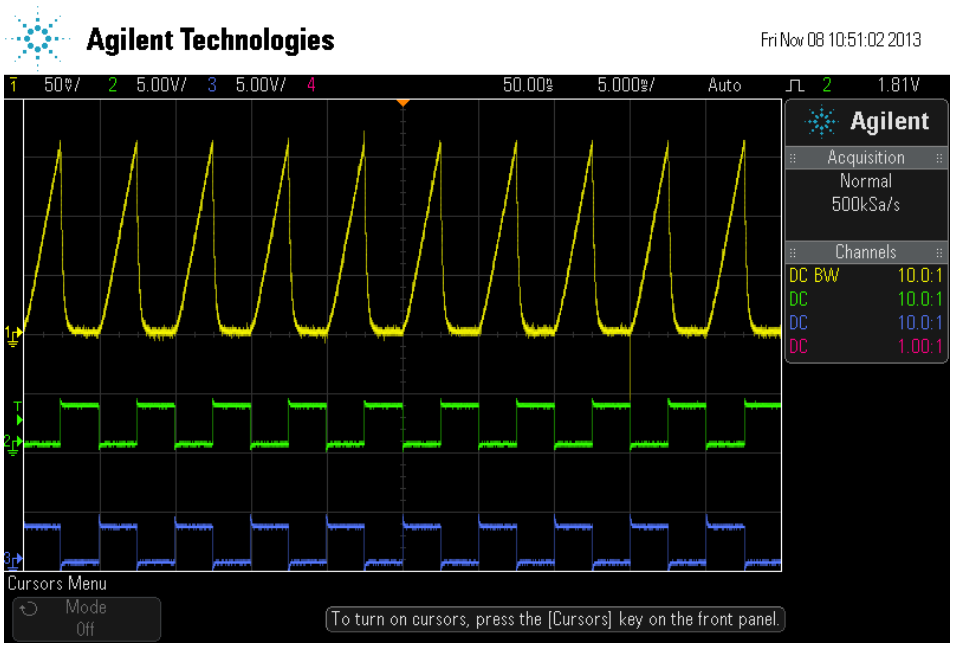

Figure 3-78 Measured output with 200 Hz clock @ Iin = 9µA

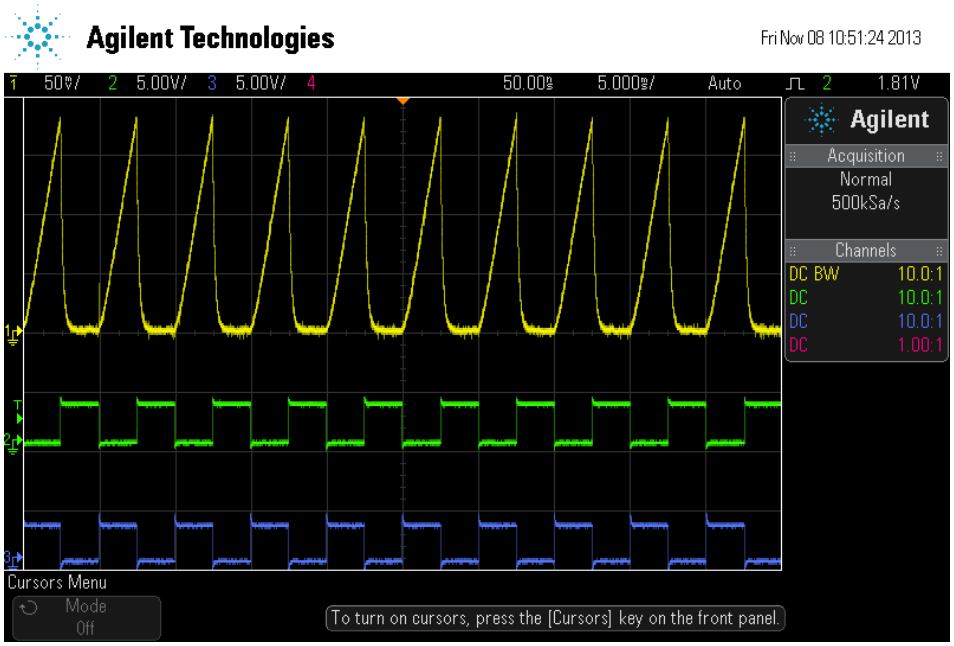

Figure 3-79 Measured output with 200 Hz clock @ Iin = 10µA

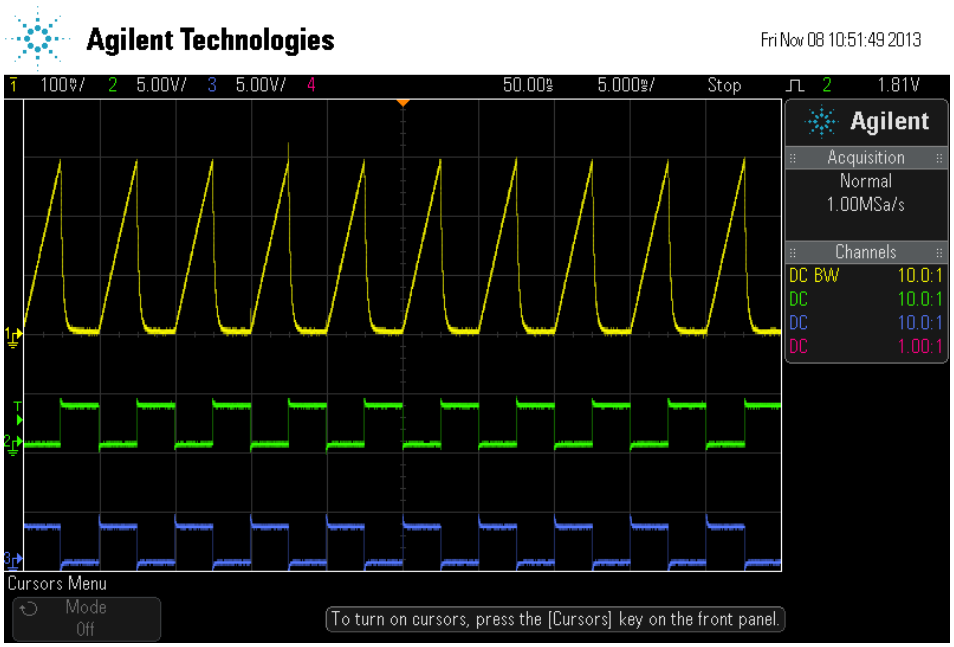

Figure 3-80 Measured output with 200 Hz clock @ Iin = 15µA

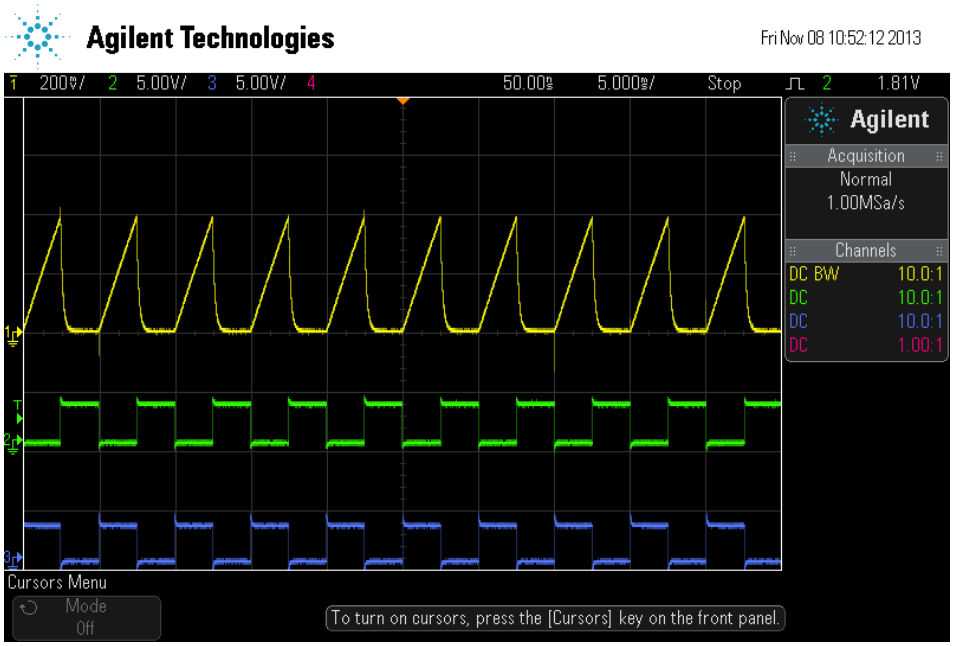

Figure 3-81 Measured output with 200 Hz clock @ Iin = 20µA

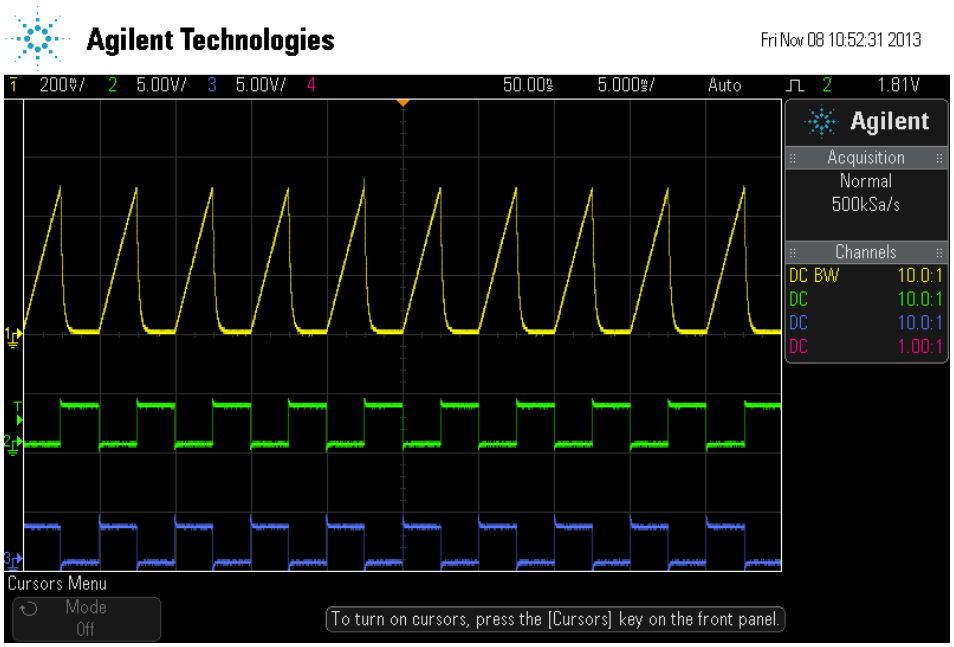

Figure 3-82 Measured output with 200 Hz clock @ Iin = 25µA

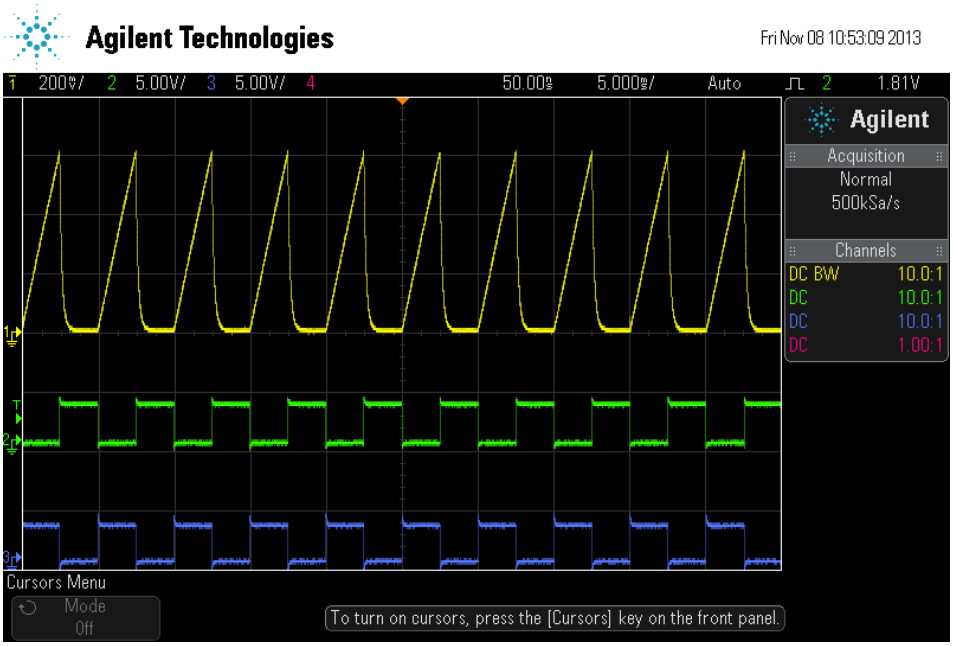

Figure 3-83 Measured output with 200 Hz clock @ Iin = 30µA

The readings of all the measurements shown from Figure 3-72 to 3-84 is tabulated in Table 3-9. The minimum glucose level that can be measured is 1mM, the corresponding sensor current is 2µA and maximum is 15mM corresponding sensor current is 30 µA.

Table 3-9 Measured results with 200 Hz clock

Glucose concentration (mM)	Electrode Resistance (kΩ)	Iin (µA)	Measured Output (mV)
1	250	2	19.25
1.5	166.6	3	49.5
2	125	4	70.75
2.5	100	5	88.25
3	83.33	6	107.5

Table 3.9—*Continued*

Glucose concentration (mM)	Electrode Resistance (kΩ)	Iin (µA)	Measured Output (mV)
3.5	71.428	7	131.25
4	62.5	8	150
4.5	55.5	9	172
5	50	10	198
7.5	33.3	15	307.5
10	25	20	412
12.5	20	25	520
15	16.66	30	624

Output voltage vs. sensor current at sampling frequency of 200 Hz is plotted in Figure 3-85. The resolution of the proposed circuit is 21.5mV/ µA which indicates that for every 1 µA change in input current the output voltage changes by 21.5mV.

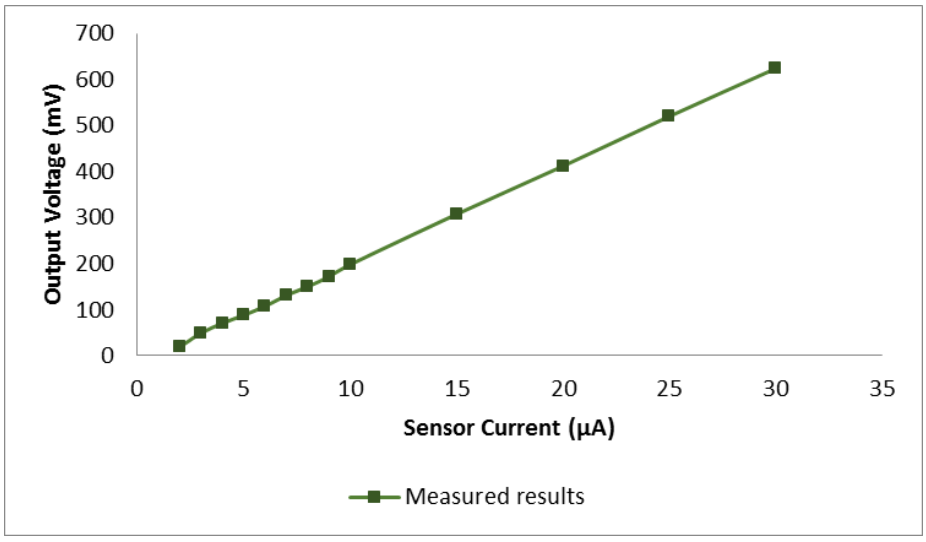

Figure 3-84 Sensor current vs. measured output voltage with 200 Hz clock

Output voltage vs. glucose concentration at sampling frequency of 200 kHz is plotted in Figure 3-86. The measured trans-impedance gain of the proposed switched capacitor trans-impedance amplifier circuits is 21.2 kΩ. Thus at 1mM glucose concentration output voltage is 19.25mV and at 15mM glucose concentration output voltage is 624mV.

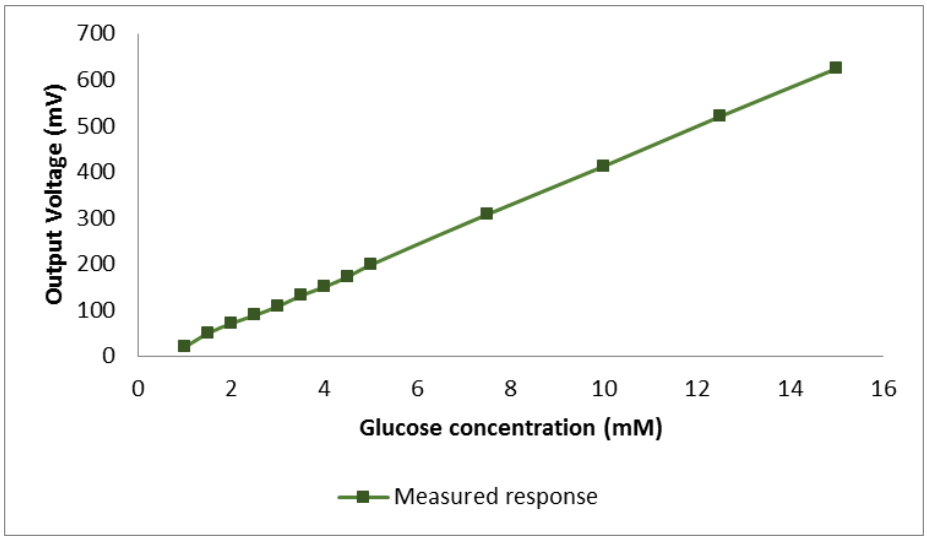

Figure 3-85 Glucose concentration vs. measured output voltage with 200 Hz clock

3.5 Comparison of simulation versus measurement results

Measurement and simulated sensor current vs. output voltage results with internal capacitor of 100pF at 200 kHz sampling frequency and with external capacitor of 100nF at 200 Hz are compared in Figure 3-85 and Figure 3-86 respectively. The comparison plots in Figure 3-85 and Figure 3-86 show that the measurement results closely matches with the simulation results with a mean percentage error of 15% between simulation and measurement results. The most likely causes for this error are gain error and offset error due to channel charge injection and body effects from transmission gate, operational

amplifier output offset introduced due to device mismatch introduced by process variation, component tolerance of the resistor used for glucose sensor emulation, component tolerance of the gain capacitor which determines the gain of switched capacitor trans-impedance amplifier.

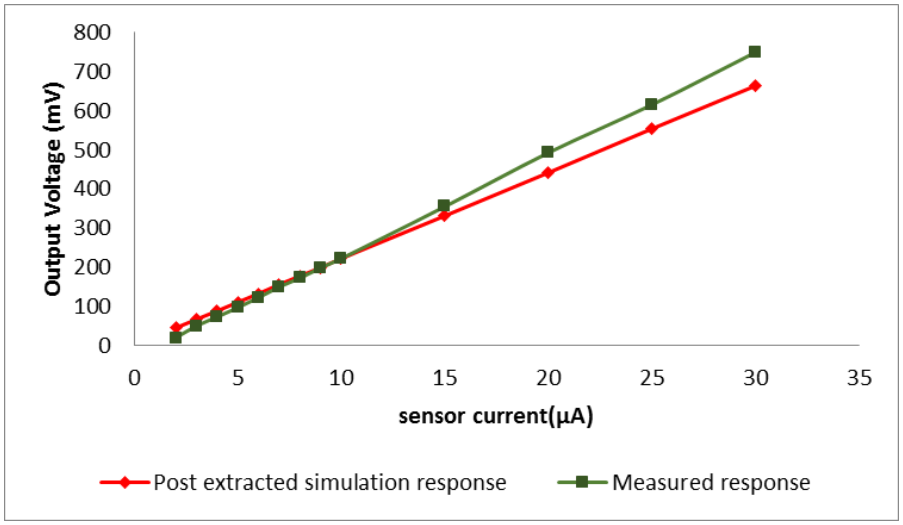

Figure 3-86 Comparison of measured and simulated results with 200 kHz clock

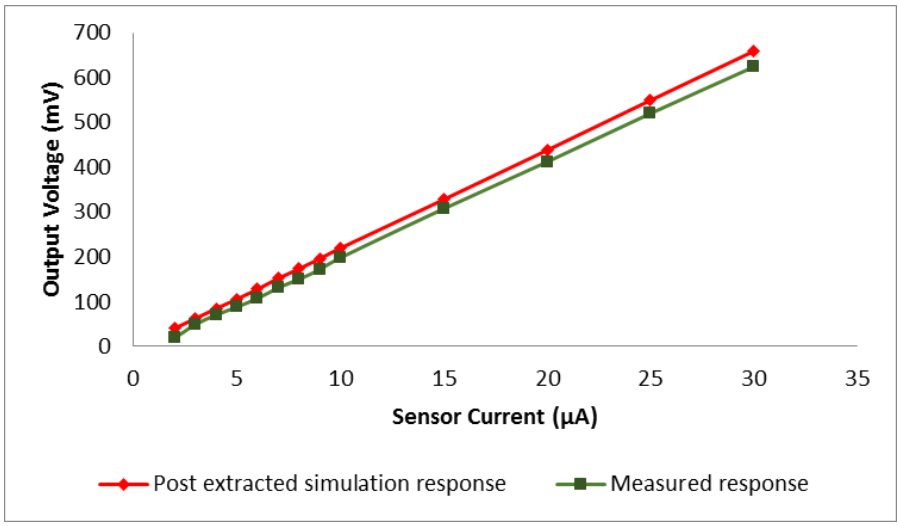

Figure 3-87 Comparison of measured and simulated results with 200 Hz clock

Charge injection problem at the output occurs due to flow of stored charge in the channel into output stage. Thus stored charge Q_{ch} in the channel of transmission gate is

$$Q_{ch} = WLC_{ox}(V_{DD} - V_{in} - V_{Th}) \tag{3.37}$$

The error caused at the output due to channel charge injection on to the holding capacitor C is given by ΔV

$$\Delta V = \frac{WLC_{ox}(V_{DD} - V_{in} - V_{Th})}{C} \tag{3.38}$$

Thus Vout is given by,

$$V_{out} = Vin\left(1 + \frac{WLC_{ox}}{C}\right) - \frac{WLC_{ox}}{C}(V_{DD} - V_{Th}) \tag{3.39}$$

where Vin is a function of sensor current and working electrode resistance.

In equation 3.39 the first term introduces gain error in the output, given by

$$Gain\ error: Vin.\left(\frac{WLC_{ox}}{C}\right) \tag{3.40}$$

and the second term introduces constant offset at the output

$$Offset: \frac{WLC_{ox}}{C}(V_{DD} - V_{Th}) \tag{3.41}$$

By including the body effect, equation 3.39 can be re-written as

$$V_{out} = Vin\left(1 + \frac{WLC_{ox}}{C}\right) + \gamma\frac{WLC_{ox}}{C}\sqrt{2\phi_B + Vin} - \frac{WLC_{ox}}{C}\left(V_{DD} - V_{Th} + \gamma\sqrt{2\phi_B}\right) \tag{3.42}$$

Thus, gain and offset error equation with body effect are:

$$Gain\ error: Vin.\left(\frac{WLC_{ox}}{C}\right)+\gamma\frac{WLC_{ox}}{C}\sqrt{2\phi_B+Vin} \tag{3.43}$$

$$Offset: \frac{WLC_{ox}}{C}\left(V_{DD}-V_{Th}+\gamma\sqrt{2\phi_B}\right) \tag{3.44}$$

The noise is measured in time domain using Agilent InfiniiVsion digital storage oscilloscope and the measured noise is shown in Figure 3-88 and Figure 3-89 at 200 kHz and 200 Hz sampling clocks. Since oscilloscope analyzes the signal in time domain, AC RMS is used to measure integrated noise. Total measured noise is around 3 mVrms at 200 kHz sampling clock and 1.3mVrms at 200 Hz sampling clock.

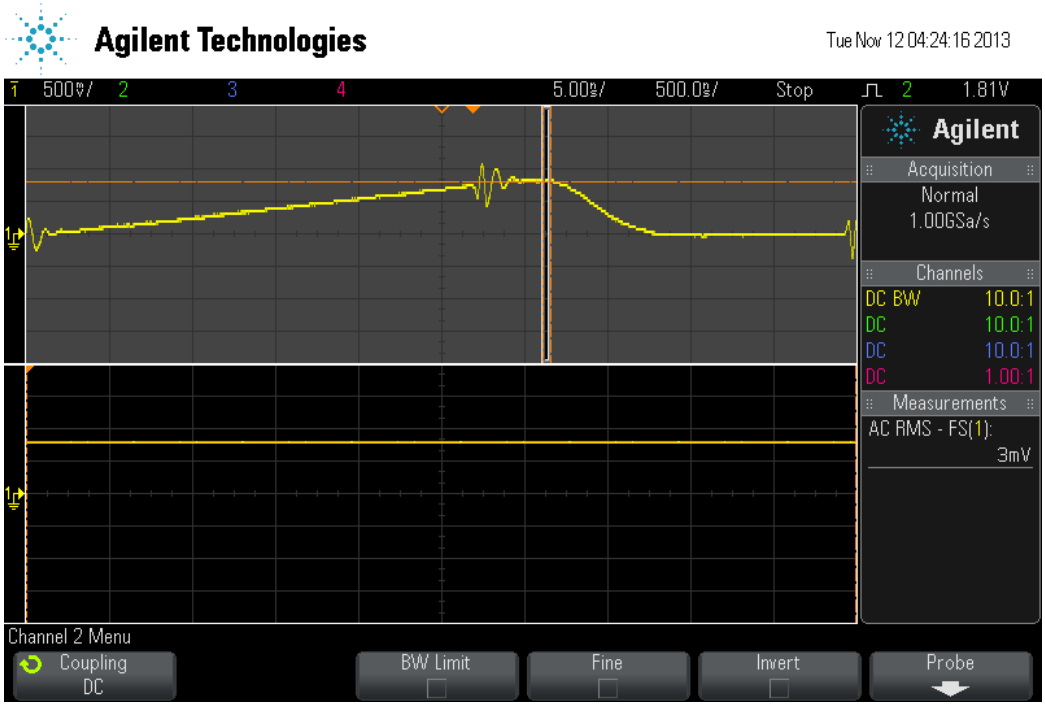

Figure 3-88 Noise measurement at 200 kHz sampling clock

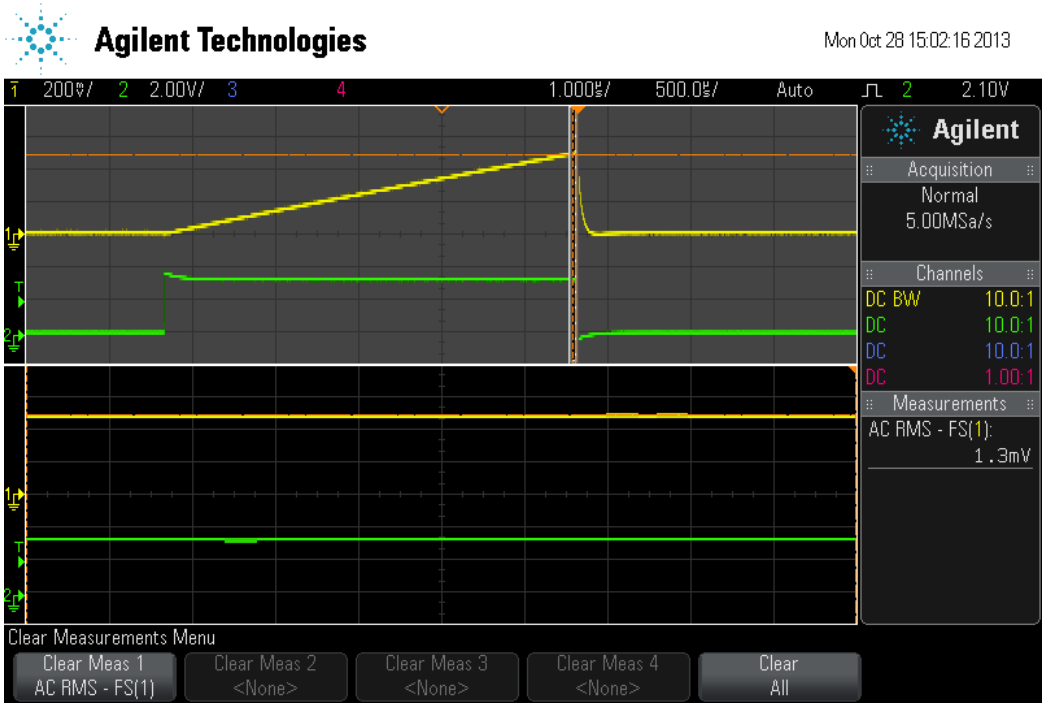

Figure 3-89 Noise measurement at 200 Hz sampling clock

Table 3-10 and 3 -11 summarizes the comparison between simulation and measurement results at 200 kHz and 200 Hz sampling clock. The measurement results closely follow the simulation results as expected. Noise at 200 kHz is higher due to higher power consumption and overshoot on the clock edges getting coupled to the output.

Table 3-10 Comparison between measurement and simulation results at 200 kHz

Parameter	Post extraction simulation	Measurement
Input Current	2µA-30µA	2µA-30µA
Output voltage	45mV-664mV	19.25mV-624mV
Total integrated noise	953.442µVrms	3mVrms
System power dissipation	3.05mW	3.33mW

Table 3-11 Comparison between measurement and simulation results at 200 Hz

Parameter	**Post extraction simulation**	**Measurement**
Input Current	2μA-30μA	2μA-30μA
Output voltage	45mV-664mV	19.25mV-624mV
Total integrated noise	803.442μVrms	1.3mVrms
System power dissipation	2.49mW	2.67mW

Chapter 4

Conclusion

In this work, a switched capacitor based trans-impedance amplifier amperometric readout circuit for microneedle glucose sensor is proposed. The designed switched capacitor based trans-impedance amplifier circuit has a linear output response for the input current range from (2µA to 30µA). Thus it will be used to amplify the complete output current range (5µA to 30µA) of a novel microneedle glucose sensor. The switched capacitor based trans-impedance amplifier offers lower noise and wider dynamic range compared to the conventional trans-impedance amplifier with resistive feedback architecture and fully differential current measurement architecture.

This switched capacitor based trans-impedance amplifier is designed and fabricated in 0.35µm CMOS process technology. The switched capacitor based trans-impedance amplifier in this work is implemented using an operational amplifier and transmission gates. The designed operational amplifier has a differential-to-single ended folded cascode structure at the core to provide high gain and the output stage is a two stage differential-to-single ended amplifier with negative feedback to drive low impedance (upto 1kΩ) loads. The PAD size for wire bonding with the QFP package is 81.4um × 81.4um. The total area of the proposed readout circuit is 160 µm x 157 µm and the area of 100pF on chip capacitance is capacitance is 900 µm x 50 µm.

The designed switched capacitor trans-impedance amplifier was simulated and tested with on chip gain capacitor of 100pF at 200 kHz and with external gain capacitor of 100nF at 200 Hz. The circuit linearly amplifies the input current from 2µA-30µA to output voltage of 45mV-664mV with a trans-impedance gain of 22kΩ. Therefore the output varies by 22mV for a 1µA change in input current. Also, from the microneedle current response

vs. glucose concentration plot it can be seen that for every 0.5mM change in glucose concentration sensor current changes by 1µA. Thus, the output voltage changes by 22mV for every 0.5mM change in glucose concentration. There is a mean percentage error of 15% between simulation and measured response due to the gain and offset error introduced by charge injection effect and also due to component tolerances. The measured noise at 200 kHz sampling clock is 3mVrms and the system power consumed is 3.33mW, whereas measured noise at 200 Hz sampling clock is 1.3mVrms and the system power consumed is 2.67mW. Since the electrochemical sensors work at speeds lower than 100 Hz, configuring the switched capacitor based trans-impedance amplifier to sample at 200 Hz provides optimal solution to conserve power. Comparison of this work with existing architectures is shown in Table

Table 4-1 Architecture comparison

Architecture	Power consumption	Noise	Complexity
Trans-impedance [33]	≈4.3mW	N/A	Less
Fully differential architecture [31]	15.84mW	N/A	Moderate
Switched capacitor based trans-impedance amplifier at 200 kHz(this work)	1.665mW	≈3mVrms	Moderate
Switched capacitor based trans-impedance amplifier at 200 Hz(this work)	1.335mW	≈1.3mVrms	Moderate

In the future work, the proposed CMOS switch capacitor based trans-impedance amplifier readout circuit is intended to be integrated with a microneedle glucose sensor. Thus creating a lab on chip platform for glucose measurement that can be interfaced with or embedded into the current portable computing platforms such as tablets and

smartphones allowing seamless flow of data for doctors to remotely monitor their patient's glucose levels and prescribe accurate treatment.

References

[1] E. H. Mathews and L. Liebenberg, “A Practical Quantification of Blood Glucose Production due to High-level Chronic Stress,” *Stress and Health*, vol. 28, no. 4, pp. 327–332, 2012.

[2] B. Alberts, D. Bray, J. Lewis, M. Raff, K. Roberts, and J. D. Watson, Molecular Biology of the Cell, 1983 :Garland

[3] A. L. Lehninger, D. L. Nelson, and M. M. Cox, Principles of Biochemistry, 1993 :Worth

[4] M. Giugliano, M. Bove, and M. Grattarola, “Insulin release at the molecular level: Metabolic-electrophysiological modeling of the pancreatic beta-cells,” IEEE Transactions on Biomedical Engineering, vol. 47, no. 5, pp. 611–623, 2000.

[5] D. D. Cunningham and J. A. Stenken, Eds., *In Vivo Glucose Sensing, Volume 174*. 2009.

[6] R. K. Clark, *Anatomy and Physiology: Understanding the Human Body*. Jones & Bartlett Learning, 2005.

[7] Y.-T. Liao, H. Yao, B. Parviz, and B. Otis, “A 3μW wirelessly powered CMOS glucose sensor for an active contact lens,” in *Solid-State Circuits Conference Digest of Technical Papers (ISSCC), 2011 IEEE International*, 2011, pp. 38 –40.

[8] J. D. Lane, D. M. Krumholz, R. A. Sack, and C. Morris, “Tear glucose dynamics in diabetes mellitus,” Curr. Eye Res., vol. 31, no. 11, pp. 895–901, Nov. 2006.

[9] J. Baca and R. Myllylä, “Tear Fluid Photonic Crystal Contact Lens Noninvasive Glucose Sensors,” in Handbook of Optical Sensing of Glucose in Biological Fluids and Tissues, vol. 20082359, V. Tuchin, Ed. Taylor & Francis, 2008, pp. 387–417.

[10] E. Wilkins and P. Atanasov, “Glucose monitoring: state of the art and future possibilities,” Medical Engineering & Physics, vol. 18, no. 4, pp. 273–288, Jun. 1996.

[11] http://usa.healthcare.siemens.com/

[12] N. S. Oliver, C. Toumazou, A. E. G. Cass, and D. G. Johnston, “Glucose sensors: a review of current and emerging technology,” Diabetic Medicine, vol. 26, no. 3, pp. 197–210, 2009.

[13] J. Zhang, W. Hodge, C. Hutnick, and X. Wang, “Noninvasive diagnostic devices for diabetes through measuring tear glucose,” Journal of diabetes science and technology, vol. 5, no. 1, pp. 166–172, Jan. 2011, PMID: 21303640.

[14] K. I. Iniewski, VLSI Circuit Design for Biomedical Applications. Artech House, 2008.

[15] M. M. Ahmadi and G. A. Jullien, “Current-Mirror-Based Potentiostats for Three-Electrode Amperometric Electrochemical Sensors,” IEEE Trans. Circuits Syst. Regul. Pap., vol. 56, no. 7, pp. 1339–1348, 2009.

[16] R. Greef, “Instruments for use in electrode process research,” J. Phys. [E], vol. 11, no. 1, p. 1, Jan. 1978.

[17] P. E. Allen and D. R. Holberg, CMOS Analog Circuit Design, 1st ed. Oxford University Press, USA, 2004.

[18] B. Goldstein, D. Kim, J. Xu, T. K. Vanderlick, and E. Culurciello, “CMOS Low Current Measurement System for Biomedical Applications,” IEEE Transactions on Biomedical Circuits and Systems, vol. 6, no. 2, pp. 111 –119, Apr. 2012.

[19] Y. Yoon, J. Kim, K. Lee, H. Song, K. Yoo, G. Lee, and J. Lee, “A novel microneedle-based non- enzymatic glucose sensor for painless diabetes testing application,” in Solid-State Sensors, Actuators and Microsystems Conference (TRANSDUCERS), 2011 16th International, 2011, pp. 2164 –2167.

[20] A. J. Bard and L. R. Faulkner, Electrochemical Methods: Fundamentals and Applications. Wiley, 2000.

[21] J. T. Maloy, “Factors affecting the shape of current-potential curves,” J. Chem. Educ., vol. 60, no. 4, p. 285, Apr. 1983.

[22] S. Gebhart, M. Faupel, R. Fowler, C. Kapsner, D. Lincoln, V. McGee, J. Pasqua, L. Steed, M. Wangsness, F. Xu, and M. Vanstory, “Glucose sensing in transdermal body fluid collected under continuous vacuum pressure via micropores in the stratum corneum,” Diabetes Technol. Ther., vol. 5, no. 2, pp. 159–166, 2003.

[23] U. Guth, W. Vonau, and J. Zosel, “Recent developments in electrochemical sensor application and technology—a review,” Measurement Science and Technology, vol. 20, no. 4, p. 042002, Apr. 2009.

[24] B. R. Eggins, Ed., Analytical Techniques in the Sciences: Chemical Sensors and Biosensors. 2007.

[25] J. Janata, “Electrochemistry Encyclopedia -- Electrochemical sensors.” [Online]. Available: http://electrochem.cwru.edu/encycl/art-s02-sensor.htm.

[26] W. Zhang and G. Li, “Third-generation biosensors based on the direct electron transfer of proteins,” Anal Sci, vol. 20, no. 4, pp. 603–609, Apr. 2004.

[27] U. Gebhardt, G. Luft, G. J. Richter, and F. von Sturm, “253 - Development of an Implantable Electrocatalytic Glucose Sensor,” Bioelectrochemistry and Bioenergetics, vol. 5, no. 4, pp. 607–624, 1978.

[28] T. R. G. C. Kathryn E, “Electrochemical Non-enzymatic Glucose Sensors: A Perspective and an Evaluation,” Int J Electrochem Sci Int. J., vol. 5, pp. 1246–1301, 2010.

[29] D. Pletcher, “Electrocatalysis: present and future,” J. Appl. Electrochem., vol. 14, no. 4, pp. 403–415, Jul. 1984.

[30] L. Busoni, M. Carlà, and L. Lanzi, “A comparison between potentiostatic circuits with grounded work or auxiliary electrode,” Rev. Sci. Instrum., vol. 73, no. 4, pp. 1921–1923, Apr. 2002.

[31] S. M. Martin, F. H. Gebara, T. D. Strong, and R. B. Brown, “A Fully Differential Potentiostat,” IEEE Sensors J., vol. 9, no. 2, pp. 135–142, 2009.

[32] J. Zhang, N. Trombly, and A. Mason, “A low noise readout circuit for integrated electrochemical biosensor arrays,” in Proceedings of IEEE Sensors, 2004, 2004, pp. 36 – 39 vol.1.

[33] “LTC2050 Data sheet”.

[34] B. Razavi, Design of Analog CMOS Integrated Circuits, 1st ed. McGraw-Hill Science/Engineering/Math, 2000.

[35] P. R. Gray, Analysis and Design of Analog Integrated Circuits. John Wiley & Sons, 2009.

[36] R. Gregorian, Introduction to CMOS OP-AMPs and Comparators, 1st ed. Wiley-Interscience, 1999.

[37] J. P. Uyemura, CMOS logic circuit design. Boston: Kluwer Academic Publishers, 2002.

[38] R. Schreier, J. Silva, J. Steensgaard, and G. C. Temes, “Design-oriented estimation of thermal noise in switched-capacitor circuits,” IEEE Transactions on Circuits and Systems I: Regular Papers, vol. 52, no. 11, pp. 2358– 2368, Nov. 2005.

[39] F. N. Hooge, “1/f noise,” Physica B+C, vol. 83, no. 1, pp. 14–23, May 1976.

[40] O. P. Hamill, A. Marty, E. Neher, B. Sakmann, and F. J. Sigworth, “Improved patch-clamp techniques for high-resolution current recording from cells and cell-free membrane patches,” Pflugers Arch., vol. 391, no. 2, pp. 85–100, Aug. 1981.

Biographical Information

Sunil Govardhan is a candidate for the Master of Science degree at the University of Texas at Arlington. He received his Bachelor's degree in Electronics & Communications Engineering from Visvesvaraya Technological University in India and worked in Robert Bosch Engineering and Business Solutions Limited in India until August 2011 as senior engineer in the area of automotive electronics. In 2011 fall, he joined the AMIC lab under the supervision of Dr. Sungyong Jung to design, integrate and test, systems and circuits for electrochemical sensors. During his Master's he has interned in Spring 2013 at BlackBerry as baseband hardware validation intern of boost converters for backlight drivers and rapid Li-Ion battery charging platforms and in Summer 2013 interned with Freescale Semiconductor Inc. as product definition and applications intern on battery management systems with passive cell balancing and isolated communication transceiver for fully electric and hybrid automotive power train. He will be joining Freescale Semiconductor as Analog Integrated Circuit Designer.